FOLDED SHELL ANALYSIS OF BOX BEAMS CURVED IN PLAN

by

M. Rehn, B.E.(Hons.)

A Thesis presented to the Faculty of Engineering of the University of Adelaide for the Degree of Doctor of Philosophy.

Civil Engineering Department
University of Adelaide

November 1971

To the best of the candidate's knowledge and belief, this thesis contains no material which has been accepted for the award of any other degree or diploma in any University, and contains no material previously published or written by another person, except where due reference is made in the text.

M. Rehn

C O N T E N T S

SUMMARY

The fundamental aim of the investigation described in this dissertation was to formulate a reliable method for analysing box beams curved in plan.

Just as a straight box beam can be considered as an assembly of rigidly connected folded plate elements, so a curved box beam can be considered as an assembly of rigidly connected folded shell elements. Based on classical thin shell elasticity equations for the various folded shell elements, a combined stiffness and flexibility matrix method is derived for the solution of loaded continuous box beams having constant curvatures in plan, non-varying cross sections, and simple supports at the extreme ends. The effects of any interior transverse stiffening diaphragms are included in the analysis, which utilizes Fourier series expansions in the circumferential direction. Since a computer is essential to perform the extremely large number of calculation steps involved, a general program has been written which is capable of analysing a wide variety of curved box beams subjected to most common load configurations.

In order to check experimentally the accuracy of the folded shell theoretical predictions, several static load tests were conducted on two independent models. The deflections and strains recorded from all tests confirmed the validity of the analysis.

ACKNOWLEDGEMENT

The author wishes to acknowledge the encouragement, advice, and constructive criticism which he at all times received from Mr G. Sved, Reader in Civil Engineering at the University of Adelaide, who supervised the project.

PRINCIPAL NOTATION

A	(8×8) element transformation matrix
A_i, B_i, C_i	Integration constants
B	Matrix used to formulate equilibrium and compatibility conditions for moveable diaphragms
C	(8×1) column matrix containing integration constants
D	Differential operator $\frac{d}{dx}$
D_r	Differential operator $\frac{d}{dr}$
E	Young's modulus
E_1, E_2, E_3	Matrices used to formulate contributions to the matrix F_D
F	$\frac{2Eh_1^3}{3(1-\nu^2)}$
F_D	Diaphragm flexibility matrix
G, H	(8×8) matrices associated with the complementary solutions of each element differential equation system
G_1, G_2, G_3, G_4 H_1, H_2, H_3, H_4	Matrices used to formulate various complementary and particular solutions required for each element
J	(3×4) Modified unit matrix
$K_1, K_2, \ldots K_{28}$	Constants
K_S	Structural stiffness matrix (complete structure)
L	Generator length of cylindrical shell element
L_1, L_2, L_3	Matrices used to formulate matrix P_J due to the action of diaphragm redundants

M	Curved edge moment stress resultant required in the formulation of matrix k_M
$M_x, M_\phi, M_{x\phi}, M_{\phi x}$	Moment stress resultants
N	Curved edge normal force stress resultant required in the formulation of matrix k_M
$N_x, N_\phi, N_{x\phi}, N_{\phi x}$	Stress resultants associated with shell membrane action
P	(8×1) column matrix containing curved edge stress resultants induced by the action of distributed loads under fixed-edge conditions
P_D	Column matrix containing all diaphragm redundants
P_J	Column matrix containing all joint loads for the complete structure
P_P	(8×1) column matrix containing particular solutions for the curved edge stress resultants due to distributed uniform loads
P_{diaph}	Column matrix containing the distributed diaphragm redundants acting on each element
P_{ext}	(2×1) column matrix used to represent uniform external loads acting on each element
P_m	Column matrix containing redundants associated with all moveable diaphragms
P_u	Column matrix containing redundants associated with all unmoveable diaphragms
Q_x, Q_ϕ	Shear force stress resultants normal to the surface of each element
R	Radius of cylindrical shell element
$R_{(a)}$	Column matrix containing the amplitudes of all desired output quantities for each element, due solely to edge movements
$R_{(b)}$	Column matrix containing the amplitudes of all desired output quantities for each element, due solely to the action of distributed loads under fixed-edge conditions

R_0	Radius to the location of a strain gauge rosette
R_1, R_2	Internal and external radii of flat plate element
S	Curved edge effective shear force stress resultant required in the formulation of matrix k_M. S is normal to the surface of each element
T	Curved edge effective shear force stress resultant required in the formulation of matrix k_M. T is tangential to the curved edge
X,Y,Z	Intensities of distributed loads acting on conical shell element in the x,ϕ,z member directions respectively
X_A, Z_A, Y_A, X_B, Z_B, Y_B	Concentrated edge redundants induced by diaphragm action. The subscripts A, B refer to the curved edges of the element
X_C, Z_C, X_D, Z_D	Distributed redundants induced by diaphragm action. The subscripts C, D refer to the one-third points (lateral) of the element width
X_n, Y_n, Z_n	Coefficients of infinite series used to represent distributed loads acting on conical shell element
a,b	Dimensionless parameters for conical shell element
$e_x, e_\phi, e_{x\phi}$	Actual-surface strains
e_1, e_2, e_3, e_4	Strains measured by four component gauges of a strain gauge rosette
$e_{1_0}, e_{2_0}, e_{3_0}, e_{4_0}$	Strains which exist at the centre of a strain gauge rosette, corresponding to the directions of the four component gauges
f_1, f_2, f_3	Linear functions
h	Thickness of cylindrical shell and of flat plate elements

h_1	Half thickness of conical shell element
i,m,n	Integers
k	$\frac{h^2}{12R^2}$
k_G	Element stiffness matrix referred to the global coordinate system
k_M	Element stiffness matrix referred to the member coordinate system
ℓ_1, ℓ_2	Length parameters for conical shell element
p	$\frac{\beta}{s}$
p_G	(8×1) column matrix containing the curved edge stress resultants required in the formulation of matrix k_G
p_M	(8×1) column matrix containing the curved edge stress resultants required in the formulation of matrix k_M
p_o, q_o	Intensities of distributed uniform external loads acting on each element in the x, z member directions respectively
r	Dimensionless variable
s	$\sin\gamma$
t	$\tan\gamma$
u,v,w	Displacement components in x, ϕ, z member directions respectively
u_C, w_C, u_D, w_D	Displacement components which correspond to X_C, Z_C, X_D, Z_D respectively
x,ϕ,z	Right-handed orthogonal coordinate system
y	Dimensionless variable
α	Angle subtended by folded shell structure at the axis of rotation
$\alpha_n, \beta_n, \gamma_n$	Infinite series coefficients

β	$\frac{m\Pi}{\alpha}$
γ	Half cone angle
δ	Common eccentricity of gauges in a strain gauge rosette
δ_P	(8×1) column matrix containing particular solutions for the curved edge displacement components due to distributed uniform loads
δ_M	(8×1) column matrix containing the curved edge displacement components required in the formulation of matrix k_M
δ_R	Column matrix containing rigid body displacement components of all moveable diaphragms
$\delta\phi$	Increment of angle ϕ
$\varepsilon_x, \varepsilon_\phi, \gamma_{x\phi}$	Middle-surface strains
ζ_A, ζ_B	Matrices calculated for each element and used in the assembly of matrix E_1. The subscripts A, B refer to the curved edges of the element
$\eta_i, \chi_i (i=1,\ldots 8)$	Ratios of integration constants
κ_A, κ_B	Matrices calculated for each element and used in the assembly of matrix L_2. The subscripts A, B refer to the curved edges of the element
$\lambda_{b_i} (i=1,\ldots 4)$	Roots of characteristic equation for flat plate bending action
$\lambda_i (i=1,\ldots 8)$	Roots of characteristic equation for cylindrical shell element
$\lambda_{m_i} (i=1,\ldots 4)$	Roots of characteristic equation for flat plate membrane action
ν	Poisson's ratio
ξ	Angular distance on a folded shell structure, measured from left support (ϕ=0)
$\xi_i (i=1,\ldots 4)$	Ratios of integration constants

ρ_1, ρ_2, ρ_3	Radii of three folded shell curved joints
$\sigma_x, \sigma_\phi, \tau_{x\phi}$	Actual-surface stresses
Δ	Column matrix containing absolute displacement components at the locations of all diaphragm redundants, due to the action of these redundants
Δ_D	Cumulative sum of Δ for all harmonics
Δ_J	Column matrix containing all joint displacement components for the complete structure
$\Delta_{m_o}, \Delta_{u_o}$	Column matrices containing absolute displacement components at the locations of all moveable and unmoveable (respectively) diaphragm redundants, due to the action of external loads
Δ_1, Δ_2	Contributions to the matrix Δ
χ_x, χ_ϕ	Curvatures
$\chi_{x\phi}$	Twist
ψ	Matrix calculated for each element and used in the assembly of matrix E_2

1. INTRODUCTION

The construction of curved bridges has become much more frequent in recent years because of the need to conform to modern complex roadway alignments. Since approximately 1940, curved box beams have been recognised as eminently suitable for highway overpasses, due to their excellent appearance and resistance to torsional loads.

Although many curved box beam bridges have been designed and constructed during the last 30 years, most of the analytical methods currently available do not adequately describe their true structural behaviour. A search through the available literature indicates that the influence of such complex structural effects as shear lag, distortion of the cross section, restraint of longitudinal (axial) warping, and secondary shear deformation can be of vital importance in determining the actual stress distribution within a loaded box beam. Consequently, many engineers are beginning to question the applicability of simple bending and torsion theory as a basis for design.

Throughout the world, much research is currently being devoted to the development of analytical methods capable of predicting the true behaviour of curved box beams. In this thesis, the results of a research programme conducted at the University of Adelaide are presented.

2. REVIEW OF LITERATURE

2.1 Introduction

The analysis of curved beams has attracted considerable attention since the first work was completed by SAINT-VENANT[1]* in 1843. Since that time, a large volume of literature has been published. Fortunately, in 1969, McMANUS, NASIR, and CULVER[2] presented a 'State of the Art' review of the developments regarding horizontally curved girders. Brief comments were made on relative costs, aesthetics, methods of analysis and design, experimental work, current work, and future needs. A comprehensive bibliography of 202 references was included covering the period from 1843 to 1968. This extensive list indicated that an ever-increasing amount of research was being applied to curved box beams treated as members of the 'thin-walled' class of structures. Further evidence of the interest in box beam behaviour was provided in 1970 by MAISEL[3], who presented an excellent review of 299 comparatively modern references dealing with the analysis and design of both straight and curved thin-walled beams, with special emphasis on box sections.

Every paper or article about curved beams written since the time of Saint-Venant could be considered to apply, at least in a general way, to the particular case of a curved box beam. However, it is now generally known that the complete response of

---

* Numbers in brackets refer to references in the bibliography.

a curved box beam is not adequately predicted by the traditional method of analysis, namely, a combination of simple bending theory and Saint-Venant torsional theory. The additional structural actions which occur are briefly listed below for future reference. In a real structure, the effects are intimately related, and so any method of analysis which treats them as independent must be approximate to some extent. Their relative significance is largely determined by the overall proportions of the box beam.

Distortion of the cross section

Displacements in the plane of the cross section cause changes in cross sectional shape.

Warping of the cross section

Warping corresponds to out-of-plane displacements of points on the cross section. It is assumed in the Saint-Venant theory of torsion that every cross section along the beam warps by the same amount, that the applied torque is uniform along the beam, that each cross section rotates without distortion, and that there is zero resistance to the warping displacements. If these conditions are violated, a more complex theory should be used. The principal effect of warping restraint is to induce axial stresses in the beam walls.

Shear lag

Shear deformation causes a redistribution of the axial bending stresses.

Torsional response of compound sections

A compound box beam is a beam whose cross section comprises any combination of closed cells, cantilever flanges attached to closed cells, and deck slabs connecting adjacent closed cells. When such a beam is subjected to torsional loads, those portions of the cross section which do not form part of a closed cell should be considered when assessing the stiffness properties of the beam, as their contribution to the overall torsional response may be significant.

Perhaps the greatest advantage of box girders is their comparatively high torsional resistance. Although various solutions to the problem of torsion in box girders have been proposed[3], unfortunately for design engineers the influence of the structural actions listed above considerably complicates any theoretical estimate of the true stresses within the structure. Analytical methods are usually based on one of the following three sets of assumptions[4], which are listed in order of increasing calculation complexity.

(a) The cross section is undistorted, and only the pure shear stresses which result from Saint-Venant torsional analysis are considered

(b) The cross section is undistorted, and the additional influence of warping restraint is considered

(c) The cross section is distorted, and this effect is also included in the torsional analysis

These three assumptions form a useful basis for classifying literature on the analysis of thin-walled beams.

The following brief survey concerns available published information on elastic methods for the analysis and design of statically loaded curved box beams. For a comprehensive general discussion of literature on the analysis of both straight and curved box beams, the torsional properties of thin-walled cross sections, and the relative importance of the listed box beam structural actions, the valuable review by Maisel[3] is again recommended.

2.2 Saint-Venant Torsional Analysis

For well over 100 years, simple Saint-Venant Torsional analysis[5] has been the standard method for analysing curved beams with any cross sectional shape. Consequently many hundreds of references could be included in this section, for in order to apply the theory to the particular case of a curved box beam, it is necessary to obtain only the appropriate cross sectional properties and then substitute them into the general equations. (BECHERT[6], for example, considered the analysis of a single-span curved box beam and gave numerical results). Only a few comparatively modern references are selected for discussion here. Since each is based on the same well-established theory, there is very little inter-dependence. Consequently, references are grouped to illustrate various applications of the theory, rather than to group them in strict chronological order.

Fixed-ended beams

An approximate solution for cantilevers curved in plan was given by MELLOR and JOHNSON[7]. The load was applied to the free end of the beam, and the solution was obtained by applying Castigliano's theorem upon consideration of the strain energy induced by combined bending and torsion. Deflections were then evaluated after assuming that the ratio of bending stiffness to torsional stiffness was equal to unity.

For the more complex case of horizontal beams curved circularly in plan and having built-in ends, MOORMAN and TATE[8] derived influence lines for shear forces, bending moments, and twisting moments. ABBASSI[9] analysed a symmetrical bow girder which was built-in at both ends, but not necessarily curved in plan. Exact and approximate formulae were given. This analysis was formulated in terms of the angle between the tangent at any point on the girder, and the tangent at the middle point. Only uniform loads and a pair of equal concentrated loads placed symmetrically about the middle point were considered. Later, in a highly theoretical paper[10], the same writer investigated the stresses in a beam whose centre-line was an arbitrary plane curve. Equations of equilibrium and compatability were derived in their general form by using complex variables and orthogonal curvilinear coordinates, and their application was illustrated by examples. By starting with an analysis which was similar to that of Mellor and Johnson for curved cantilevers[7], STAMPF[11] employed the principle of superposition to analyse horizontal

circularly curved beams with fixed ends and subjected to both general loading and longitudinally symmetrical loading. Longitudinal prestressing was also briefly discussed. TERRINGTON[12] gave an initial discussion of both Saint-Venant torsion and warping torsion. However, for closed box sections of commercial proportions, he suggested that the shear centre should be first located, and then the shear stresses resulting from only Saint-Venant torsion need be calculated. Warping torsional stresses were assumed to be secondary and negligible. Results for a circular arc girder built-in at both ends and subjected to either a concentrated load or a uniformly distributed load were displayed in graphical form. Further detailed workings for a series of examples, including multicell box sections, were later given in a supplementary paper[13].

Single-span beams with various end conditions

For analysing any arbitrary planar curved member with varying cross section, DONALD and GODDEN[14] suggested a numerical forward integration technique. By approximating the beam as a series of short chords, any applied loading was reduced to an equivalent nodal point load system. All chords were assumed rigid, and overall beam flexibility was assumed to be concentrated at the nodes. Moments and deflections at these points were obtained. The concept of approximating a beam with continually varying curvature or cross section by a large number of connected short segments has also been used by other writers. Two such

examples in which the flexibility matrix method was applied to curved beam problems have been given by REDDY and TUMA[15] and by YOUNG[16]. Reddy and Tuma considered a planar arbitrarily curved bar of variable section, and suggested that numerical methods such as elemental or segmental flexibilities should be used[17,18]. For the familiar case of a circularly curved bar with uniform cross section, flexibility coefficients were calculated by direct integration. Young briefly treated the general problem of a beam curved in three dimensions by using a discrete nodal representation. Cross sectional properties were assumed to vary along the axis. It was realised that a three-dimensional curved beam had little practical application, and so the solution was developed in detail for the particular case of planar curved beams.

The effects of prestressing curved beams were thoroughly discussed in a paper by MENN[19]. However, a simple analysis of prestressed beams curved in plan and having torsional restraint at the supports has recently been outlined by GARRETT and COCHRAINE[20]. They stated that the torsional moments induced by prestress cables placed symmetrically about the vertical axis of the cross section were dependent only upon the support bending moments which could be calculated in most cases by using the 'equivalent' straight beam approximation*. Conditions of concordancy for curved prestressed beams were prescribe

---

* One of the most common assumptions made by design engineers is that a curved member can be designed as an 'equivalent' straight member[21,22,23].

Continuous beams

Before the development of electronic computers, moment distribution was often used to analyse complex curved beam problems. From the expression for total strain energy due to combined bending and torsion of a circularly curved beam with constant cross section, VELUTINI[24] used Castigliano's theorem to derive expressions for the necessary stiffness and carry-over factors. A calculation procedure for continuous beams was then described in which support bending moments were kept separate from support torsional moments. This same moment distribution technique is still used by modern designers to analyse continuous curved beams. It is by no means obsolete.

The concept of an influence line is very useful in the design of continuous beam structures. One paper which details these calculations for circularly curved girders was presented by FICKEL[25]. He used a flexibility method to derive influence lines for bending moments, twisting moments, and shear forces in the cases of both simply supported and continuous girders. Effects of variable moments of inertia and elasticity of the torsional supports were discussed.

Several papers have been published on the general analysis of continuous beams curved in plan, and a few of these merit special mention. COURBON[26] derived a three-moment equation for continuous planar beams curved circularly in plan and loaded normal to the plane of the central fibre. For curved spans which had small subtended angles, he calculated the errors

associated with the 'equivalent' straight beam approximation. In a final section of the paper, the theory was extended to bridges with variable curvature. BRETTHAUER and NOETZOLD[27] investigated continuous curved beams in which each span was of constant curvature, and torsion supports could be specified as either fixed or elastic. Similar structures were analysed by STAMPF[28]. The curve was again approximated by a series of circular arcs with colinear radii at the connection points, and external elastic constraints occurred at the beam ends and at any intermediate supports. Loads applied to the structure were either torsional moments, or forces normal to the plane of curvature. Governing equations were derived from strain energy considerations, and it was suggested that they could be solved by a direct matrix procedure. (Such a direct procedure was later used by PETERSEN[29] in the form of a matrix progression (transfer matrix) technique. The direction of the progression was along the beam axis, and hence both structural and load discontinuities could be incorporated by analysing successive short lengths of the curved beam). TOPPLER, CHAUDHURI, and VAN DEN BERG[30] considered the effects of circular curvature on the reactions and stresses which result when a girder of closed cross section is subjected to combined bending, shear, and torsion. Typical load systems were applied to beams of up to four continuous spans. It was assumed that the cross section remained constant along the full length of the beam, and that the degree of torsional restraint was identical at every support.

In addition, the ratio of bending stiffness to torsional stiffness was taken as unity. Results were tabulated for two finite degrees of torsional restraint, and it was implied that other cases could be deduced by interpolation. A three-span curved box girder with a twin-cell cross section was presented as an example. The 'equivalent' straight beam approximation was also investigated by the writers, and charts were given to indicate the differences between bending moments, torsional moments, and shear forces for straight members and for curved members subtending central angles of up to 60 degrees. On the basis of these charts, they deduced that for subtended angles less than 30 degrees, the straight beam approximation could be used to calculate the magnitudes of the torsional moments, reactions, and shearing stresses within limits of accuracy suitable for design. A deficiency of the paper is the lack of comment on the effects of altering the ratio of bending stiffness to torsional stiffness. For a beam in which this ratio is not equal to unity, the results should be treated with some caution.

For many years, there were no complete reference works published on the general Saint-Venant torsional analysis of curved beams, and designers were forced to search through individual papers in order to find the required information. Recently, however, a number of excellent comprehensive works have been made available. In 1964, WITTFOHT published a book[31] on the linear elastic analysis of curved beams loaded normal to the plane of curvature. A circularly curved beam with torsionally

rigid end supports was first treated in detail. From this solution, the case of a multispan curved girder was solved by using a flexibility method which was conceptually similar to that which is often applied to straight continuous beams. Formulae for bending moments, twisting moments, deflections, and influence lines were derived, and the results of calculations given in numerous extensive tables and graphs. All necessary explanations of the design aids were included in one section, enabling the engineer to extract information without necessary recourse to the details of the theory. (Wittfoht later extended the theory to include the effects of eccentric torsional loads[32]). In 1964, VREDEN also published a book[33] on the analysis of curved continuous girders. Many load cases were first considered for a single curved span with torsionally rigid ends, and from these solutions flexibility coefficients for bending moments, twisting moments, and shear forces were derived for continuous beams. In a later volume[34], Vreden evaluated some of these coefficients, and thereby considerably reduced the number of tedious calculations to be completed by the designer. Unfortunately, some of the analytical steps were explained a little too briefly, and several of the derivations are difficult to follow. Although SCHULZ[35] analysed most of the same problems as Wittfoht and Vreden, he did include all necessary explanations of the analytical steps involved. For continuous beams which had intermediate supports with zero torsional restraint, the solution obtained by Schulz was more direct than that of Vreden, and

prestress loads were also analysed very simply. Useful graphs were given to facilitate evaluation of moment distribution factors for a large variety of curved beams.

Frame systems with curved members

In an early paper, MICHALOS[36] applied moment distribution to the analysis of plane frames with curved members. Although modern computer techniques are essential to analyse highly redundant frame systems with a very large number of members, iterative moment distribution is still used to solve problems involving relatively few members[35].

The derivation of influence lines for space frames with curved members was recently undertaken by YAMASAKI and OHTA[37]. Influence lines were deduced for general forces on an arbitrary space frame by applying the Muller-Breslau principle to the deflection profiles caused by corresponding unit deformations. As an illustrative example, a space frame with a combination of both straight and curved members was given.

Direct stiffness and flexibility matrix methods coupled with an electronic digital computer constitute a very powerful tool of structural analysis. A number of papers applicable to curved beam systems have been published. In a well written paper, TEZCAN and OVUNC[38] obtained general stiffness matrices for circularly curved beams with doubly symmetrical cross sections. A series of successive orthogonal transformations were described in order to refer the member stiffness matrices to a global (common) coordinate system. By specifying

a sufficiently large radius and a correspondingly small subtended angle, each curved beam stiffness matrix could be reduced to that of a straight beam element. MICHALOS[39] considered a single branch structure arbitrarily curved in space and subjected to an arbitrary static load system. By dividing the structure into a number of relatively short segments, members with variable cross section were analysed. Fixed-end moments and fixed-end forces were deduced. SAWKO[40] applied the direct stiffness method to a beam grillage containing circularly curved members. Flexibility coefficients for the curved member ends were calculated, and by inversion, the stiffness matrix of a single member was obtained. Methods for calculating fixed-end moments and forces were outlined, and a computer program capable of analysing a grillage of both straight and curved members was briefly discussed. Sawko also investigated the 'equivalent' straight beam approximation, and concluded that the error involved was substantial, even for spans with subtended angles as small as 1 degree, and rose rapidly for larger angles. (This conclusion is in marked contrast with that reached by Toppler et al.[30]). The curved beam stiffness matrices derived by MORRIS[41], LEE[42], and WANG[43] were essentially similar to those proposed earlier by Tezcan and Ovunc[38]. Wang also listed the required transformation matrices.

Although many papers have been written on the analysis of curved beams, comparatively few have been written on general design aspects. Only three such references are included in the

bibliography[44,45,46]. Of particular interest is the paper by BRAMALD and GRALTON[46], in which extensive discussion was given concerning practical design considerations of a continuous box beam roadway structure with non-uniform horizontal curvature. Saint-Venant torsional analysis was briefly outlined using a strain energy approach. This analysis was assumed to be satisfactory for all parts of the structure except at the supports and at points of locally applied torque. (In these areas, warping torsional analysis was used). Basic Saint-Venant torsional calculations were programmed for computer solution by using moment distribution, and all parasitic moments due to prestress were incorporated. Comments were made on such problems as the choice of cross section, types of bearing, number of diaphragms, distribution of maximum principal diagonal tensile stresses, stability at supports, and construction procedure. This paper is a valuable contribution to the literature of curved beams, although it is surprising that an iterative moment distribution technique was chosen for the computer solution rather than a more direct matrix formulation.

2.3 Warping Torsional Analysis

When any thin-walled beam is subjected to non-uniform torsion or free warping is prevented, corresponding changes are induced in the stress distribution within the structure. If it is assumed that the cross section remains undistorted throughout the beam length, then the theory which predicts the internal stress distribution is known as warping torsional

analysis. Some important contributions to the theory of curved beam warping torsion are discussed in this section. Many papers have been published on this relatively young research topic, and several apparently independent solutions have been derived for essentially similar problems. Where possible, papers are grouped herein according to the original source reference.

VLASOV was probably the first to derive differential equations for warping torsion of curved beams. In 1961, the English translation of a book[47] was published summarizing the work contained in a large number of his early papers on the analysis of thin-walled beam structures. Straight members formed the subject of most of the book, and many chapters were devoted to the analysis of both open and closed cross sections with non-deformable profiles. The analysis was then extended to the case of circularly curved thin-walled beams. Equations obtained were approximate, and all forces were referred to the beam centroidal axis. For a beam with a radius greater than ten times the largest cross sectional dimension, errors associated with the approximations were stated to be insignificant. (It is of interest to note that in this same book, Vlasov also considered the analysis of a straight prismatic multicell beam with deformable profile, firstly including the effects of shear deformation, and secondly neglecting them. All rectilinear elements of the beam cross section were assumed to be hinged at their inter-connection points, and to remain straight while the

cross section warped and distorted. On the basis of these calculations and some supporting experimental evidence, it was concluded that for thin prismatic multicell structures, deformation of the cross section was an important factor in determining the final state of stress, but the effect of shear deformation was secondary, and could be neglected. The calculations were not extended to curved multicell beams). Another early work containing an approximate warping torsional analysis of curved beams was published by WANSLEBEN[48], who used simplifying assumptions which were similar to those of Vlasov. A single-span beam was first analysed, and the solution was then extended to continuous beams by utilizing the continuity conditions at intermediate supports. No formulae were given for evaluating the various cross sectional properties required in the general analysis.

DABROWSKI[49] derived four general differential equations for the torsional behaviour of a loaded curved beam. Several terms omitted by Vlasov were included, and whereas Vlasov referred his equations to the centroidal axis, Dabrowski's more accurate equations involved displacements of points on the shear centre axis. In another paper[50] by the same writer, the warping torsional theory of circularly curved thin-walled beams with mono-symmetrical open profiles was considered. The governing differential equation for the warping moment (bimoment) of members loaded normal to the plane of curvature was derived and solved for deformations and internal stresses. Formulae for

these quantities were given for statically determinate beams under various load conditions. Formulae for influence coefficients were stated, and their use in the analysis of continuous structures was clearly indicated. Limiting conditions of the method were also given, together with a numerical example to illustrate the procedure. (Further applications of the theory can be found in a paper[51] in which influence lines for bending moments and torsional moments were presented for single- and two-span curved beams of open cross section). Dabrowski also extended this method[52] to analyse single-span curved beams with closed cross sections. Bimoments and other properties of circularly curved box beams were deduced, and the treatment of continuous box beam structures was briefly outlined. The three previous papers[50,51,52] were later incorporated into a book[53] on the general analysis and design of curved thin-walled beams with open or closed cross sections. All relevant equations and expressions for warping torsion were detailed, together with extensive tables of internal forces and displacements for multi-span beams with constant section properties. These tables were arranged in terms of stiffness parameters and subtended span angles. Although the publication of tables is often made redundant by the availability of modern computing facilities, the book can be recommended for the preliminary design of curved box beam structures.

KONISHI and KOMATSU[54] developed from first principles a torsion-bending theory for a circularly curved girder with

a multicell cross section of arbitrary shape. Strain energy considerations formed the basis of the analysis, and formulae for finding the shear centre of the cross section and various other quantities related to cross sectional geometry were explicitly defined. Both simply supported and continuous beams were completely analysed under many typical load conditions. In order to further illustrate the method, a three-span bridge was numerically analysed, in which the cross section consisted of a single-cell composite box with side cantilevers. The central bridge span was curved, and the outer spans were straight. Influence lines for stress resultants and deformations were calculated, and brief comments were made concerning the general response of the bridge. This paper is very concise, and emphasizes the need to consider warping torsional stresses in box beams. The theory is based on several earlier papers by the same writers[55,56,57,58]. Curved beams with closed thin-walled cross sections were also analysed by KONISHI, SHIRAISHI, and KAMBE[59]. The principle of complementary virtual work was used to derive governing equations which included the effects of non-uniform rate of twist along the beam, and the associated secondary shear deformation. This analysis was based on BENSCOTER's hypothesis[60] concerning lateral variation of warping displacements, and on the work of HEILIG[61]. Unfortunately, the paper lacks an illustrative numerical example.

By employing the assumption that each cross section remains plane after bending, a circularly curved beam with

either open or closed non-deformable thin-walled profile was analysed by KURANISHI[62]. Cross sectional properties required for warping torsional analysis were explicitly formulated, taking into account the radius of the shear centre axis and also the geometry of the cross section. A differential equation which was similar to that of a beam on an elastic foundation was derived and solved for the shear centre axis twists and deflections.

FUKAZAWA[63] extended the Wagner theory of unit warping for loaded thin-walled straight bars to the static analysis of circularly curved bars with thin-walled arbitrary cross section. Effects of curvature were included in all formulae for cross sectional properties, and the differences between the torsional properties of open and closed cross sections were carefully stated. General differential equations were obtained in terms of the displacement components of any arbitrary point on the cross section, and it was pointed out that these equations could be more simply expressed in terms of the displacement components of either the neutral axis or the shear centre. In another paper[64], Fukazawa considered the analysis of thin-walled curved beams with variable cross section, taking the discontinuity of the shear centre axis into account. Fundamental warping torsion equations were first derived for a curved segment of constant radius and constant cross section, loaded normal to its plane of curvature. A transfer matrix which related static quantities at one point of the beam to those

at any neighbouring point was then deduced after solving these equations with the aid of Laplace transforms. Where the cross section or radius suddenly changed, continuity relationships were expressed in matrix form, and an example of a simply-supported S-shaped box girder with varying section was worked. At the abrupt change of beam curvature, there was a finite discontinuity in the radial position of the shear centre axis, and the effect of this was included. The calculations were repeated, this time neglecting the discontinuity, and substantially different results were obtained. Curved thin-walled beams with varying cross section had been analysed earlier by BAZANT[65], but the variations were assumed to be continuous and gradual and the profiles were assumed to be mono-symmetrical. The theory for beams with varying open cross sections was similar to that of Vlasov for constant cross sections. The theory for beams with varying closed cross sections was based on Umanskiy's assumption that non-uniform torsion in closed profiles caused warping of the initially plane cross sections which was proportional to the warping predicted by pure Saint-Venant torsional analysis. Bazant stated that for variable mono-symmetrical profiles, torsion and horizontal bending were not independent, but were connected by a system of two simultaneous differential equations. However, the solution was approximate due to the initial assumptions, and he pointed out that some experimental verification was needed to establish the conditions for which reasonable accuracy could be expected.

A paper which gave an approximate theory for an arbitrarily curved beam with fixed ends was presented by WASHIZU[66]. Warping was assumed to be prevented at the supports, and the effects of transverse shear deformation were included in the analysis. Six equilibrium differential equations were derived from virtual work considerations, and a seventh equation was obtained by relating warping to other deformations. All properties were referred to the beam centroidal axis. GREBEN[67] obtained similar results. A theory for continuous thin-walled circularly curved beams has been reported by VESELOVSKII[68], who assumed that all supports were on the axis of the centres of flexure, and that these supports prevented movement normal to the plane of beam curvature. A flexibility approach enabled the problem to be reduced to the solution of a canonical equation system, and a numerical example was given.

2.4 Distortional Analysis

Associated with any loaded thin-walled beam, there is an inherent tendency for the cross section to distort. The influence of cross sectional distortion in hollow members was noted in 1911 by KARMAN[69], who observed that the flexibility of a curved tube was greater, and the strength less, than predicted by simple bending theory. Analogous results were obtained by TIMOSHENKO[70] in 1923 during an investigation into the flexure of curved tubes with rectangular cross section. These observations were supported by ANDERSON[71] in 1950, when the flexure of curved rectangular box sections was again

investigated. Experimental evidence confirmed the conclusion that flange distortion was accompanied by lateral bending stresses which, under certain circumstances, could be of greater magnitude than the circumferential bending stresses. In this paper, Anderson also reviewed the history of the theory of flexure for curved beams, with special reference to the effects of distortion. Analyses similar to those of Anderson and Timoshenko were conducted by CORNELIS and CARTILIER[72] in 1960, and by DZIEWOLSKI[73] in 1964 respectively. Perhaps because of the greater complexity of the calculations, the important additional influence of torsional loads on the distortion of curved box beam cross sections has only recently received some attention. In the following paragraphs, those few references which consider combined bending and torsional analysis of curved box beams with deformable profiles are discussed.

DABROWSKI[74] analysed a curved beam with a deformable mono-symmetrical closed cross section, and included the effects of warping torsion. Deformation of the cross section was characterized by an angle which was governed by a fourth order differential equation analogous to that of a beam on an elastic foundation. The solution could be found either by employing the analogy, or by using Fourier series expansions. Due to the nature of the assumed simplified deformation pattern, the method must be regarded as approximate. (This work was incorporated into a section of Dabrowski's book[53] on curved thin-walled beams). Later, based on the principle of minimum

potential energy of deformation, BAZANT[75] derived a system of linear differential equations for the behaviour of thin-walled members with varying deformable cross sections and with thick stiffening diaphragms. The method was first applied to straight structural members of either open or closed cross section. An analysis was then deduced for a beam circularly curved in plan, and it was stated that these calculations were reasonably accurate for closed cross sections. However, no numerical examples were given to illustrate the use of the derived equations. Like the method of Dabrowski, the accuracy of the approach is limited by the nature of the assumed deformation pattern.

If the ratio of width to depth of a circularly curved multicell box beam is sufficiently large, then the net structural action may be approximated by treating the beam as a thin flat slab curved in polar coordinates. COULL and DAS[76] have presented an analysis based on the elasticity theory for simply supported single-span curved slabs. Loads and resultant deflections were expressed by Fourier series in the circumferential direction, with the Fourier coefficients being functions of the radial coordinate only. Concentrated loads were incorporated as discontinuities of shear force in the radial direction by using an artifice similar to the method of Macaulay's brackets in ordinary beam theory. Experiments on two models made of perspex and asbestos-cement gave reasonable agreement with the theory after only three non-zero Fourier terms were taken.

Unfortunately, application of the solution to real bridge structures is severely restricted because of the initial assumption that the plate is isotropic. A similar approach was provided by CERADINI[77], who considered the more realistic case of an orthotropic polar flat plate. In addition to the rigorous analysis, a simplified version was given in which the plate was assumed to be stiffened by rigid transverse beams. YONEZAWA[78] obtained a rigorous solution for a uniformly loaded polar orthotropic plate simply supported along its radial edges and having elastic beams rigidly attached to its curved edges. From the results, he concluded that simple curved beam theory was inadequate to describe the true behaviour of this type of deformable structure. By using a method analogous to the slope-deflection method for planar rigid frames, BELL and HEINS[79,80,81,82] analysed continuous orthotropic or isotropic bridge decks on curved flexible girders. Basic slope-deflection matrices were derived to include the effects of girder warping stiffness and of radial diaphragms, and girder deflections and internal forces at any desired location on the span were computed for both concentrated and uniformly distributed loads. The solution allowed for either composite or non-composite interaction between the beams and slab. As part of the same general research programme into the behaviour of curved viaducts, the finite difference technique has also been applied to the same type of structure[83,84,85]. Comparison of computed results with experimental data from model tests has indicated that this technique provides a valid and reliable solution. Continuous

curved plates have also been studied by YÜKSEL[86].

During recent years, the finite element technique has been successfully applied to a wide variety of structural problems[87]. ANEJA and ROLL[88,89] applied this method to a typical horizontally curved box beam. They constructed a plastic model to test the validity of the theoretical predictions, and found good agreement for the lateral stress distribution, but not for the circumferential stress distribution. CHAPMAN, DOWLING, LIM, and BILLINGTON[90] have reported results of a general analytical investigation into the influence of cross sectional deformation on the stresses induced in straight, skewed, and curved box beams. By using three methods of analysis, namely Saint-Venant torsion, the beam on elastic foundation analogy, and the finite element method, both steel and concrete forms of construction were considered. No details of the finite element solution were given in the paper, and very little discussion was given on the fixed-ended curved box beams quoted as examples. However, the importance of allowing for cross sectional distortion even for concrete box girders was clearly illustrated, and some useful comments were made concerning the effects of stiffening diaphragms. Further details of the finite element solutions, together with model test results, have been presented in other papers[91,92]. SISODIYA, CHEUNG, and GHALI[93] discussed the application of finite elements to a skew curved single-cell box beam with vertical webs. The problem was treated by using rectangular finite elements for the

webs, and either parallelogram or triangular finite elements for the top and bottom slabs. Analytical results were checked against experimental values obtained from an aluminium model, and comments were made concerning computer storage requirements and relative accuracies of the various chosen element configurations. CHEUNG, KING, and ZIENKIEWICZ[94] applied the orthotropic plate idealization to analyse a curved cellular bridge deck with large ratio of width to depth. A series of triangular finite elements simulated the equivalent bridge slab. It was stated that since the chosen elements did now allow for in-plane forces, a three-dimensional box beam structure whose cell depth was large compared to the overall width of the bridge could not be analysed by the same system. An important variant of the usual finite element method, known as the 'finite strip' method, was suggested by CHEUNG[95] for the analysis of curved orthotropic plate bridge decks simply supported at the two radial ends. This approach required far less computer storage locations. Each strip spanned the full length of the bridge, and was joined to its neighbour along its curved edges. Boundary conditions at the supports were automatically satisfied by using the familiar separation of variables technique based on Fourier series expansions in the circumferential direction. By starting with an assumed displacement function, element stiffness matrices were calculated in terms of the displacements and forces which existed at each of the element curved edges, and a complete structure could then be analysed by the standard stiffness method. Comparisons with the results of Coull and

Das[76] indicated excellent agreement. MEYER and SCORDELIS[96] have recently extended the finite strip approach to analyse three-dimensional curved box beams simply supported at the two ends. In this case each elemental strip consisted, in general, of a segment of a conical frustrum. The approximate nature of the finite strip method was clearly indicated in this work, and its limitations were outlined. Although calculated results were presented for a typical double-cell super-elevated curved box beam with cantilevered flanges, some experimental evidence would have been extremely useful in establishing the degree of approximation involved. In addition to the finite element references mentioned above, certain others which may be of interest have been included in the bibliography[97,98,99,100]. However, copies of these were not available for perusal at the time of writing this thesis.

2.5 Summary

Several contributions to the elastic theory of curved box girders have been reviewed in the preceding sections. To a design engineer, the 'best' analysis is the simplest one which gives reliable predictions of the critical stress conditions within the structure. Since it is very difficult to determine the relative importance of the various structural actions of a box beam in any particular design situation, the engineer should always be acutely aware of the assumptions associated with any approximate analysis. Unfortunately, the range of conditions for which the simplifying assumptions are valid is not adequately

defined in most papers, and this fact considerably complicates the choice of a suitable design approach.

Several independent references have emphasized the particular importance of cross sectional distortion in both concrete and steel box beam bridges of typical proportions. It follows that neither Saint-Venant torsional analysis nor the more accurate warping torsional analysis will necessarily predict the actual stress conditions, and a more comprehensive theory should be used. Since any analysis which incorporates distortion of the cross section is necessarily complex, a digital computer is usually required to execute the calculations.

For three-dimensional curved box beams, the most powerful method of distortional analysis described in the literature is the finite element method, as this can handle structures with arbitrary profiles, load configurations, and support conditions. However, traditional elements require large amounts of computer storage in order to achieve suitable representation of a bridge, and so this method is not yet widely used by bridge designers. Another reason why finite element techniques are not more widely used in design is that very little work has been published on the true accuracies of the discrete approximations involved. The finite strip method for simply supported beams with constant cross section and curvature offers large savings in computer storage, but as yet this solution has not been extended to incorporate either intermediate stiffening diaphragms or intermediate supports.

From the literature survey, it is evident that there is a need to develop general analyses which will give accurate solutions to the problem of curved continuous box girder structures, including all of their structural actions. The analyses should be capable of predicting the internal stress distribution for beams of all common proportions when subjected to all common load configurations. They could then be used either for the direct analysis and design of structures, or as powerful aids in determining the specific limitations and relative accuracies of other analyses. The latter usage is particularly important, for very little work has been done on the correlation of the analytical solutions currently available.

3. FOLDED SHELL ANALYSIS

3.1 Introduction

One traditional method of analysing a redundant structure is to use a combined stiffness and flexibility approach. The structure without the redundants (released or primary structure) is first analysed subject to the influence of the applied external loads, and the displacement components at the location of the absent redundants are evaluated. This is the stiffness part of the solution. The redundant forces are then calculated by applying the compatibility relationships which must exist at their points of application. This is the flexibility part of the solution. The primary structure is then loaded with only the known redundant forces, and is again analysed by the stiffness method. Finally, results from the latter calculations are superimposed on those obtained from the first stiffness calculations to give the complete solution for the redundant structure.

A relevant example of the method is the folded plate analysis of continuous straight thin-walled beam structures, in which the redundants are taken to be the reactions due to interior support diaphragms. The problem is complex, since the lateral distribution of the interaction forces between the diaphragms and the folded plate elements is unknown. In order to approximate this distribution, PULTAR[101] assumed that each supporting diaphragm was infinitely rigid in its own plane, and that the interaction forces were uniformly distributed over the small thickness

of the diaphragm. Compatibility was enforced at the folded plate joints and at a finite number of selected points in between. It was further assumed that compatibility need be enforced only at the centre of the diaphragm thickness. A Fourier harmonic analysis in the longitudinal direction was used to solve classical elasticity equations for the structural behaviour of each plate, and these calculations were programmed to obtain a computer solution for continuous structures with simply supported ends. Recently, it has been shown[102,103] that satisfactory results could be obtained even with relatively crude approximations for the nature of the diaphragm redundants. Based on the procedure proposed by Pultar[101], SCORDELIS and LO[104,105] developed a general computer program for the matrix analysis of continuous cellular folded plate structures which were simply supported at the two ends. In addition to the previous assumptions, each diaphragm was assumed to be perfectly flexible normal to its own plane. Joint redundants were essentially the same as those suggested by Pultar, but the plate distributed redundants were assumed to vary linearly between the longitudinal edges of the plate. Compatibility was enforced at the plate edges and at the one-third points only. Once again Fourier series were used to solve the elasticity equations for thin flat plates. This solution has been checked against experiments and calculations of other writers, and has been found to give excellent predictions of the true elastic behaviour of prismatic folded plate systems.

Just as a straight box beam may be considered as a series of rigidly connected folded plates, so a curved box beam may be considered as a series of rigidly connected folded shells. If the radius of curvature is constant, then the particular shells involved are segments of cylinders, flat plates, and cones. In the sections which follow, a rigorous solution is formulated for a continuous box beam which has a constant radius and a constant thin-walled cross section. The traditional combined stiffness and flexibility approach is clearly evident in the procedure, and all calculations are based on classical elasticity equations for thin shells.

Since shell calculations are necessarily complex, it is considered vital to provide independent checks on the developed solution. For this reason, the assumptions regarding the nature of the diaphragm redundants are directly analogous to those made by Scordelis and Lo[105]. By specifying a very large beam radius and a correspondingly small subtended span angle, a curved beam can be made to closely approximate a straight beam, and the folded shell results could then be directly compared with folded plate results.

For evaluating the stiffness coefficients of thin flat plates, Scordelis and Lo were able to use explicit mathematical formulae which had been previously derived by GOLDBERG and LEVE[106]. No such formulae are currently available for folded shell elements. However, in Section 3.3.1, a systematic unified

approach for finding the complete stiffness matrices of the three element types is presented. These calculations form the key to the folded shell solution, and the philosophy employed therein is strongly reflected throughout all other aspects of the computational procedure.

Calculations for cylindrical and conical shells are based on equation systems taken from particular references by FLÜGGE[107] and WILSON[108] respectively, whereas calculations for curved flat plates are based on the familiar equations for separate plate bending and membrane action[109,110].

For the sake of uniformity, chosen coordinate systems are always right handed.

3.2 Definition of a Folded Shell Structure

Consider a thin-walled beam circularly curved in plan. The beam subtends an angle α at the axis of rotation, and has a constant cross section consisting of a series of rigidly jointed straight elements made from homogeneous isotropic elastic material. The cross section may be open, closed, or a combination of both open and closed parts. Some examples of folded shell cross sections are given in Figure 3.1.

Figure 3.1 Examples of folded shell cross sections

At the two ends of the beam (taken as $\phi = 0$ and $\phi = \alpha$) there are externally supported thin diaphragms. They are infinitely rigid in their own plane, thereby maintaining the initial shape of the complete cross section, and are supported so that no rotation of the cross section can occur as a result of torsional reactions. In contrast, however, the end diaphragms are perfectly flexible normal to their own plane, and hence present zero resistance to warping displacements which occur at the beam ends. Rotations about the intersections between folded shell elements and end diaphragms are also free to take place. Under these conditions, the beam is considered to be 'simply supported' at its ends.

There may be additional diaphragms at various intermediate cross sections along the beam. Such diaphragms subtend 'small' angles $\delta\phi$ at the axis of rotation of the beam, and are termed 'internal' to distinguish them from those at the extreme ends. An internal diaphragm may be either of two types. An 'unmoveable' diaphragm is one which is supported externally in the same manner as an end diaphragm, whereas a 'moveable' diaphragm is supported by the beam itself. Each internal diaphragm is, like an end diaphragm, considered infinitely rigid in its own plane but perfectly flexible normal to its own plane. However, unlike an end diaphragm, an internal diaphragm need not be connected to every element of the beam cross section. A beam which has no internal diaphragms is defined as a 'primary' structure.

Certain preliminary assumptions must be made concerning the nature of the redundant forces which occur as a direct result of the interaction between a folded shell element and an internal diaphragm. In a real structure, the connection is continuous over the full width and thickness of the diaphragm, and the true force distribution is unknown. The following simplifying assumptions are made[104].

(a) All redundant forces are uniformly distributed across the diaphragm thickness

(b) Between the curved edges of the element, normal and in-plane distributed redundants exist which vary linearly in the lateral (transverse) direction

(c) Concentrated line load redundants exist at the curved edges of the element

Since the diaphragm is perfectly flexible normal to its own plane, no forces are transmitted in this direction.

Figure 3.2 shows the nature of the assumed diaphragm distributed redundants acting on any general folded shell element. (The redundants are termed 'distributed' to distinguish them from the 'concentrated' line loads which co-exist at the element curved edges). As indicated in the diagrams by dashed lines, each linearly distributed redundant may be considered as the sum of two triangularly distributed redundants. Provided that $\delta\phi$, the angle subtended by the diaphragm at the axis of rotation, is small,

IN-PLANE REDUNDANTS

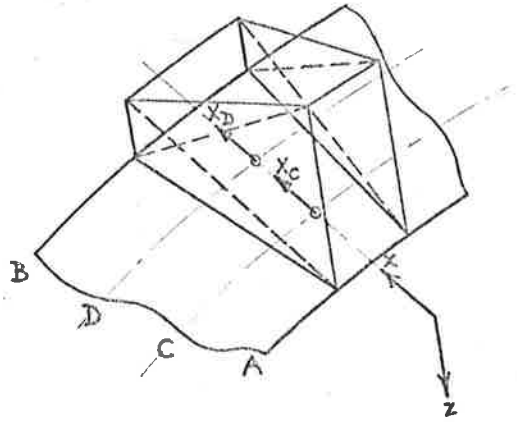

(a) General view

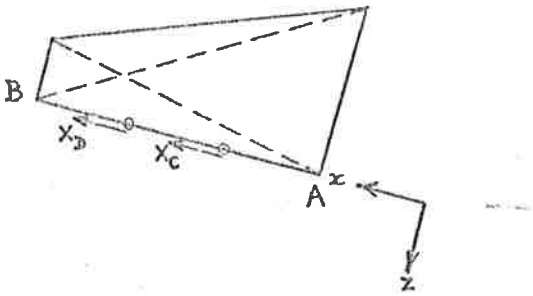

(b) Cross sectional view

NORMAL REDUNDANTS

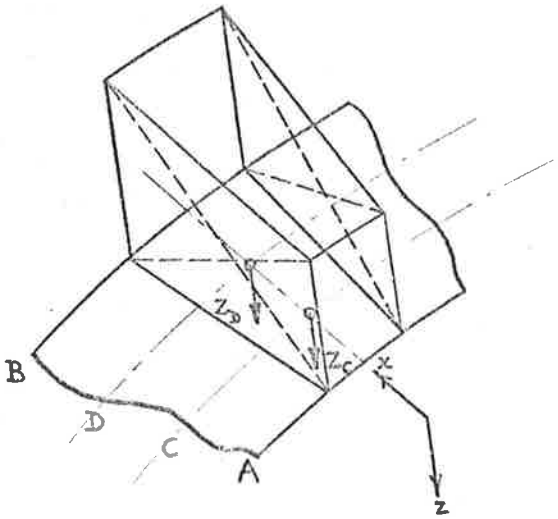

(a) General view

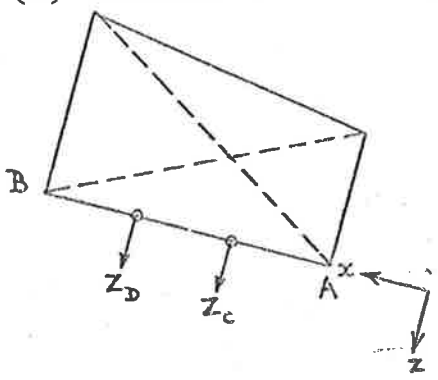

(b) Cross sectional view

Figure 3.2 Distributed redundants caused by diaphragm action

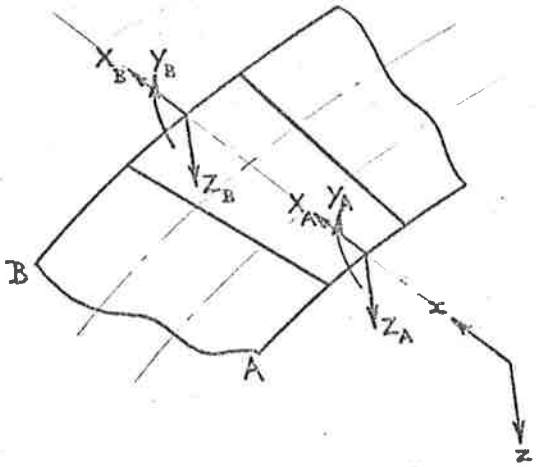

Figure 3.3 Concentrated edge redundants caused by diaphragm action

then the triangularly distributed redundants will have resultants which act at distances one-third of the element width from the curved edges A and B. The loci of points on the element which are one-third of the element width from each of the curved edges A and B are referred to as C and D respectively, and the resultants of the triangularly distributed redundants are accordingly denoted X_C, Z_C, X_D, Z_D. These four resultants act at the centre of the diaphragm thickness, and are expressed in a coordinate system which is member orientated ('member' coordinate system).

Figure 3.3 shows the nature of the assumed diaphragm concentrated redundants acting on any general folded shell element. At each curved edge A and B there are two line forces (one in-plane (lateral); one normal) and one line moment, all of which are uniformly distributed across the thickness of the diaphragm. The resultants of the uniformly distributed redundants are accordingly denoted X_A, Z_A, Y_A, X_B, Z_B, Y_B as shown in the diagram. These six resultants act at the centre of the diaphragm thickness, and are expressed in a coordinate system which is common to all of the folded shell elements ('global' coordinate system).

3.3 Analysis of Primary Structure

Element stiffness matrices, element fixed-edge solutions for externally applied distributed loads, and element transformation matrices are the three principal quantities associated with the stiffness solution of any folded shell primary structure. Consequently, detailed methods for their calculation are described

in the following first three sections. The method for calculating the element stiffness matrices is particularly important, since extensive use is made of the developed concepts throughout the whole of the folded shell analysis as presented in this thesis. A general description of the solution for a primary structure is given in Section 3.3.4.

3.3.1 Element stiffness matrices*

Introduction

The stiffness matrices of the following three folded shell elements are investigated in succession.

(a) a sector of a circular cylindrical shell bounded by two straight edges (generators) and by two circular edges in parallel planes;

(b) a sector of a flat circular plate bounded by two straight radial edges and by two concentric circular edges;

(c) a sector of a right conical shell bounded by two straight generators and by two circular edges in parallel planes.

Each element is assumed to be simply supported along its straight edges. 'Simple support' implies that displacements in the direction of the normal to the surface and displacements parallel to the support are prevented, whereas circumferential displacements (at right angles to the normal and to the edge) and rotations about

---

* The principal contents of this section have been published in a previous paper[111].

the edge are free to take place.

The stiffness matrices sought express the relationships between the stress resultants acting along the curved edges, and the corresponding curved edge displacement components. A sinusoidal variation with an integral number of half wavelengths within the sector is assumed circumferentially for the stress resultants and the displacement components. (Such a resolution of forces and displacements automatically satisfies the boundary conditions which exist at the straight edges of the element. Any other configuration compatible with the prescribed support conditions is easily handled by using Fourier expansions). Under these circumstances, the amplitude of the harmonic function describing the circumferential variation of a stress resultant or displacement component completely defines that quantity along each curved edge, and the amplitudes may be regarded as generalised forces and displacements. The stiffness coefficients obtained refer to the relationships between these amplitudes.

There are four degrees of freedom along each curved edge; three displacements and one rotation about the edge tangent. Thus the element as a whole has eight degrees of freedom, and the edge loading is completely described by eight stress resultants, consisting of three force resultants and one moment resultant acting along each of the two edges. The size of the stiffness matrix is therefore (8 × 8).

For all three types of element, the stiffness matrix is generated as the product of two (8 × 8)

matrices. The first matrix relates the edge displacement components to the eight integration constants which arise from the solution of the eighth order differential equation system describing the behaviour of the element. The second matrix relates the edge stress resultants to the same eight constants. In the particular case of the flat plate element, the theory implies no interaction between in-plane and out-of-plane forces and displacements, and hence the stiffness matrix contains 32 zero coefficients. Although it is therefore possible to analyse the flat plate as two separate fourth order problems, for the sake of uniformity, the eighth order system is maintained.

Following the accepted practice for thin shells, edge force resultants are expressed in (force/length) units, and edge moment resultants are expressed in (force × length/length) units.

Cylindrical Shell Element Stiffness Matrix

The middle surface of a cylindrical thin shell element is shown in Figure 3.4. Positive directions of the coordinates and the corresponding displacements are shown, together with geometric information necessary to define the element. One of the curved edges ($x = 0$) is labelled A, and the other ($x = L$) is labelled B. The curved edge stress resultants required in the stiffness matrix are N, T, S, M and they are subscripted with either A or B, depending on which edge is being referenced. T and S are the effective (Kirchoff) edge shear stress resultants.

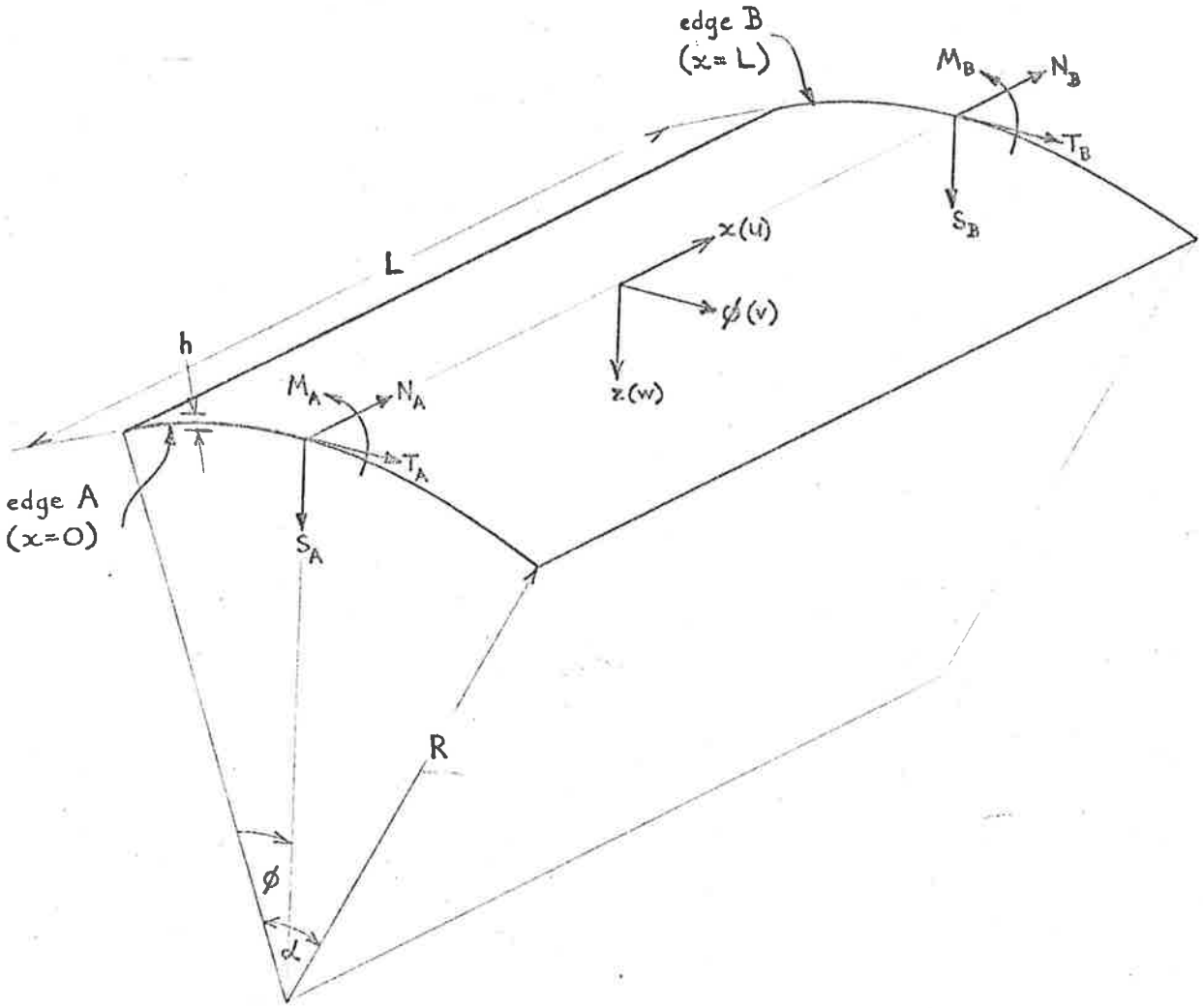

Figure 3.4 Middle surface of cylindrical shell element

In order to calculate stiffness coefficients, all terms which describe the influence of externally applied distributed surface loads must be omitted from the governing equilibrium equations. Thus the three partial differential equations describing equilibrium of the shell element become[107]

$$R^2u''+\frac{1-\nu}{2}u\ddot{}+R\left(\frac{1+\nu}{2}\right)v'\dot{}-\nu Rw'+k\left(\frac{1-\nu}{2}u\ddot{}+R^3w'''-\frac{1-\nu}{2}Rw'\ddot{}\right)=0 \qquad \ldots (1a)$$

$$\frac{1+\nu}{2}Ru'\dot{}+v\ddot{}+\frac{1-\nu}{2}R^2v''-w\dot{}+k\left(\frac{3}{2}(1-\nu)R^2v''+\frac{3-\nu}{2}R^2w''\dot{}\right)=0 \qquad \ldots (1b)$$

$$\nu Ru'+v\dot{}-w+k\left(\frac{1-\nu}{2}Ru'\ddot{}-R^3u'''-\frac{3-\nu}{2}R^2v''\dot{}-R^4w''''\right.$$

$$\left.-2R^2w''\ddot{}-w''''-2w\ddot{}-w\right)=0 \qquad \ldots (1c)$$

where $k=\dfrac{h^2}{12R^2}$, $(\ )'=\dfrac{\partial(\ )}{\partial x}$, and $(\ )\dot{}=\dfrac{\partial(\ )}{\partial\phi}$

Since the displacement components vary sinusoidally in the circumferential direction, the following equations may be written

$$u = u(x)\sin\beta\phi \qquad \ldots (2a)$$

$$v = v(x)\cos\beta\phi \qquad \ldots (2b)$$

$$w = w(x)\sin\beta\phi \qquad \ldots (2c)$$

where $\beta=\dfrac{m\Pi}{\alpha}$, and m is a positive integer.

Expressions (2a-c) satisfy the desired boundary conditions along the straight edges. At this stage u(x), v(x), w(x) are unknown

functions to be determined in such a way that equations (1a-c) are satisfied. When expressions (2a-c) are substituted into equations (1a-c), a symmetric homogeneous system of three simultaneous differential equations in u(x), v(x), w(x) results.

$$-[R^2D^2-\frac{1-\nu}{2}\beta^2(1+k)]u(x)+[\frac{1+\nu}{2}R\beta D]v(x)+[\nu RD-k(R^3D^3+\frac{1-\nu}{2}R\beta^2D)]w(x)=0 \quad \ldots (3a)$$

$$[\frac{1+\nu}{2}R\beta D]u(x)+[-\beta^2+\frac{1-\nu}{2}R^2(1+3k)D^2]v(x)+[-\beta+\frac{3-\nu}{2}kR^2\beta D^2]w(x)=0 \quad \ldots (3b)$$

$$[\nu RD-k(R^3D^3+\frac{1-\nu}{2}R\beta^2D)]u(x)+[-\beta+\frac{3-\nu}{2}kR^2\beta D^2]v(x)$$
$$+[-1-k(R^4D^4-2R^2\beta^2D^2+(\beta^2-1)^2)]w(x)=0 \quad \ldots (3c)$$

where $D = \frac{d}{dx}$. These equations are abbreviated in the following way.

$$-[R^2D^2-K_1]u(x)-[K_2RD]v(x)-RD[K_3R^2D^2+K_4]w(x)=0 \quad \ldots (4a)$$

$$-[K_2RD]u(x)+[K_5R^2D^2+K_6]v(x)+[K_7R^2D^2+K_8]w(x)=0 \quad \ldots (4b)$$

$$-RD[K_3R^2D^2+K_4]u(x)+[K_7R^2D^2+K_8]v(x)+[K_9R^4D^4+K_{10}R^2D^2+K_{11}]w(x)=0 \quad \ldots (4c)$$

where $K_1 = \frac{1-\nu}{2} \beta^2(1+k)$

$K_2 = - \frac{1+\nu}{2} \beta$

$K_3 = k$

$K_4 = - \nu + \frac{1-\nu}{2} \beta^2 k$

$K_5 = \frac{1-\nu}{2} (1+3k)$

$K_6 = - \beta^2$

$K_7 = \frac{3-\nu}{2} \beta k$

$K_8 = - \beta$

$K_9 = -k$

$K_{10} = 2\beta^2 k$

$K_{11} = - 1 - (\beta^2-1)^2 k$

A simple but tedious procedure can be used to systematically eliminate any two of the functions u(x), v(x), w(x) from this equation system, thereby obtaining a single eighth order differential equation with constant coefficients for the remaining

function. The exact form of this equation will depend on any approximations introduced prior to and during the elimination process. (HOUGHTON and JOHNS[112] list eleven slightly different forms of the characteristic equations which correspond to the eleven eighth order differential equations derived by various authors). It is emphasized here that any approximation made whilst manipulating the basic equations may destroy the symmetry of the desired stiffness matrix. Therefore, in this work, having decided on the form of the original equilibrium equations[107] and of the stress resultant expressions[App.B], no approximations are made in the manipulations described. The following characteristic equation is derived. To facilitate comparison with equations of other authors[112], the equation is written in its complete form.

$$\lambda^8+\frac{2}{(1+3k)(k-1)}\left[\{\beta^2[\tfrac{9}{4}(1-\nu)k^2+\tfrac{1}{4}(11-3\nu)k+2]-\nu(1+3k)\}\frac{\lambda^6}{R^2}\right.$$

$$+\{\beta^4[\frac{\nu^2k^2}{2}+\frac{3}{2}(\nu-2)k-3]+3\beta^2[\frac{(\nu^2-\nu+2)}{2}k+1]+\frac{(\nu^2-1-k)(1+3k)}{2k}\}\frac{\lambda^4}{R^4}$$

$$+\beta^2\{\beta^4[\tfrac{3}{4}(1-\nu)k^2+\tfrac{1}{4}(7-3\nu)k+2]+\beta^2[-\tfrac{3}{2}(1-\nu)k^2+\tfrac{1}{2}(5\nu-7)k+\nu-4]$$

$$\left.+[\tfrac{3}{4}(1-\nu)k^2+\tfrac{7}{4}(1-\nu)k+2-\nu]\}\frac{\lambda^2}{R^6}-\frac{\beta^4(\beta^2-1)^2(1+k)}{2R^8}\right]=0 \qquad \ldots (5)$$

Equation (5) does eventually lead to a symmetrical stiffness matrix. The eight roots (complex) of this equation are denoted

$\lambda_i (i = 1,2,\ldots 8)$ and the solution of equation system (1a-c) is therefore

$$u(x) = \sum_{i=1}^{8} A_i e^{\lambda_i x}; \quad v(x) = \sum_{i=1}^{8} B_i e^{\lambda_i x}; \quad w(x) = \sum_{i=1}^{8} C_i e^{\lambda_i x} \qquad \ldots (6a\text{-}c)$$

where A_i, B_i, C_i are complex constants governed by the curved edge boundary conditions. However, since there are only eight such conditions, it follows that only eight of these constants can be independent. Substitution of expressions (6a-c) into equations (4a-c) gives the complex matrix equation (7).

$$\begin{bmatrix} -[R^2\lambda_i^2 - K_1] & -[K_2 R\lambda_i] & -[K_3 R^3\lambda_i^3 + K_4 R\lambda_i] \\ -[K_2 R\lambda_i] & +[K_5 R^2\lambda_i^2 + K_6] & +[K_7 R^2\lambda_i^2 + K_8] \\ -[K_3 R^3\lambda_i^3 + K_4 R\lambda_i] & +[K_7 R^2\lambda_i^2 + K_8] & +[K_9 R^4\lambda_i^4 + K_{10} R^2\lambda_i^2 + K_{11}] \end{bmatrix} \cdot \begin{bmatrix} A_i \\ B_i \\ C_i \end{bmatrix} = 0$$

$$\ldots (7)$$

Since equation (5) is identical to the one found by setting the determinant of the (3 × 3) matrix in equation (7) equal to zero, the homogeneous equation system (7) has non-trivial solutions. The ratios A_i/C_i and B_i/C_i can therefore be calculated. Hence

$$\eta_i = A_i/C_i$$

$$= - \frac{[K_3K_5R^5\lambda_i^5+(K_4K_5+K_6K_3-K_7K_2)R^3\lambda_i^3+(K_4K_6-K_8K_2)R\lambda_i]}{[K_5R^4\lambda_i^4+(K_6-K_1K_5+K_2^2)R^2\lambda_i^2-K_1K_6]} \quad \ldots (8a)$$

$$\chi_i = B_i/C_i$$

$$= - \frac{[(K_2K_3+K_7)R^4\lambda_i^4+(K_2K_4-K_1K_7+K_8)R^2\lambda_i^2-K_1K_8]}{[K_5R^4\lambda_i^4+(K_6-K_1K_5+K_2^2)R^2\lambda_i^2-K_1K_6]} \quad \ldots (8b)$$

The displacement component expressions (6a-c) can be rewritten to incorporate the quantities η_i and χ_i.

$$u(x) = \sum_{i=1}^{8} \eta_i e^{\lambda_i x} . C_i; \quad v(x) = \sum_{i=1}^{8} \chi_i e^{\lambda_i x} . C_i; \quad w(x) = \sum_{i=1}^{8} e^{\lambda_i x} . C_i$$

...(9a-c)

An expression is also needed for edge rotations. Hence

$$- \frac{dw(x)}{dx} = - \sum_{i=1}^{8} \lambda_i e^{\lambda_i x} . C_i \quad \ldots (9d)$$

where the minus sign is necessary to make the curved edge rotations comply with the positive direction of the edge moment stress

resultants defined in Figure 3.4.

The stress resultants corresponding to the above four displacement components can also be expressed in terms of the quantities η_i and χ_i. After direct application of equations (2a-c) and (9a-c) to the general expressions[107,App.B], these resultants are

$$N = N(x)\sin\beta\phi$$

$$= \frac{Eh}{R(1-\nu^2)} \{\sum_{i=1}^{8} [R\eta_i\lambda_i - \nu\beta\chi_i - \nu + \frac{h^2}{12}\lambda_i^2] e^{\lambda_i x}.C_i\}\sin\beta\phi \qquad \ldots (10a)$$

$$T = T(x)\cos\beta\phi$$

$$= \frac{Eh}{2R(1+\nu)} \{\sum_{i=1}^{8} [\beta\eta_i + R\lambda_i\chi_i + \frac{h^2}{4R}(\lambda_i\chi_i + \beta\lambda_i)] e^{\lambda_i x}.C_i\}\cos\beta\phi \qquad \ldots (10b)$$

$$S = S(x)\sin\beta\phi$$

$$= -\frac{Eh^3}{12R^2(1-\nu^2)} \{\sum_{i=1}^{8} [R^2\lambda_i^3 - \nu\beta^2\lambda_i - \nu\beta\lambda_i\chi_i + R\lambda_i^2\eta_i$$

$$+ (1-\nu)(-2\beta^2\lambda_i + \frac{\beta^2\eta_i}{2R} - \frac{3}{2}\beta\lambda_i\chi_i)] e^{\lambda_i x}.C_i\}\sin\beta\phi \qquad \ldots (10c)$$

$$M = M(x)\sin\beta\phi$$

$$= -\frac{Eh^3}{12R^2(1-\nu^2)}\{\sum_{i=1}^{8}[R^2\lambda_i^2-\nu\beta^2+R\lambda_i\eta_i-\nu\beta\chi_i]e^{\lambda_i x}.C_i\}\sin\beta\phi \quad ...(10d)$$

Expressions (9a-d) and (10a-d) hold for all values of x in the range $0 \leq x \leq L$. However, for the specific purpose of calculating stiffness coefficients, only the extreme values x = 0 and x = L need be considered. In order to comply with the positive directions defined in Figure 3.4, the stress resultant expressions (10a-d) must be reversed in sign when evaluated at x = 0.

By using convenient matrix notation, expressions for the amplitudes of the required displacement components and corresponding stress resultants at the edges A and B may be written as follows.

$$\begin{bmatrix} u_A \\ v_A \\ w_A \\ \left(-\frac{dw}{dx}\right)_A \\ u_B \\ v_B \\ w_B \\ \left(-\frac{dw}{dx}\right)_B \end{bmatrix} = \begin{bmatrix} u_{1A} & u_{2A} & u_{3A} & u_{4A} & u_{5A} & u_{6A} & u_{7A} & u_{8A} \\ v_{1A} & & & & & & & \cdot \\ w_{1A} & & & & & & & \cdot \\ \left(-\frac{dw}{dx}\right)_{1A} & & & & & & & \cdot \\ u_{1B} & & & & & & & \cdot \\ v_{1B} & & & & & & & \cdot \\ w_{1B} & & & & & & & \cdot \\ \left(-\frac{dw}{dx}\right)_{1B} & \cdot & \cdot & \cdot & \cdot & \cdot & \cdot & \left(-\frac{dw}{dx}\right)_{8B} \end{bmatrix} \cdot \begin{bmatrix} C_1 \\ C_2 \\ C_3 \\ C_4 \\ C_5 \\ C_6 \\ C_7 \\ C_8 \end{bmatrix} \quad \ldots(11)$$

$$\begin{bmatrix} N_A \\ T_A \\ S_A \\ M_A \\ N_B \\ T_B \\ S_B \\ M_B \end{bmatrix} = \begin{bmatrix} N_{1A} & N_{2A} & N_{3A} & N_{4A} & N_{5A} & N_{6A} & N_{7A} & N_{8A} \\ T_{1A} & & & & & & & \cdot \\ S_{1A} & & & & & & & \cdot \\ M_{1A} & & & & & & & \cdot \\ N_{1B} & & & & & & & \cdot \\ T_{1B} & & & & & & & \cdot \\ S_{1B} & & & & & & & \cdot \\ M_{1B} & \cdot & \cdot & \cdot & \cdot & \cdot & \cdot & M_{8B} \end{bmatrix} \cdot \begin{bmatrix} C_1 \\ C_2 \\ C_3 \\ C_4 \\ C_5 \\ C_6 \\ C_7 \\ C_8 \end{bmatrix} \quad \ldots(12)$$

Each of the elements in the square matrices of equations (11) and (12) is found from one of the expressions (9a-d) or (10a-d). For example,

u_{1A} = (coefficient of C_1 in expression for u(x) at x = 0)

= η_1

$(-\frac{dw}{dx})_{7B}$ = (coefficient of C_7 in expression for $-\frac{dw(x)}{dx}$ at x = L)

= $-\lambda_7 e^{\lambda_7 L}$

T_{2A} = (coefficient of C_2 in expression for T(x) at x = 0)

= $\frac{Eh}{2R(1+\nu)} [\beta\eta_2+R\lambda_2\chi_2+\frac{h^2}{4R} (\lambda_2\chi_2+\beta\lambda_2)]$

M_{8B} = (coefficient of C_8 in expression for M(x) at x = L)

= $- \frac{Eh^3}{12R^2(1-\nu^2)} [R^2\lambda_8^2-\nu\beta^2+R\lambda_8\eta_8-\nu\beta\chi_8] e^{\lambda_8 L}$

In symbolic form, equations (11) and (12) are

$$\delta_M = G.C \qquad \ldots (13a)$$

and

$$p_M = H.C \qquad \ldots (13b)$$

where the subscript M indicates reference to the member coordinate system. δ_M is the column matrix of the edge displacement components $\{u_A \ldots (-\frac{dw}{dx})_B\}$, p_M is the column matrix of the

corresponding edge stress resultants $\{N_A \ldots M_B\}$, G and H are square matrices, and C is the column matrix of the constants $\{C_1 \ldots C_8\}$. Equations (13a) and (13b) may be combined to give

$$p_M = H.G^{-1}.\delta_M \qquad \ldots (14)$$

or, from the definition of a stiffness matrix,

$$k_M = H.G^{-1} \qquad \ldots (15)$$

Computer Calculations:

From the physical and geometrical properties of the cylindrical shell, the coefficients which appear in the characteristic equation (5) can be evaluated. A standard library subroutine is then used to calculate the eight complex roots. (The method employed is an iteration based on a combination of Newton's and Bairstow's procedures). By using the expressions given, matrices G and H are then assembled, and the product $k_M = H.G^{-1}$ is calculated.

Some checks which may be applied to the stiffness matrix in any particular case are

(a) All elements are real

(b) The main diagonal elements are positive

(c) The first four and the second four main diagonal elements are identical

(d) The matrix is symmetrical

Flat Plate Element Stiffness Matrix

The middle surface of a thin flat plate element is shown in Figure 3.5. Positive directions of the coordinates and the corresponding displacements are shown, together with the geometric information necessary to define the element. The inner curved edge ($x = R_1$) is labelled A, and the outer curved edge ($x = R_2$) is labelled B. All required curved edge stress resultants N, T, S, M are subscripted accordingly. The plate is simply supported along the straight (radial) edges, and it is assumed that there are no externally applied distributed surface loads. Curved edge stress resultants (and hence all displacement components) are assumed to vary sinusoidally in the circumferential direction.

The governing equilibrium equations in terms of u, v, w may be expressed as follows[109,110].

$$\frac{Eh}{1-\nu^2}\left[u''+\nu\left(-\frac{u}{x^2}+\frac{u'}{x}+\frac{v''}{x}-\frac{v}{x^2}\right)\right]+\frac{Eh}{x(1+\nu)}\left(u'-\frac{u}{x}-\frac{v}{x}\right)$$

$$+\frac{Eh}{2x(1+\nu)}\left(\frac{u}{x}+v''-\frac{v}{x}\right)=0 \qquad \ldots(16a)$$

$$\frac{Eh}{x(1-\nu^2)}\left(\frac{u}{x}+\frac{v}{x}+\nu u''\right)+\frac{Eh}{2(1+\nu)}\left(\frac{u''}{x}-\frac{u}{x^2}+v''+\frac{v}{x^2}-\frac{v'}{x}\right)$$

$$+\frac{Eh}{x(1+\nu)}\left(\frac{u}{x}+v'-\frac{v}{x}\right)=0 \qquad \ldots(16b)$$

$$\nabla^2(\nabla^2(w))=0 \qquad \ldots(16c)$$

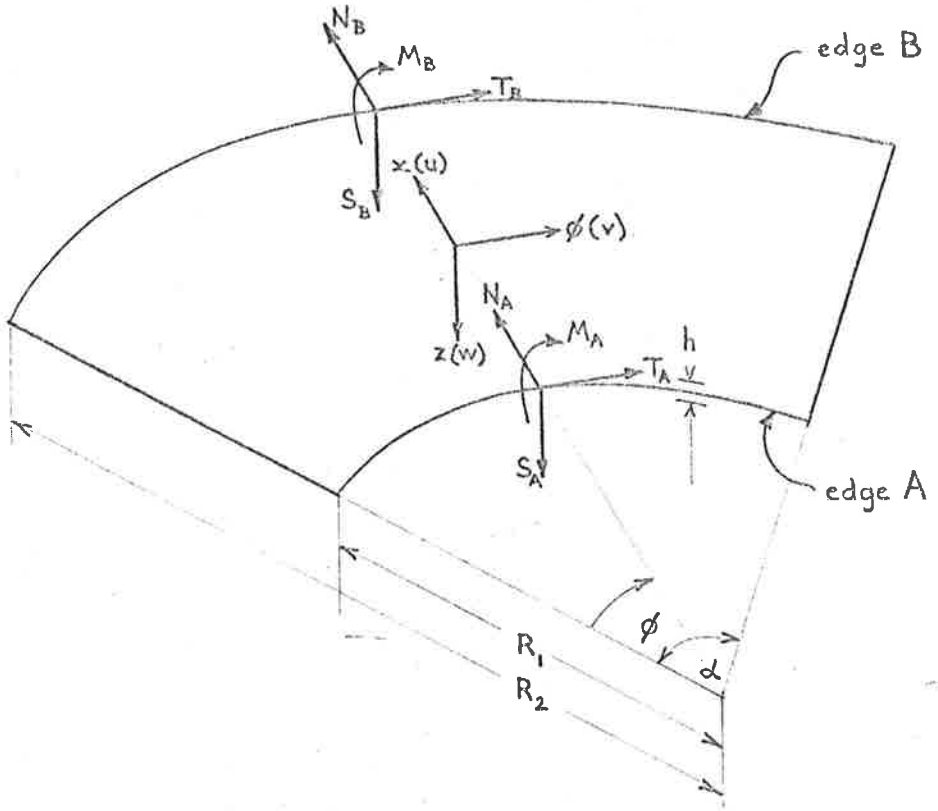

Figure 3.5 Middle surface of flat plate element

where $(\ )' = \frac{\partial(\ )}{\partial x}$, $(\ )^{\cdot} = \frac{\partial(\ )}{\partial \phi}$, and $\nabla^2(\ ) = (\ )'' + \frac{(\ )'}{x} + \frac{(\ )^{\cdot\cdot}}{x^2}$

Equations (16a) and (16b) govern the membrane action of the plate and are completely decoupled from equation (16c) which governs the normal bending action of the plate.

Expressions (2a-c) may be substituted into equations (16a-c), and the following equation system results.

$$[D^2+\frac{1}{x}D-\frac{1}{x^2}(1+\frac{1-\nu}{2}\beta^2)]u(x)+[-\frac{\beta}{2x}(1+\nu)D+\frac{\beta}{2x^2}(3-\nu)]v(x)=0 \quad \ldots (17a)$$

$$[\frac{\beta}{2x}(1+\nu)D+\frac{\beta}{2x^2}(3-\nu)]u(x)+[\frac{1-\nu}{2}D^2+\frac{1-\nu}{2x}D-\frac{1}{x^2}(\beta^2+\frac{1-\nu}{2})]v(x)=0 \quad \ldots (17b)$$

$$[D^4+\frac{2}{x}D^3-\frac{1}{x^2}(1+2\beta^2)D^2+\frac{1}{x^3}(1+2\beta^2)D+\frac{1}{x^4}(\beta^4-4\beta^2)]w(x)=0 \quad \ldots (17c)$$

where $D = \frac{d}{dx}$

These equations can be reduced to linear differential equations with constant coefficients by using the transformation $x = x_o e^r$. Hence

$$[D_r^2-(1+\frac{1-\nu}{2}\beta^2)]u(x)+[-\frac{\beta}{2}(1+\nu)D_r+\frac{\beta}{2}(3-\nu)]v(x)=0 \quad \ldots (18a)$$

$$[\frac{\beta}{2}(1+\nu)D_r+\frac{\beta}{2}(3-\nu)]u(x)+[\frac{1-\nu}{2}D_r^2-(\beta^2+\frac{1-\nu}{2})]v(x)=0 \quad \ldots (18b)$$

$$[D_r^4-4D_r^3+2(2-\beta^2)D_r^2+4\beta^2D_r+\beta^2(\beta^2-4)]w(x)=0 \quad \ldots (18c)$$

where $D_r = \frac{d}{dr}$

If either of the functions u(x), v(x) is systematically eliminated from the membrane equations (18a) and (18b), a single fourth order differential equation is obtained for the remaining function. The characteristic equation corresponding to membrane action thus becomes

$$\lambda_m^4 - 2(1+\beta^2)\lambda_m^2 + (\beta^2-1)^2 = 0 \qquad \ldots (19)$$

where the subscript m refers to membrane action. The characteristic equation corresponding to bending action follows directly from equation (18c).

$$\lambda_b^4 - 4\lambda_b^3 + 2(2-\beta^2)\lambda_b^2 + 4\beta^2\lambda_b + \beta^2(\beta^2-4)=0 \qquad \ldots (20)$$

where the subscript b refers to bending action. The roots (all real) of the two characteristic equations are

$$\lambda_{m_1} = -(1-\beta) \qquad \lambda_{b_1} = +\beta$$

$$\lambda_{m_2} = +(1-\beta) \qquad \lambda_{b_2} = -\beta$$

$$\lambda_{m_3} = -(1+\beta) \qquad \lambda_{b_3} = +\beta+2$$

$$\lambda_{m_4} = +(1+\beta) \qquad \lambda_{b_4} = -\beta+2$$

Thus the solution of the plate differential equations may be written

$$u(x) = \sum_{i=1}^{4} A_i (x_o e^r)^{\lambda_{m_i}} = \sum_{i=1}^{4} A_i x^{\lambda_{m_i}} \qquad \ldots (21a)$$

$$v(x) = \sum_{i=1}^{4} B_i (x_o e^r)^{\lambda_{m_i}} = \sum_{i=1}^{4} B_i x^{\lambda_{m_i}} \qquad \ldots (21b)$$

$$w(x) = \sum_{i=1}^{4} C_i (x_o e^r)^{\lambda_{b_i}} = \sum_{i=1}^{4} C_i x^{\lambda_{b_i}} \qquad \ldots (21c)$$

and $$- \frac{dw(x)}{dx} = - \sum_{i=1}^{4} C_i \lambda_{b_i} x^{\lambda_{b_i} - 1} \qquad \ldots (21d)$$

where the minus sign is necessary to make the curved edge rotations comply with the positive directions of the edge moment stress resultants defined in Figure 3.5.

From equations (18a) and (18b), the ratios B_i/A_i can be found in the same way as for the cylindrical shell.

$$\xi_i = B_i/A_i = \frac{-[\lambda_{m_i}^2 - (1+\frac{1-\nu}{2}\beta^2)]}{[-\frac{\beta}{2}(1+\nu)\lambda_{m_i} + \frac{\beta}{2}(3-\nu)]} \qquad \ldots (22)$$

(The constants A_i and B_i are completely independent of the bending constants C_i). Displacement component expressions

(21a-d) can now be written to incorporate the quantities ξ_i.

$$u(x) = \sum_{i=1}^{4} x^{\lambda_{m_i}}.A_i \qquad \ldots (23a)$$

$$v(x) = \sum_{i=1}^{4} \xi_i x^{\lambda_{m_i}}.A_i \qquad \ldots (23b)$$

$$w(x) = \sum_{i=1}^{4} x^{\lambda_{b_i}}.C_i \qquad \ldots (23c)$$

$$-\frac{dw(x)}{dx} = -\sum_{i=1}^{4} \lambda_{b_i} x^{\lambda_{b_i}-1}.C_i \qquad \ldots (23d)$$

The stress resultants which correspond to the above four displacement components can also be expressed using the quantities ξ_i. After direct application of equations (2a-c) and (23a-d) to the general expressions[109,110,App.B], these resultants become

$$N = N(x)\ \sin\beta\phi$$

$$= \frac{Eh}{1-\nu^2}\{\sum_{i=1}^{4}[\lambda_{m_i}+\nu(1-\beta\xi_i)]x^{\lambda_{m_i}-1}.A_i\}\sin\beta\phi \qquad \ldots (24a)$$

$$T = T(x)\ \cos\beta\phi$$

$$= \frac{Eh}{2(1+\nu)}\{\sum_{i=1}^{4}[\beta+\xi_i\lambda_{m_i}-\xi_i]x^{\lambda_{m_i}-1}.A_i\}\cos\beta\phi \qquad \ldots (24b)$$

$$S = S(x)\ \sin\beta\phi$$

$$= -\frac{Eh^3}{12(1-\nu^2)}\{\sum_{i=1}^{4}[\lambda_{b_i}^3-2\lambda_{b_i}^2+\lambda_{b_i}-\lambda_{b_i}(1+\beta^2)+2\beta^2 - (1-\nu)\beta^2(\lambda_{b_i}-1)]x^{\lambda_{b_i}-3}.C_i\}\sin\beta\phi \quad \ldots (24c)$$

$$M = M(x)\ \sin\beta\phi$$

$$= -\frac{Eh^3}{12(1-\nu^2)}\{\sum_{i=1}^{4}[\lambda_{b_i}(\lambda_{b_i}-1)+\nu(\lambda_{b_i}-\beta^2)]x^{\lambda_{b_i}-2}.C_i\}\sin\beta\phi \quad \ldots (24d)$$

As is the case with the cylindrical shell, for the purpose of finding stiffness coefficients, expressions for the stress resultants must be reversed in sign when evaluated at edge A.

Matrix notation is again used to write expressions for the amplitudes of the required displacement components and corresponding stress resultants at the curved edges A and B.

$$\begin{bmatrix} u_A \\ v_A \\ w_A \\ \left(-\frac{dw}{dx}\right)_A \\ u_B \\ v_B \\ w_B \\ \left(-\frac{dw}{dx}\right)_B \end{bmatrix} = \begin{bmatrix} u_{1A} & u_{2A} & 0 & 0 & u_{3A} & u_{4A} & 0 & 0 \\ v_{1A} & v_{2A} & 0 & 0 & v_{3A} & v_{4A} & 0 & 0 \\ 0 & 0 & w_{1A} & w_{2A} & 0 & 0 & w_{3A} & w_{4A} \\ 0 & 0 & \left(-\frac{dw}{dx}\right)_{1A} & \left(-\frac{dw}{dx}\right)_{2A} & 0 & 0 & \left(-\frac{dw}{dx}\right)_{3A} & \left(-\frac{dw}{dx}\right)_{4A} \\ u_{1B} & u_{2B} & 0 & 0 & u_{3B} & u_{4B} & 0 & 0 \\ v_{1B} & v_{2B} & 0 & 0 & v_{3B} & v_{4B} & 0 & 0 \\ 0 & 0 & w_{1B} & w_{2B} & 0 & 0 & w_{3B} & w_{4B} \\ 0 & 0 & \left(-\frac{dw}{dx}\right)_{1B} & \left(-\frac{dw}{dx}\right)_{2B} & 0 & 0 & \left(-\frac{dw}{dx}\right)_{3B} & \left(-\frac{dw}{dx}\right)_{4B} \end{bmatrix} \cdot \begin{bmatrix} A_1 \\ A_2 \\ C_1 \\ C_2 \\ A_3 \\ A_4 \\ C_3 \\ C_4 \end{bmatrix}$$

... (25)

$$\begin{bmatrix} N_A \\ T_A \\ S_A \\ M_A \\ N_B \\ T_B \\ S_B \\ M_B \end{bmatrix} = \begin{bmatrix} N_{1A} & N_{2A} & 0 & 0 & N_{3A} & N_{4A} & 0 & 0 \\ T_{1A} & T_{2A} & 0 & 0 & T_{3A} & T_{4A} & 0 & 0 \\ 0 & 0 & S_{1A} & S_{2A} & 0 & 0 & S_{3A} & S_{4A} \\ 0 & 0 & M_{1A} & M_{2A} & 0 & 0 & M_{3A} & M_{4A} \\ N_{1B} & N_{2B} & 0 & 0 & N_{3B} & N_{4B} & 0 & 0 \\ T_{1B} & T_{2B} & 0 & 0 & T_{3B} & T_{4B} & 0 & 0 \\ 0 & 0 & S_{1B} & S_{2B} & 0 & 0 & S_{3B} & S_{4B} \\ 0 & 0 & M_{1B} & M_{2B} & 0 & 0 & M_{3B} & M_{4B} \end{bmatrix} \cdot \begin{bmatrix} A_1 \\ A_2 \\ C_1 \\ C_2 \\ A_3 \\ A_4 \\ C_3 \\ C_4 \end{bmatrix}$$

... (26)

Each of the elements in the square matrices of equations (25) and (26) is found from one of the expressions (23a-d) or (24a-d). For example,

u_{1A} = (coefficient of A_1 in expression for u(x) at $x = R_1$)

$(-\frac{dw}{dx})_{3B}$ = (coefficient of C_3 in expression for $-\frac{dw(x)}{dx}$ at $x = R_2$)

T_{2A} = (coefficient of A_2 in expression for T(x) at $x = R_1$)

M_{4B} = (coefficient of C_4 in expression for M(x) at $x = R_2$)

Equations (25) and (26) can be written in the same symbolic form as equations (13a) and (13b) for the cylindrical shell element. Hence, again $k_M = H.G^{-1}$.

Computer Calculations:

Since the roots of the two characteristic equations are known, the flat plate stiffness matrix calculations are considerably faster than those for the cylindrical shell. The matrix is not symmetrical since the curved edges A and B are of different lengths. (The calculations may be checked by premultiplying k_M by the diagonal matrix $\lceil R_1 R_1 R_1 R_1 R_2 R_2 R_2 R_2 \rfloor$. The matrix thus obtained should be symmetrical).

Conical Shell Element Stiffness Matrix

The middle surface of a thin conical shell element is shown in Figure 3.6. Positive directions of

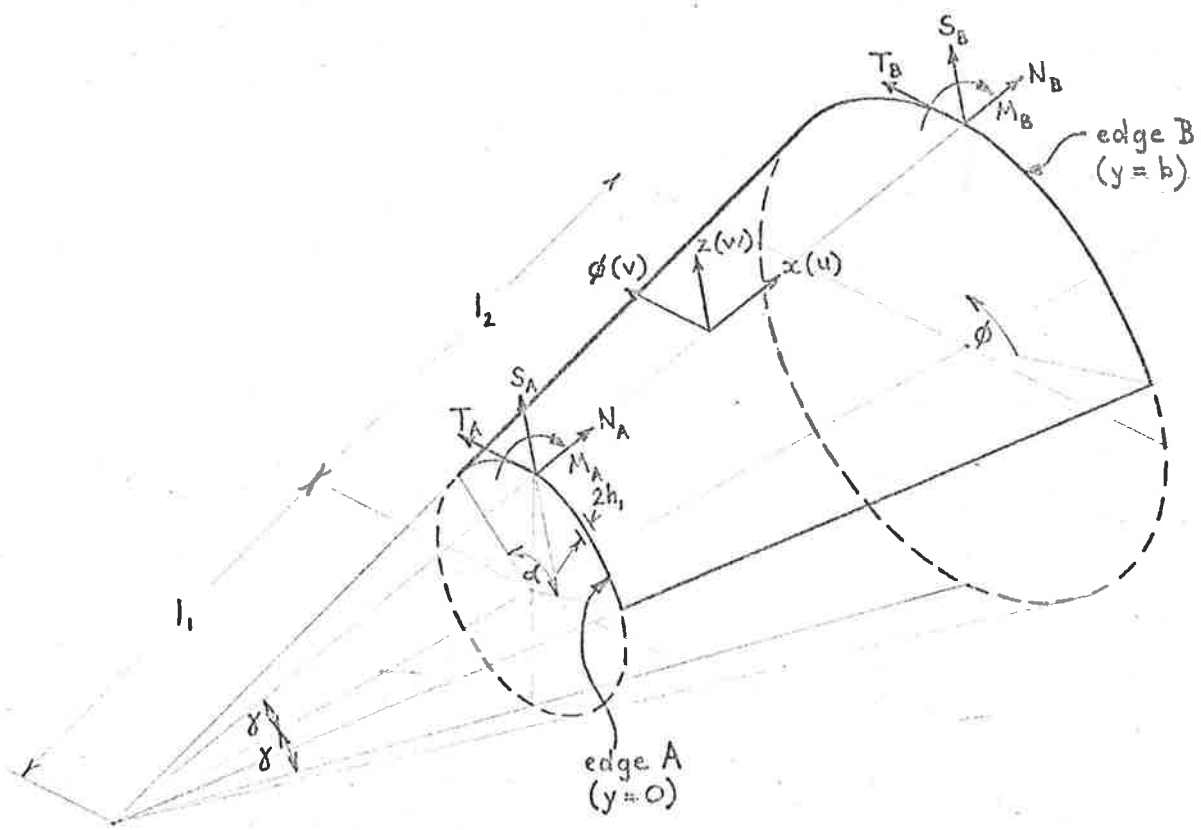

Figure 3.6 Middle surface of conical shell element

the coordinates and the corresponding displacement components are shown; the positive z-direction is the outward normal to the shell surface. The shell is simply supported along its straight edges, and all surface loads are taken to be zero. Once again, the curved edge stress resultants (and hence all displacement components) are assumed to vary sinusoidally in the circumferential direction. With reference to Figure 3.6, the following quantities are defined.

$$F = \frac{2Eh_1^3}{3(1-\nu^2)} \qquad t = \tan\gamma \qquad s = \sin\gamma$$

$$a = \frac{\ell_1}{h_1} \qquad b = \frac{\ell_2}{\ell_1} \qquad y = \frac{x}{ah_1} - 1$$

where $a >> 1$. The amplitudes of all stress resultants and displacement components are to be expressed in terms of the dimensionless variable y.

Displacements u, v, w may be written

$$u = h_1 u(y)\sin\beta\phi \qquad \ldots (27a)$$

$$v = ph_1 v(y)\cos\beta\phi \qquad \ldots (27b)$$

$$w = h_1 w(y)\sin\beta\phi \qquad \ldots (27c)$$

where $\beta = \frac{m\Pi}{\alpha}$, and $p = \frac{\beta}{s}$. Solutions of the governing differential equation system[108] are sought in the form

$$u(y) = \sum_{n=o}^{\infty} \alpha_n y^n \; ; \quad v(y) = \sum_{n=o}^{\infty} \beta_n y^n \; ; \quad w(y) = \sum_{n=o}^{\infty} \gamma_n y^n \qquad \ldots (28a\text{-}c)$$

which converge provided $|y| < 1$ [108]. Recurrence formulae have been derived by Wilson for calculating the coefficients in these series, but for the sake of brevity they are not reproduced here in precise detail. Equations (29a-c) represent them in an abbreviated form.

$$\alpha_{n+2} = f_1(\alpha_{n+1},\alpha_n,\beta_{n+1},\beta_n,\gamma_{n+1},\gamma_n) \quad \ldots (29a)$$

$$\beta_{n+2} = f_2(\alpha_{n+1},\alpha_n,\alpha_{n-1},\alpha_{n-2},\beta_{n+1},\beta_n,\beta_{n-1},\beta_{n-2},$$
$$\gamma_{n+2},\gamma_{n+1},\gamma_n,\gamma_{n-1},\gamma_{n-2}) \ldots (29b)$$

$$\gamma_{n+4} = f_3(\alpha_{n+1},\alpha_n,\alpha_{n-1},\alpha_{n-2},\beta_{n+2},\beta_{n+1},\beta_n,\beta_{n-1},\beta_{n-2},$$
$$\gamma_{n+3},\gamma_{n+2},\gamma_{n+1},\gamma_n,\gamma_{n-1},\gamma_{n-2}) \ldots (29c)$$

where f_1, f_2, f_3 are linear functions. Equations (28a-c) apply for all n = 0,1,2.... Quantities with negative subscripts are taken to be zero.

Following the solution as presented by Wilson, each of the displacement functions (28a-c) can be expressed as a combination of eight linearly independent parts. The eight leading coefficients are set $\alpha_0 = 1$, $\alpha_1 = \beta_0 = \beta_1 = \gamma_0 = \gamma_1 = \gamma_2 = \gamma_3 = 0$, and the remaining coefficients α_n, β_n, γ_n are found from the recurrence formulae. The series solutions (28a-c), evaluated by using these coefficients, are denoted

$u_1(y), v_1(y), w_1(y)$. Similarly $u_2(y), v_2(y), w_2(y)$ are found by prescribing all leading coefficients to zero except $\alpha_1 = 1$. This process is repeated until $u_8(y), v_8(y), w_8(y)$ are found. Then the complete solution may be written

$$u = h_1[\sum_{i=1}^{8} C_i u_i(y)]\sin\beta\phi \qquad \ldots (30a)$$

$$v = ph_1[\sum_{i=1}^{8} C_i v_i(y)]\cos\beta\phi \qquad \ldots (30b)$$

$$w = h_1[\sum_{i=1}^{8} C_i w_i(y)]\sin\beta\phi \qquad \ldots (30c)$$

where C_i (i=1,2...8) are, at this stage, unknown constants governed by the curved edge boundary conditions. An expression for the required edge rotation can be deduced from expression (30c).

$$-\frac{dw}{dx} = -\frac{1}{a}[\sum_{i=1}^{8} C_i w_i'(y)]\sin\beta\phi \qquad \ldots (30d)$$

where $(\,)' = \frac{d(\,)}{dy}$, and the minus sign is necessary to suit the chosen convention for positive edge moments defined in Figure 3.6.

The stress resultant expressions for N and M may be taken directly from Wilson[108], but expressions for T and S must be derived from their constituent components[113].

$$N = N(y)\sin\beta\phi$$

$$= \frac{3F}{h_1^2 a}\{\sum_{i=1}^{8}[u_i' + \frac{\nu}{(y+1)}(u_i - p^2 v_i + \frac{1}{t}w_i)].C_i\}\sin\beta\phi \qquad \ldots (31a)$$

$$T = T(y)\cos\beta\phi$$

$$= \frac{Fp(1-\nu)}{h_1^2 a}\{\sum_{i=1}^{8}[\frac{3}{2}[\frac{1}{(y+1)}(u_i - v_i) + v_i'] - \frac{2}{a^2 t(y+1)^3}[(y+1)w_i' - w_i$$

$$- \frac{(y+1)}{t}v_i' + \frac{1}{t}v_i]].C_i\}\cos\beta\phi \qquad \ldots (31b)$$

$$S = S(y)\sin\beta\phi$$

$$= -\frac{F}{a^3 h_1^2 (y+1)^3}\{\sum_{i=1}^{8}[(y+1)^3 w_i''' + (y+1)^2 w_i'' - (p^2+1)(y+1)w_i'$$

$$+ 2p^2 w_i + \frac{p^2}{t}(y+1)v_i' - \frac{2p^2}{t}v_i$$

$$- p^2(1-\nu)[(y+1)w_i' - w_i - \frac{(y+1)}{t}v_i' + \frac{1}{t}v_i]].C_i\}\sin\beta\phi \qquad \ldots (31c)$$

$$M = M(y)\sin\beta\phi$$

$$= \frac{F}{h_1 a^2}\{\sum_{i=1}^{8}[-w_i'' - \frac{\nu}{(y+1)^2}[(y+1)w_i' - p^2 w_i + \frac{p^2}{t}v_i]].C_i\}\sin\beta\phi$$

$$\ldots (31d)$$

where as before, $( )' = \frac{d( )}{dy}$. Once again, for the purpose of calculating stiffness coefficients, the stress resultant expressions must be reversed in sign when evaluated at the edge A in order to comply with the sign convention of Figure 3.6.

Inspection of the displacement component expressions (30a-d) and the stress resultant expressions (31a-d) reveals that the amplitudes may be grouped into matrix equations which are directly analogous to equations (13a) and (13b) for the cylindrical shell element. The constants $C_i (i = 1,2 \ldots 8)$ are real in this case, and formulae for the elements of the matrices G and H are easily obtained from expressions (30a-d) and (31a-d). For example,

u_{1A} = (coefficient of C_1 in expression for amplitude of u at y = 0)

$\left(-\frac{dw}{dx}\right)_{7B}$ = (coefficient of C_7 in expression for amplitude of $-\frac{dw}{dx}$ at y = b)

T_{2A} = (coefficient of C_2 in expression for T(y) at y = 0)

M_{8B} = (coefficient of C_8 in expression for M(y) at y = b)

Thus, once again $k_M = H.G^{-1}$.

Computer Calculations:

For practical calculations, the infinite series associated with this solution must be truncated. In the present work, 50 terms are used. Because of these series, the conical shell stiffness matrix calculations require much more computing time than the corresponding calculations for either of the two previous element types. As is the case with the flat plate element, the final stiffness matrix k_M is not symmetrical since edges A and B are of different lengths. However, if k_M is premultiplied by an (8 × 8) diagonal matrix which has the first four diagonal elements equal to the arclength of edge A, and the second four equal to the arclength of edge B, then the product matrix should be symmetrical. A further check on the calculations is obtained by prescribing the angle γ equal to $\Pi/2$, for then the conical shell becomes a flat plate, and the stiffness matrix can be directly compared with the one predicted by the flat plate calculations.

3.3.2 Fixed-edge solutions for distributed uniform loads

Due to various desired combinations of dead load, wind load, and live load, any folded shell element may be subjected to loads which are uniformly distributed across the lateral dimension of the element. They can be resolved into two components. One component is normal to the shell surface, and the other is an in-plane load in the lateral direction. For each type of folded shell element, a simple method is described

for calculating the fixed-edge stress resultants under these two separate load conditions. It is shown that the same general equation can always be used, irrespective of which load condition or element is being considered. This equation involves the appropriate element stiffness matrix k_M, and two column matrices which contain particular solutions of the appropriate differential equation system.

For reasons which are made clear in the following description, the particular solutions for a flat plate element cannot be used when $\beta = 1,2,3$ or 4. Under these conditions, each flat plate must be analysed as a special case of a conical shell.

Cylindrical shell

(a) Normal load (positive in z-direction) uniform in x-direction

Let the applied normal load per unit surface area be $q = q_c \sin\beta\phi$, where q_c is constant (independent of x). Equation system (4a-c) must be modified to include a load term on the right hand side of equation (4c).

$$-[R^2D^2-K_1]u(x) - [K_2RD]v(x) - RD[K_3R^2D^2+K_4]w(x)=0 \quad \ldots (32a)$$

$$-[K_2RD]u(x) + [K_5R^2D^2+K_6]v(x) + [K_7R^2D^2+K_8]w(x)=0 \quad \ldots (32b)$$

$$-RD[K_3R^2D^2+K_4]u(x) + [K_7R^2D^2+K_8]v(x) + [K_9R^4D^4+K_{10}R^2D^2+K_{11}]w(x)$$

$$= -\frac{q_cR^2(1-\nu^2)}{Eh} \quad \ldots (32c)$$

Equations (32a-c) constitute a non-homogeneous system, and the complete solution is the sum of a complementary solution and a particular solution. For the particular solution, the following expressions are chosen.

$$u = u_c \sin\beta\phi \qquad \ldots (33a)$$

$$v = v_c \cos\beta\phi \qquad \ldots (33b)$$

$$w = w_c \sin\beta\phi \qquad \ldots (33c)$$

where u_c, v_c, w_c are constants. If expressions (33a-c) are substituted into equations (32a-c), equations (34a-c) result.

$$-[-K_1]u_c - [0]v_c - [0]w_c = 0 \qquad \ldots (34a)$$

$$-[0]u_c + [K_6]v_c + [K_8]w_c = 0 \qquad \ldots (34b)$$

$$-[0]u_c + [K_8]v_c + [K_{11}]w_c = -\frac{q_c R^2(1-\nu^2)}{Eh} \qquad \ldots (34c)$$

It follows that

$$u_c = 0 \qquad \ldots (35a)$$

$$v_c = \frac{K_8 q_c R^2(1-\nu^2)}{Eh(K_6K_{11}-K_8^2)} \qquad \ldots (35b)$$

$$w_c = -\frac{K_6 q_c R^2(1-\nu^2)}{Eh(K_6K_{11}-K_8^2)} \qquad \ldots (35c)$$

For fixed edges, the boundary conditions may be written

$$G.C + \begin{bmatrix} 0 \\ v_c \\ w_c \\ 0 \\ 0 \\ v_c \\ w_c \\ 0 \end{bmatrix} = 0 \qquad \ldots (36)$$

where G and C are defined by equations (11) and (13a). If δ_P is used to denote the particular solution for the edge displacement amplitudes, equation (36) becomes

$$G.C + \delta_P = 0 \qquad \ldots (37)$$

and so $$C = - G^{-1}.\delta_P \qquad \ldots (38)$$

The particular solutions for stress resultants are deduced by substituting expressions (33a-c) into the general stress resultant expressions[107,App.B], and the complete fixed-edge solutions are therefore

$$P = H.C + \begin{bmatrix} \frac{Eh\nu}{R(1-\nu^2)}(\beta v_c + w_c) \\ 0 \\ 0 \\ -\frac{Eh^3\nu\beta}{12(1-\nu^2)R^2}(\beta w_c + v_c) \\ -\frac{Eh\nu}{R(1-\nu^2)}(\beta v_c + w_c) \\ 0 \\ 0 \\ \frac{Eh^3\nu\beta}{12(1-\nu^2)R^2}(\beta w_c + v_c) \end{bmatrix} \quad \ldots (39)$$

$$= H.C + P_P \quad \ldots (40)$$

where H is defined by equations (12) and (13b). Equations (38) and (40) may be combined to give

$$P = - H.G^{-1}.\delta_P + P_P \quad \ldots (41)$$

Hence,

$$P = - k_M.\delta_P + P_P \quad \ldots (42)$$

where k_M is the stiffness matrix of the cylindrical shell element.

(b) In-plane load (positive in x-direction) uniform in x-direction

Let the applied in-plane load per unit surface area be $p = p_c \sin\beta\phi$, where p_c is constant (independent of x). Equation system (4a-c) must be modified to include a load term on the right hand side of equation (4a).

$$-[R^2D^2-K_1]u(x) - [K_2RD]v(x) - RD[K_3R^2D^2+K_4]w(x) = \frac{p_cR^2(1-\nu^2)}{Eh} \quad \ldots (43a)$$

$$-[K_2RD]u(x) + [K_5R^2D^2+K_6]v(x) + [K_7R^2D^2+K_8]w(x)=0 \quad \ldots (43b)$$

$$-RD[K_3R^2D^2+K_4]u(x) + [K_7R^2D^2+K_8]v(x) + [K_9R^4D^4+K_{10}R^2D^2+K_{11}]w(x)=0 \quad \ldots (43c)$$

For the particular solutions, the following expressions are chosen.

$$u = u_c \sin\beta\phi \quad \ldots (44a)$$

$$v = v_c \cos\beta\phi \quad \ldots (44b)$$

$$w = w_c \sin\beta\phi \quad \ldots (44c)$$

where again u_c, v_c, w_c are constants. If expressions (44a-c) are substituted into equations (43a-c), it follows that

$$u_c = \frac{p_cR^2(1-\nu^2)}{EhK_1} \quad \ldots (45a)$$

$$v_c = 0 \quad \ldots (45b)$$

$$w_c = 0 \quad \ldots (45c)$$

Particular solutions for stress resultants are deduced by substituting expressions (44a-c) into the general expressions (107, App.B). The complete fixed-edge stress resultants may then be calculated according to equation (42), where

$$\delta_P = \begin{bmatrix} u_c \\ 0 \\ 0 \\ 0 \\ u_c \\ 0 \\ 0 \\ 0 \end{bmatrix} \qquad \ldots (46)$$

and

$$P_P = \begin{bmatrix} 0 \\ \frac{-Eh\beta u_c}{2R(1+\nu)} \\ \frac{Eh^3\beta^2 u_c}{24R^3(1+\nu)} \\ 0 \\ 0 \\ \frac{Eh\beta u_c}{2R(1+\nu)} \\ \frac{-Eh^3\beta^2 u_c}{24R^3(1+\nu)} \\ 0 \end{bmatrix} \qquad \ldots (47)$$

Flat plate

(a) Normal load (positive in z-direction) uniform in x-direction

Let the applied normal load per unit surface area be $q = q_c \sin\beta\phi$, where q_c is constant (independent of x). Equation (18c) must be modified to include a load term on the right hand side.

$$[D_r^4 - 4D_r^3 + 2(2-\beta^2)D_r^2 + 4\beta^2 D_r + \beta^2(\beta^2-4)]w(x) = \frac{12x^4 q_c(1-\nu^2)}{Eh^3} \quad \ldots (48)$$

For the particular solution, the following expression is chosen

$$w = w_c x^4 \sin\beta\phi \quad \ldots (49)$$

where w_c is a constant. If expression (49) is substituted into equation (48), it follows that

$$w_c = \frac{12q_c(1-\nu^2)}{Eh^3(64-20\beta^2+\beta^4)} \quad \ldots (50)$$

where $\beta \neq 2$ or 4. Particular solutions for stress resultants are deduced by substituting expression (49) into the general expressions[109,110,App.B]. The complete fixed-edge stress resultants may then be calculated according to equation (42), where

$$\delta_P = \begin{bmatrix} 0 \\ 0 \\ w_c R_1^4 \\ -4w_c R_1^3 \\ 0 \\ 0 \\ w_c R_2^4 \\ -4w_c R_2^3 \end{bmatrix} \qquad \ldots (51)$$

and

$$P_P = \begin{bmatrix} 0 \\ 0 \\ \frac{Eh^3 w_c R_1}{12(1-\nu^2)}(32-5\beta^2+3\nu\beta^2) \\ \frac{Eh^3 w_c R_1^2}{12(1-\nu^2)}(12+\nu(4-\beta^2)) \\ 0 \\ 0 \\ \frac{-Eh^3 w_c R_2}{12(1-\nu^2)}(32-5\beta^2+3\nu\beta^2) \\ \frac{-Eh^3 w_c R_2^2}{12(1-\nu^2)}(12+\nu(4-\beta^2)) \end{bmatrix} \qquad \ldots (52)$$

and k_M is the stiffness matrix of the flat plate element.

(b) In-plane load (positive in x-direction) uniform in x-direction

Let the applied in-plane load per unit surface area be $p = p_c \sin\beta\phi$, where p_c is constant (independent of x). Equation system (18a-b) must be modified to include a load term on the right hand side of equation (18a).

$$[D_r^2 - (1+\frac{1-\nu}{2}\beta^2)]u(x) + [-\frac{\beta}{2}(1+\nu)D_r + \frac{\beta}{2}(3-\nu)]v(x) = -\frac{p_c x^2(1-\nu^2)}{Eh} \quad \ldots (53a)$$

$$[\frac{\beta}{2}(1+\nu)D_r + \frac{\beta}{2}(3-\nu)]u(x) + [\frac{1-\nu}{2}D_r^2 - (\beta^2+\frac{1-\nu}{2})]v(x) = 0 \quad \ldots (53b)$$

For the particular solutions, the following expressions are chosen.

$$u = u_c x^2 \sin\beta\phi \quad \ldots (54a)$$

$$v = v_c x^2 \cos\beta\phi \quad \ldots (54b)$$

where u_c and v_c are constants. If expressions (54a-b) are substituted into equations (53a-b), equations (55a-b) are obtained by equating coefficients of x^2.

$$[K_{12}]u_c + [K_{13}]v_c = -\frac{p_c(1-\nu^2)}{Eh} \quad \ldots (55a)$$

$$[K_{14}]u_c + [K_{15}]v_c = 0 \quad \ldots (55b)$$

where $K_{12} = 3 - \frac{1-\nu}{2}\beta^2$

$K_{13} = \frac{\beta}{2}(1-3\nu)$

$K_{14} = \frac{\beta}{2}(5+\nu)$

$K_{15} = \frac{3}{2}(1-\nu) - \beta^2$

Solutions of equations (55a-b) are

$$u_c = -\frac{p_c(1-\nu^2)K_{15}}{Eh(K_{12}K_{15}-K_{13}K_{14})} \qquad \ldots (56a)$$

$$v_c = \frac{p_c(1-\nu^2)K_{14}}{Eh(K_{12}K_{15}-K_{13}K_{14})} \qquad \ldots (56b)$$

where $\beta \neq 1$ or 3. Particular solutions for stress resultants are deduced by substituting expressions (54a-b) into the general stress resultant expressions[109,110,App.B]. The complete fixed-edge stress resultants may then be calculated according to equation (42), where

$$\delta_p = \begin{bmatrix} u_c R_1^2 \\ v_c R_1^2 \\ 0 \\ 0 \\ u_c R_2^2 \\ v_c R_2^2 \\ 0 \\ 0 \end{bmatrix} \qquad \ldots (57)$$

$$\text{and } P_P = \begin{bmatrix} -\frac{EhR_1}{1-\nu^2}((2+\nu)u_c - \nu\beta v_c) \\ -\frac{EhR_1}{2(1+\nu)}(\beta u_c + v_c) \\ 0 \\ 0 \\ \frac{EhR_2}{1-\nu^2}((2+\nu)u_c - \nu\beta v_c) \\ \frac{EhR_2}{2(1+\nu)}(\beta u_c + v_c) \\ 0 \\ 0 \end{bmatrix} \quad \ldots (58)$$

Conical shell

(a) Normal load (positive in z-direction) uniform in x-direction

Let the applied normal load per unit surface area be $Z = q_c \sin\beta\phi$, where q_c is constant (independent of x). Wilson assumes that normal surface loads can always be expressed in the form

$$Z = \frac{3Fh_1}{x^4}\left[\sum_{n=o}^{\infty} Z_n\left(\frac{x}{ah_1} - 1\right)^n\right]\sin\beta\phi \quad \ldots (59)$$

If the amplitude is to be independent of x, then the coefficients Z_n must be chosen such that $Z_0 = 1$, $Z_1 = 4$, $Z_2 = 6$, $Z_3 = 4$, $Z_4 = 1$, $Z_5 = Z_6 = \ldots = 0$. Hence equation (59) becomes

$$Z = \frac{3F}{a^4 h_1^3}\sin\beta\phi \quad \ldots (60)$$

It follows that for the amplitude to be the simple constant q_c, then each of the Z_n coefficients should be multiplied by

$$\frac{a^4 h_1^3 q_c}{3F} .$$

Particular solutions for the displacement functions (28a-c) are deduced from the recurrence formulae[108] by setting the eight loading coefficients ($\alpha_0, \alpha_1, \beta_0, \beta_1, \gamma_0, \gamma_1, \gamma_2, \gamma_3$) equal to zero, and the Z_n loading coefficients equal to the values suggested above. (All X_n and Y_n loading coefficients are taken to be zero in the recurrence formulae). The particular solutions thus found are denoted $u_9(y)$, $v_9(y)$, $w_9(y)$. Particular solutions for stress resultants are deduced by substituting the functions $u_9(y)$, $v_9(y)$, $w_9(y)$ into the expressions (31a-d). The complete fixed-edge stress resultants may then be calculated according to equation (42), where

$$\delta_p = \begin{bmatrix} 0 \\ 0 \\ 0 \\ 0 \\ h_1 u_9 \\ p h_1 v_9 \\ h_1 w_9 \\ -\frac{1}{a} w_9' \end{bmatrix} \qquad \ldots (61)$$

and P_p =

$$\begin{bmatrix} 0 \\ 0 \\ 0 \\ 0 \\ \frac{3F}{h_1^2 a}\left[u_9' + \frac{\nu}{(b+1)}(u_9 - p^2 v_9 + \frac{1}{t} w_9)\right] \\ \frac{3Fp(1-\nu)}{2h_1^2 a}\left[\frac{1}{(b+1)}(u_9 - v_9) + v_9'\right] - \frac{2Fp(1-\nu)}{a^3 h_1^2 t (b+1)^3}\left[(b+1)w_9' - w_9 - \frac{(b+1)}{t} v_9' + \frac{1}{t} v_9\right] \\ \frac{-F}{h_1^2 a^3 (b+1)^3}\left[(b+1)^3 w_9''' + (b+1)^2 w_9'' - (p^2+1)(b+1) w_9' + 2p^2 w_9 + \frac{p^2}{t}(b+1) v_9' - \right. \\ \left. \frac{2p^2}{t} v_9\right] + \frac{Fp^2(1-\nu)}{a^3 h_1^2 (b+1)^3}\left[(b+1)w_9' - w_9 - \frac{(b+1)}{t} v_9' + \frac{1}{t} v_9\right] \\ \frac{F}{h_1 a^2}\left[-w_9'' - \frac{\nu}{(b+1)^2}\left((b+1)w_9' - p^2 w_9 + \frac{p^2}{t} v_9\right)\right] \end{bmatrix} \quad \ldots (62)$$

and k_M is the stiffness matrix of the conical shell element. In equations (61) and (62), the shorthand notation u_9, v_9, w_9 is used to represent $u_9(b)$, $v_9(b)$, $w_9(b)$ respectively.

(b) In-plane load (positive in x-direction) uniform in x-direction

Let the applied in-plane load per unit surface area be $X = p_c \sin\beta\phi$, where p_c is constant (independent of x). Wilson assumes that in-plane surface loads can always be expressed in the form

$$X = \frac{3F}{h_1 x^2} \left[\sum_{n=o}^{\infty} X_n \left(\frac{x}{a h_1} - 1 \right)^n \right] \sin\beta\phi \qquad \ldots (63)$$

If the amplitude is to be independent of x, then the coefficients X_n must be chosen such that $X_0 = 1$, $X_1 = 2$, $X_2 = 1$, $X_3 = X_4 = \ldots = 0$. Hence equation (63) becomes

$$X = \frac{3F}{a^2 h_1^3} \sin\beta\phi \qquad \ldots (64)$$

It follows that for the amplitude to be the simple constant p_c, then each of the X_n coefficients should be multiplied by $\frac{a^2 h_1^3 p_c}{3F}$.

Particular solutions for the displacement functions (28a-c) are deduced from the recurrence formulae[108] by setting the eight leading coefficients ($\alpha_0, \alpha_1, \beta_0, \beta_1, \gamma_0, \gamma_1, \gamma_2, \gamma_3$) equal to zero, and the X_n loading coefficients equal to the values suggested above. (All Y_n and Z_n loading coefficients are taken to be zero in the recurrence formulae). The particular solutions thus found are denoted $u_9(y)$, $v_9(y)$, $w_9(y)$ as before,

and the complete fixed-edge stress resultants may then be calculated according to equation (42), where δ_P and P_P are defined by equations (61) and (62) respectively.

3.3.3 Element transformation matrices

Each folded shell element has its own particular member coordinate system. Hence for each element, a matrix can be deduced which describes the transformation of the eight curved edge displacement components associated with the stiffness matrix, from the member coordinate system to the common, or 'global', coordinate system. Hence if δ_M denotes the column matrix which contains the eight curved edge displacement components in member coordinates, and if δ_G denotes the column matrix which contains the same eight displacement components in global coordinates, then the transformation matrix A is defined such that

$$\delta_M = A \cdot \delta_G \qquad \ldots (65)$$

and

$$\delta_G = A^T \cdot \delta_M \qquad \ldots (66)$$

where A^T is the transpose of the orthogonal matrix A.

For the global system, cylindrical coordinates (x, ϕ, z) are chosen as shown in Figure 3.7. The z axis is parallel to the axis of rotation, and the plane $z = 0$ passes through the uppermost joint (s) of the folded shell structure. The x-coordinate indicates radial distance from the axis

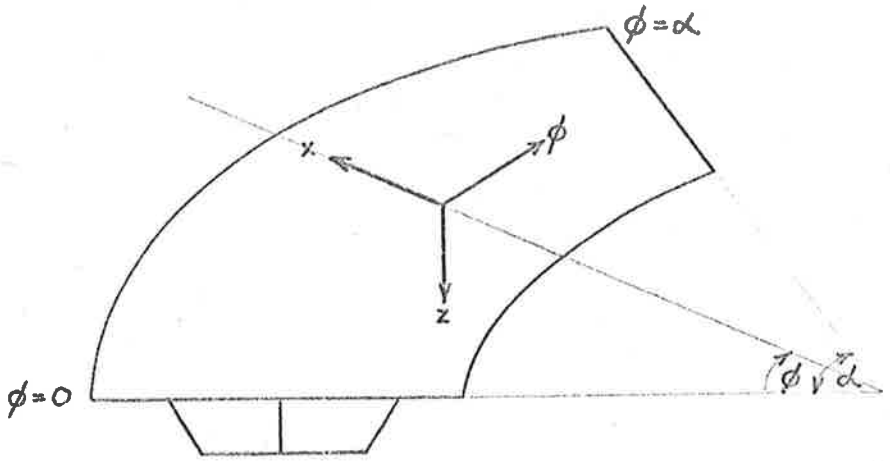

Figure 3.7 Global coordinate system

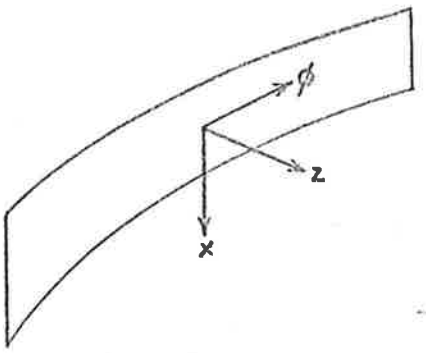

(a) Cylindrical shell element

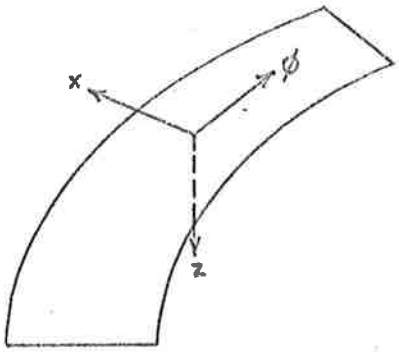

(b) Flat plate element

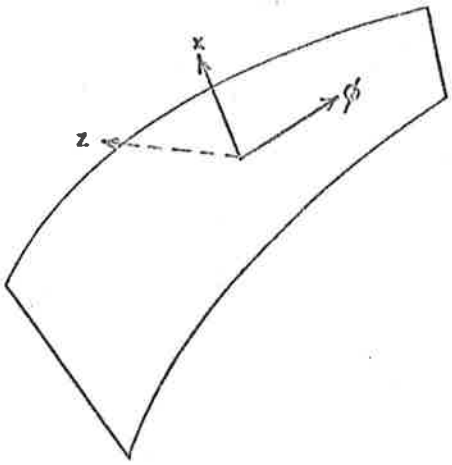

(c) Inverted conical shell element

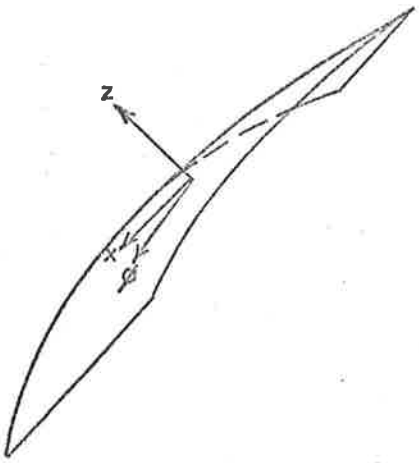

(d) Upright conical shell element

Figure 3.8 Member coordinate systems

of rotation, and the circumferential ϕ-coordinate is measured from the near end ($\phi = 0$) to the far end ($\phi = \alpha$) of the structure.

Member coordinate systems for cylindrical shell, flat plate, and conical shell elements are defined in Section 3.3.1, and they are summarized in Figure 3.8. A curved beam such as the one sketched in Figure 3.7 incorporates two possible types of conical shell element. One has the apex of the cone below the element, and the other has its apex above. These two types are referred to as 'inverted' and 'upright' conical shell elements respectively. With regard to the calculation of transformation matrices, an upright conical shell element requires special consideration, since it is the only folded shell element with its member ϕ-direction opposite to the global ϕ-direction.

Cylindrical shell element transformation matrix

$$A = \left[\begin{array}{cccc|cccc} 0 & 0 & 1 & 0 & & & & \\ 0 & 1 & 0 & 0 & & & & \\ -1 & 0 & 0 & 0 & & \text{zero} & & \\ 0 & 0 & 0 & 1 & & & & \\ \hline & & & & 0 & 0 & 1 & 0 \\ & & & & 0 & 1 & 0 & 0 \\ & \text{zero} & & & -1 & 0 & 0 & 0 \\ & & & & 0 & 0 & 0 & 1 \end{array}\right] \quad \ldots (67)$$

Flat plate element transformation matrix

$$A = \left[\begin{array}{cccc|cccc} 1 & 0 & 0 & 0 & & & & \\ 0 & 1 & 0 & 0 & & & & \\ 0 & 0 & 1 & 0 & & \text{zero} & & \\ 0 & 0 & 0 & 1 & & & & \\ \hline & & & & 1 & 0 & 0 & 0 \\ & & & & 0 & 1 & 0 & 0 \\ & \text{zero} & & & 0 & 0 & 1 & 0 \\ & & & & 0 & 0 & 0 & 1 \end{array}\right] \quad \ldots (68)$$

Upright conical shell element transformation matrix

$$A = \left[\begin{array}{cccc|cccc} -S\cos m\Pi & 0 & -C\cos m\Pi & 0 & & & & \\ 0 & -\cos m\Pi & 0 & 0 & & & & \\ -C\cos m\Pi & 0 & S\cos m\Pi & 0 & & \multicolumn{3}{c}{\text{zero}} & \\ 0 & 0 & 0 & \cos m\Pi & & & & \\ \hline & & & & -S\cos m\Pi & 0 & -C\cos m\Pi & 0 \\ & & & & 0 & -\cos m\Pi & 0 & 0 \\ & \multicolumn{3}{c}{\text{zero}} & & & & \\ & & & & -C\cos m\Pi & 0 & S\cos m\Pi & 0 \\ & & & & 0 & 0 & 0 & \cos m\Pi \end{array}\right] \quad \ldots (69)$$

where $S = \sin\gamma$, and $C = \cos\gamma$. The upright cone is the only folded shell element which has its transformation matrix dependent upon the value of m.

Inverted conical shell element transformation matrix

$$A = \left[\begin{array}{cccc|cccc} S & 0 & -C & 0 & & & & \\ 0 & 1 & 0 & 0 & & \multicolumn{3}{c}{\text{zero}} & \\ C & 0 & S & 0 & & & & \\ 0 & 0 & 0 & 1 & & & & \\ \hline & & & & S & 0 & -C & 0 \\ & & & & 0 & 1 & 0 & 0 \\ & \multicolumn{3}{c}{\text{zero}} & & & & \\ & & & & C & 0 & S & 0 \\ & & & & 0 & 0 & 0 & 1 \end{array}\right] \quad \ldots (70)$$

3.3.4 General method of solution

A brief description is given for the folded shell solution of any primary structure. For each successive Fourier harmonic of the applied loads, the structure is completely analysed by the direct stiffness method, and the results are accumulated. Therefore, only the general m^{th} harmonic need be considered when describing the solution. Final results are obtained by terminating the calculations after a sufficient number of Fourier harmonics have been taken to ensure adequate representation of the applied loads and of the structural response.

Structural stiffness matrix K_S

Each folded shell element has an associated stiffness matrix which describes the direct relationship between the curved edge displacements and the corresponding stress resultants. This relationship can be expressed in the form

$$p_M = k_M \cdot \delta_M \qquad \ldots (71)$$

where the subscript M indicates reference to the member coordinate system. Details for calculating k_M are given in Section 3.3.1. Each folded shell element also has an associated coordinate transformation matrix A such that

$$\delta_M = A \cdot \delta_G \qquad \ldots (72)$$

and

$$p_M = A \cdot p_G \qquad \ldots (73)$$

where the subscript G indicates reference to the global coordinate system. Details of all transformation matrices are given in Section 3.3.3. If equations (72) and (73) are substituted into equation (71), then

$$p_G = [A^{-1} \cdot k_M \cdot A] \cdot \delta_G \qquad \ldots (74)$$

However, the inverse of the orthogonal matrix A is equal to its transpose A^T, and so equation (74) becomes

$$p_G = [A^T \cdot k_M \cdot A] \cdot \delta_G = k_G \cdot \delta_G \qquad \ldots (75)$$

where k_G is thus defined as the element stiffness matrix referred to the global coordinate system. The matrix equation (75) may be partitioned as follows,

$$\left[\frac{p_A}{p_B}\right]_G = \left[\begin{array}{c|c} k_{AA} & k_{AB} \\ \hline k_{BA} & k_{BB} \end{array}\right]_G \cdot \left[\frac{\delta_A}{\delta_B}\right]_G \qquad \ldots (76)$$

where k_{AA}, k_{AB}, k_{BA}, k_{BB} are (4 × 4) submatrices, and A and B are the two curved edges of the element being considered. By using these partitions, the complete structural stiffness matrix K_S can be assembled in the usual way[87]. Thus, for the complete structure, the relationship between the curved joint loads

(in global coordinates) and the corresponding joint displacement components (in global coordinates) is defined by the equation

$$P_J = K_S \cdot \Delta_J \qquad \ldots (77)$$

where P_J is the column matrix which contains the amplitudes of the joint loads, and Δ_J is the column matrix which contains the amplitudes of the resulting joint displacement components.

Joint load matrix P_J

There are two distinct contributions to the matrix P_J. The contribution due to any external loads which are directly applied to the joints is first calculated by using Fourier expansions (A.1-7). Secondly, the contribution due to the joint loads which are indirectly induced by the action of any external distributed loads on the surfaces of the shell elements is calculated. For this purpose, all curved joints of the structure are assumed to be temporarily fixed against any movements. Under these so-called 'fixed-edge' conditions, shell surface loads will induce certain stress resultants at the edges of each element, which can be calculated in the case of distributed laterally-uniform surface loads by using Fourier expansions (A.8-12) together with the analysis detailed in Section 3.3.2. Equal and opposite reactions to the fixed-edge stress resultants thus obtained must then be transformed into the global coordinate system before including them in the joint load matrix P_J.

Element curved edge displacement components in member coordinates

From equation (77), it follows that

$$\Delta_J = K_S^{-1} \cdot P_J \qquad \ldots (78)$$

Having thus calculated Δ_J, the curved edge displacement components δ_G for each element are easily extracted. Equation (72) can then be used to evaluate δ_M, the curved edge displacement components in member coordinates.

Final results, in member coordinates, at selected points on each element

General expressions for all desired results are given in Appendix B. (Results include displacement components, middle-surface strains and curvatures, various stress resultants, and actual-surface stresses and strains). At any location within an element, each output quantity must be calculated as the sum of two separate additive components. The first is due solely to the curved edge movements, and the second is due solely to the action of distributed loads under fixed-edge conditions.

(a) Results due solely to curved edge movements:

Let $R_{(a)}$ denote the column matrix which is to contain the amplitudes of the results at all desired lateral locations across the edge-loaded element. In a similar

way as matrix H is calculated during the formation of the element stiffness matrix, so a matrix H_1 can be calculated such that

$$R_{(a)} = H_1 \cdot C \qquad \ldots (79)$$

where C is the column matrix of eight integration constants governed by the boundary conditions at the curved edges. However, these boundary conditions are known, since at this stage δ_M is known. Hence

$$\delta_M = G \cdot C \qquad \ldots (80)$$

where the matrix G is defined in Section 3.3.1. Equations (79) and (80) can therefore be combined to give

$$R_{(a)} = [H_1 \cdot G^{-1}] \cdot \delta_M \qquad \ldots (81)$$

(b) Results due solely to the action of distributed loads under fixed-edge conditions:

Let $R_{(b)}$ denote the column matrix which is to contain the amplitudes of the results at all desired lateral locations across the element under fixed-edge conditions. Particular solutions must be included for the distributed laterally-uniform loads. In the case of a cylinder or a flat plate, these solutions are obtained by substituting the displacement component particular solutions (derived in Section 3.3.2) into the general

expressions for output quantities (App.B). In the case of a conical shell, the solutions are obtained by using the prescribed values of the load coefficients X_n and Z_n (derived in Section 3.3.2) when evaluating the general expressions for the output quantities (App.B).

For any distributed laterally-uniform load, if p_o and q_o are the actual load intensities in the x and z member directions respectively, then a (2X1) column matrix P_{ext} can be defined as follows.

$$P_{ext} = \begin{bmatrix} K_{16} & 0 \\ 0 & K_{16} \end{bmatrix} \cdot \begin{bmatrix} p_o \\ q_o \end{bmatrix} \qquad \ldots (82)$$

where

$K_{16} = \sin \frac{m\Pi(2\xi+\delta\phi)}{2\alpha} \sin \frac{m\Pi\delta\phi}{2\alpha}$ for partial uniform load

$K_{16} = 1$ for uniform load

$K_{16} = \frac{m\Pi}{2R\alpha} \sin \frac{m\Pi\xi}{\alpha}$ for line load on cylinder

$K_{16} = \frac{m\Pi}{(R_1+R_2)\alpha} \sin \frac{m\Pi\xi}{\alpha}$ for line load on flat plate

$K_{16} = \frac{m\Pi}{ah_1(b+2)\alpha\sin\gamma} \sin \frac{m\Pi\xi}{\alpha}$ for line load on cone

(The values of K_{16} are chosen so that the product $\frac{4}{m\Pi} \cdot K_{16}$ will, in every case, give the complete amplitudes of the m^{th} terms in Fourier expansions (A.8-12) respectively).

The particular solutions can then be added to the complementary solutions as indicated by equation (83).

$$R_{(b)} = H_1 \cdot C + H_2 \cdot P_{ext} \qquad \ldots (83)$$

where C is the column matrix of eight integration constants governed by the fixed-edge boundary conditions. In the same way as matrix H_2 can be calculated from the particular solution formulae, so a matrix G_1 can be calculated such that

$$\delta_M = G \cdot C + G_1 \cdot P_{ext} = 0 \qquad \ldots (84a)$$

It follows directly from equation (84a), that

$$C = -G^{-1} \cdot G_1 \cdot P_{ext} \qquad \ldots (84b)$$

and so equation (83) can be written

$$R_{(b)} = [H_2 - H_1 \cdot G^{-1} \cdot G_1] \cdot P_{ext} \qquad \ldots (85)$$

The solution for this harmonic is the sum of $R_{(a)}$ and $R_{(b)}$. Hence

$$R_{(a)} + R_{(b)} = [H_1 . G^{-1}] \cdot \delta_M + [H_2 - H_1 . G^{-1} . G_1] \cdot P_{ext} \quad \ldots (86)$$

Appropriate sine and cosine factors are then applied to these amplitudes in order to evaluate the contribution of this harmonic (m^{th}) to the 'absolute' results at the desired circumfer-

ential locations. The final solution is obtained by accumulating the absolute results for all Fourier harmonics.

3.4 Analysis of Diaphragm Structure

The analysis of a diaphragm structure requires much more calculation than the analysis of a primary structure with the same number of folded shell elements. One reason for the extra calculation is that particular solutions associated with distributed diaphragm redundants are more complex than those associated with externally applied laterally-uniform loads. As described in Section 3.2, each linearly distributed redundant can be considered as the sum of two triangularly distributed redundants. Particular solutions associated with the latter are derived in detail in Section 3.4.1. A description of the general method of solving a loaded diaphragm structure is then given in Section 3.4.2.

Just as there are some restrictions on the values of β in the analysis of a primary structure, so there are some additional restrictions on the values of β in the analysis of a diaphragm structure. Specifically for any flat plate which is connected to an internal diaphragm, the chosen particular solutions cannot be used when $\beta = 1,2,3,4$, or 5. However, for the corresponding harmonics, the flat plate can again be treated as a special case of a conical shell.

3.4.1 Particular solutions associated with triangularly distributed diaphragm redundants

Cylindrical shell element

(a) Let the applied normal load per unit surface area be $q = Z_C a_1(x+b_1)\sin\beta\phi$, where a_1 and b_1 are constants (independent of x) obtained from Fourier expansion (A.13). Then equation system (4a-c) must be modified to include a load term on the right hand side of equation (4c).

$$-[R^2D^2-K_1]u(x)-[K_2RD]v(x)-RD[K_3R^2D^2+K_4]w(x) = 0 \qquad \ldots(87a)$$

$$-[K_2RD]u(x)+[K_5R^2D^2+K_6]v(x)+[K_7R^2D^2+K_8]w(x) = 0 \qquad \ldots(87b)$$

$$-RD[K_3R^2D^2+K_4]u(x)+[K_7R^2D^2+K_8]v(x)+[K_9R^4D^4+K_{10}R^2D^2+K_{11}]w(x)$$

$$= -\frac{Z_C a_1(x+b_1)(1-\nu^2)R^2}{Eh} \qquad \ldots(87c)$$

Equations (87a-c) constitute a non-homogeneous system, and the complete solution is the sum of a complementary solution and a particular solution. For the particular solution, the following expressions are chosen.

$$u = Z_C(c_1x+d_1)\sin\beta\phi \qquad \ldots(88a)$$

$$v = Z_C(e_1x+f_1)\cos\beta\phi \qquad \ldots(88b)$$

$$w = Z_C(g_1x+i_1)\sin\beta\phi \qquad \ldots(88c)$$

where c_1, d_1, e_1, f_1, g_1, i_1 are constants. If expressions (88a-c) are substituted into equations (87a-c), equations (89a-c) result.

$$-[-K_1](c_1x+d_1)-[K_2R]e_1-[K_4R]g_1 = 0 \qquad \ldots(89a)$$

$$-[K_2R]c_1+[K_6](e_1x+f_1)+[K_8](g_1x+i_1) = 0 \qquad \ldots(89b)$$

$$-[K_4R]c_1+[K_8](e_1x+f_1)+[K_{11}](g_1x+i_1) = -\frac{a_1(x+b_1)(1-\nu^2)R^2}{Eh} \qquad \ldots(89c)$$

It follows that

$$c_1 = 0$$

$$d_1 = -\frac{(K_6K_4-K_8K_2)a_1R^3(1-\nu^2)}{(K_6K_{11}-K_8^2)K_1Eh}$$

$$e_1 = \frac{K_8a_1R^2(1-\nu^2)}{(K_6K_{11}-K_8^2)Eh}$$

$$f_1 = \frac{K_8a_1b_1R^2(1-\nu^2)}{(K_6K_{11}-K_8^2)Eh}$$

$$g_1 = -\frac{K_6a_1R^2(1-\nu^2)}{(K_6K_{11}-K_8^2)Eh}$$

$$i_1 = -\frac{K_6a_1b_1R^2(1-\nu^2)}{(K_6K_{11}-K_8^2)Eh}$$

(b) Let the applied in-plane load per unit surface area be $p = X_C a_1 (x+b_1)\sin\beta\phi$. Then equation system (4a-c) must be modified to include a load term on the right hand side of equation (4a).

$$-[R^2D^2-K_1]u(x)-[K_2RD]v(x)-RD[K_3R^2D^2+K_4]w(x) = \frac{X_C a_1 (x+b_1)(1-\nu^2)R^2}{Eh} \quad \ldots(90a)$$

$$-[K_2RD]u(x)+[K_5R^2D^2+K_6]v(x)+[K_7R^2D^2+K_8]w(x) = 0 \quad \ldots(90b)$$

$$-RD[K_3R^2D^2+K_4]u(x)+[K_7R^2D^2+K_8]v(x)+[K_9R^4D^4+K_{10}R^2D^2+K_{11}]w(x) \quad \ldots(90c)$$

For the particular solution, the following expressions are chosen.

$$u = X_C(c_2x+d_2)\sin\beta\phi \quad \ldots(91a)$$

$$v = X_C(e_2x+f_2)\cos\beta\phi \quad \ldots(91b)$$

$$w = X_C(g_2x+i_2)\sin\beta\phi \quad \ldots(91c)$$

where c_2, d_2, ... i_2 are constants. If expressions (91a-c) are substituted into equations (90a-c), equations (92a-c) result.

$$-[-K_1](c_2x+d_2)-[K_2R]e_2-[K_4R]g_2 = \frac{a_1(x+b_1)(1-\nu^2)R^2}{Eh} \quad \ldots(91a)$$

$$-[K_2R]c_2+[K_6](e_2x+f_2)+[K_8](g_2x+i_2) = 0 \quad \ldots(91b)$$

$$-[K_4R]c_2+[K_8](e_2x+f_2)+[K_{11}](g_2x+i_2) = 0 \quad \ldots(91c)$$

It follows that

$$c_2 = \frac{a_1R^2(1-\nu^2)}{K_1Eh}$$

$$d_2 = \frac{a_1b_1R^2(1-\nu^2)}{K_1Eh}$$

$$e_2 = 0$$

$$f_2 = \frac{(K_2K_{11}-K_4K_8)a_1R^3(1-\nu^2)}{(K_6K_{11}-K_8^2)K_1Eh}$$

$$g_2 = 0$$

$$i_2 = \frac{(K_6K_4-K_8K_2)a_1R^3(1-\nu^2)}{(K_6K_{11}-K_8^2)K_1Eh}$$

(c) Let the applied normal load per unit surface area be $q = Z_D a_2(x+b_2)\sin\beta\phi$, where a_2 and b_2 are constants (independent of x) obtained from Fourier expansion (A.14). For the particular solution, the following expressions are chosen.

$$u = Z_D(c_3x+d_3)\sin\beta\phi \qquad \ldots(92a)$$

$$v = Z_D(e_3x+f_3)\cos\beta\phi \qquad \ldots(92b)$$

$$w = Z_D(g_3x+i_3)\sin\beta\phi \qquad \ldots(92c)$$

where c_3, d_3, ... i_3 are constants. The similarity between this load case and load case (a) is obvious, and the values of c_3, d_3, ... i_3 can be deduced directly from the expressions for c_1, d_1, ... i_1 respectively by appropriate change of subscripts.

(d) Let the applied in-plane load per unit surface area be $p = X_D a_2(x+b_2)\sin\beta\phi$. For the particular solution, the following expressions are chosen.

$$u = X_D(c_4x+d_4)\sin\beta\phi \qquad \ldots(93a)$$

$$v = X_D(e_4x+f_4)\cos\beta\phi \qquad \ldots(93b)$$

$$w = X_D(g_4x+i_4)\sin\beta\phi \qquad \ldots(93c)$$

where c_4, d_4, ... i_4 are constants. The similarity between this load case and load case (b) is also obvious, and the values of c_4, d_4, ... i_4 can be deduced directly from the expressions for c_2, d_2, ... i_2 respectively again by appropriate change of subscripts.

Flat plate element

(a) Let the applied normal load per unit surface area be $q = Z_C a_1 (x+b_1)\sin\beta\phi$, where a_1 and b_1 are constants (independent of x) obtained from Fourier expansion (A.15). Then equation (18c) must be modified to include a load term on the right hand side.

$$[D_r^4 - 4D_r^3 + 2(2-\beta^2)D_r^2 + 4\beta^2 D_r + \beta^2(\beta^2-4)]w(x) = \frac{12x^4 Z_C a_1 (x+b_1)(1-\nu^2)}{Eh^3} \quad \ldots(94)$$

where $x = x_o e^r$ and $D_r = \frac{d}{dr}$. For the particular solution, the following expression is chosen.

$$w = Z_C(c_1 x^5 + d_1 x^4)\sin\beta\phi \quad \ldots(95)$$

where c_1 and d_1 are constants. If expression (95) is substituted into equation (94), two equations may be deduced. The first is obtained by equating the coefficients of e^{5r}, and the second is obtained by equating the coefficients of e^{4r}. Hence

$$c_1 = \frac{12a_1(1-\nu^2)}{Eh^3(225-34\beta^2+\beta^4)}, \text{ where } \beta \neq 3 \text{ or } 5$$

$$d_1 = \frac{12a_1 b_1(1-\nu^2)}{Eh^3(64-20\beta^2+\beta^4)}, \text{ where } \beta \neq 2 \text{ or } 4$$

(b) Let the applied in-plane load per unit surface area be $p = X_C a_1 (x+b_1)\sin\beta\phi$. Then equation system (18a) and (18b) must be modified to include a load term on the right hand side of equation (18a).

$$[D_r^2 - (1+\frac{1-\nu}{2}\beta^2)]u(x) + [-\frac{\beta}{2}(1+\nu)D_r + \frac{\beta}{2}(3-\nu)]v(x)$$

$$= - \frac{X_C a_1 (x+b_1) x^2 (1-\nu^2)}{Eh} \qquad \ldots(96a)$$

$$[\frac{\beta}{2}(1+\nu)D_r + \frac{\beta}{2}(3-\nu)]u(x) + [\frac{1-\nu}{2}D_r^2 - (\beta^2 + \frac{1-\nu}{2})]v(x) = 0 \qquad \ldots(96b)$$

For the particular solution, the following expressions are chosen.

$$u = X_C (c_2 x^3 + d_2 x^2)\sin\beta\phi \qquad \ldots(97a)$$

$$v = X_C (e_2 x^3 + f_2 x^2)\cos\beta\phi \qquad \ldots(97b)$$

where c_2, d_2, e_2, f_2 are constants. If expressions (97a) and (97b) are substituted into equations (96a) and (96b), two equations may be obtained by equating coefficients of e^{3r}, and two further equations may be obtained by equating coefficients of e^{2r}. These four equations can be written as follows.

$$[K_{19}]c_2 + [K_{20}]e_2 = -\frac{a_1(1-\nu^2)}{Eh} \qquad \ldots(98a)$$

$$[K_{21}]c_2 + [K_{22}]e_2 = 0 \qquad \ldots(98b)$$

$$[K_{23}]d_2 + [K_{24}]f_2 = -\frac{a_1 b_1(1-\nu^2)}{Eh} \qquad \ldots(98c)$$

$$[K_{25}]d_2 + [K_{26}]f_2 = 0 \qquad \ldots(98d)$$

where

$$K_{19} = 8 - \frac{1-\nu}{2}\beta^2 \qquad K_{20} = -2\nu\beta$$

$$K_{21} = \beta(3+\nu) \qquad K_{22} = 4(1-\nu) - \beta^2$$

$$K_{23} = 3 - \frac{1-\nu}{2}\beta^2 \qquad K_{24} = \frac{\beta}{2}(1-3\nu)$$

$$K_{25} = \frac{\beta}{2}(5+\nu) \qquad K_{26} = \frac{3}{2}(1-\nu) - \beta^2$$

It follows that

$$\left.\begin{aligned} c_2 &= -\frac{a_1(1-\nu^2)K_{22}}{(K_{19}K_{22}-K_{21}K_{20})Eh} \\ e_2 &= \frac{a_1(1-\nu^2)K_{21}}{(K_{19}K_{22}-K_{21}K_{20})Eh} \end{aligned}\right\} \quad \beta \neq 2 \text{ or } 4$$

$$\left.\begin{aligned} d_2 &= -\frac{a_1 b_1(1-\nu^2)K_{26}}{(K_{23}K_{26}-K_{25}K_{24})Eh} \\ f_2 &= \frac{a_1 b_1(1-\nu^2)K_{25}}{(K_{23}K_{26}-K_{25}K_{24})Eh} \end{aligned}\right\} \quad \beta \neq 1 \text{ or } 3$$

(c) Let the applied normal load per unit surface area be $q = Z_D a_2(x+b_2)\sin\beta\phi$, where a_2 and b_2 are constants (independent of x) obtained from Fourier expansion (A.16). For the particular solution, the following expression is chosen.

$$w = Z_D(c_3x^5+d_3x^4) \qquad ...(99)$$

where c_3 and d_3 are constants. The values of c_3 and d_3 can be deduced directly from the expressions for c_1 and d_1 respectively.

(d) Let the applied in-plane load per unit surface area be $p = X_D a_2(x+b_2)\sin\beta\phi$. For the particular solution, the following expressions are chosen.

$$u = X_D(c_4x^3+d_4x^2)\sin\beta\phi \qquad ...(100a)$$

$$v = X_D(e_4x^3+f_4x^2)\cos\beta\phi \qquad ...(100b)$$

where c_4, d_4, e_4, f_4 are constants. The values of c_4, d_4, e_4, f_4 can be deduced directly from the expressions for c_2, d_2, e_2, f_2 respectively.

Conical shell element

(a) Let the applied normal load per unit surface area be $q = Z_C a_1 (x+b_1)\sin\beta\phi$, where a_1 and b_1 are constants (independent of x) obtained from Fourier expansion (A.17). Wilson assumes that normal surface loads can be expressed according to equation (59). If $K_{27} = \frac{(ah_1)^4}{3Fh_1}$, then the coefficients Z_n must be chosen such that

$$Z_0 = K_{27} a_1 (b_1 + ah_1) Z_C$$

$$Z_1 = K_{27} a_1 (4b_1 + 5ah_1) Z_C$$

$$Z_2 = K_{27} a_1 (6b_1 + 10ah_1) Z_C$$

$$Z_3 = K_{27} a_1 (4b_1 + 10ah_1) Z_C$$

$$Z_4 = K_{27} a_1 (b_1 + 5ah_1) Z_C$$

$$Z_5 = K_{27} a_1 ah_1 Z_C$$

and $Z_6 = Z_7 = \ldots = 0$.

(b) Let the applied in-plane load per unit surface area be $p = X_C a_1 (x+b_1)\sin\beta\phi$. Wilson assumes that in-plane surface loads can be expressed according to equation (63). If $K_{28} = \frac{(ah_1)^2 h_1}{3F}$, then the coefficients X_n must be chosen such that

$$X_0 = K_{28}a_1(b_1+ah_1)X_C$$

$$X_1 = K_{28}a_1(2b_1+3ah_1)X_C$$

$$X_2 = K_{28}a_1(b_1+3ah_1)X_C$$

$$X_3 = K_{28}a_1ah_1X_C$$

and $X_4 = X_5 = \ldots = 0$.

(c) Let the applied normal load per unit surface area be $q = Z_D a_2(x+b_2)\sin\beta\phi$, where a_2 and b_2 are constants (independent of x) obtained from Fourier expansion (A.18). The values for the coefficients Z_n can be deduced directly from load case (a).

(d) Let the applied in-plane load per unit surface area be $p = X_D a_2(x+b_2)\sin\beta\phi$. The values for the coefficients X_n can be deduced directly from load case (b).

3.4.2 General method of solution

In the following paragraphs, a brief description is given of the solution of a folded shell structure with one or more internal diaphragms. For every Fourier harmonic, the primary structure is analysed under the influence of all external loads, and the absolute displacement components at the diaphragm redundant locations are accumulated. After a sufficient number of Fourier terms have been considered to

ensure adequate convergence, the redundants are calculated by enforcing the appropriate compatibility and equilibrium conditions. The redundants alone are then applied to the primary structure, and the results from this Fourier analysis are added to those obtained earlier, in order to give the final solution for the complete diaphragm structure.

Definition of diaphragm redundant matrix P_D

The assumed nature of all diaphragm redundants is detailed in Section 3.2. A matrix P_D can be defined as the column matrix which is to contain the absolute values of all of these, including both 'distributed' surface redundants (Figure 3.2) and 'concentrated' line-load joint redundants (Figure 3.3). Before P_D can be evaluated, it is necessary to formulate what effects these loads alone would have on the primary structure. Only the m^{th} harmonic will be considered in describing this important part of the complete solution. Diaphragm compatibility and equilibrium conditions will then determine the actual values of the redundants.

Fixed-edge stress resultants induced by unit values of the distributed diaphragm redundants

In Section 3.4.1, particular solutions associated with the various triangularly distributed redundants acting on each element are derived. Fixed-edge solutions induced by unit values of the redundants can be obtained from these by using the same general procedure as described in Section

3.3.2 for obtaining the fixed-edge solutions induced by distributed laterally-uniform external loads. Stress resultants thus found are later used during the assembly of the matrix P_J.

Joint load matrix P_J

As described in Section 3.3.4, there are two contributions to the joint load matrix P_J. In considering the influence of diaphragm redundants on the primary structure, one contribution is due to the direct application of concentrated line-load joint redundants, and the other is due to the indirect application of joint loads caused by the action of distributed redundants under fixed-edge conditions. P_J may therefore be assembled in two stages as suggested by the following matrix equation.

$$P_J = [L_1 + L_2] \cdot P_D = L_3 \cdot P_D \qquad \ldots (101)$$

Matrix L_1 is derived directly from the Fourier expansion (A.2) for unit values of the concentrated joint line-load redundants directly induced by diaphragm action. Matrix L_2 is assembled from equal and opposite reactions to the calculated fixed-edge stress resultants indirectly induced by unit values of the distributed redundants. During this assembly procedure, appropriate coordinate transformations must be performed to ensure that the complete joint load matrix P_J is finally obtained in global coordinates.

Joint displacement matrix Δ_J

The equation which relates the curved joint loads P_J to the corresponding curved joint displacement components Δ_J can be written

$$P_J = L_3 \cdot P_D = K_S \cdot \Delta_J \qquad \ldots (102)$$

and so

$$\Delta_J = K_S^{-1} \cdot L_3 \cdot P_D \qquad \ldots (103)$$

Displacement components at the locations of all diaphragm redundants

(a) Due solely to joint movements:

Under these conditions, let Δ_1 denote the column matrix which is to contain the contribution of this harmonic (m^{th}) to the absolute displacement components at the locations of the diaphragm redundants. (Matrix Δ_1 is thus the same size as matrix P_D). By considering only the homogeneous solutions of the differential equation systems of each folded shell element, and by performing appropriate coordinate transformations, a matrix E_1 can be assembled such that

$$\Delta_1 = E_1 \cdot \Delta_J \qquad \ldots (104)$$

It follows from equation (103) that

$$\Delta_1 = E_1 \cdot K_S^{-1} \cdot L_3 \cdot P_D \qquad \ldots (105)$$

(b) Due solely to the action of distributed redundants under fixed-edge conditions:

Under these conditions, let Δ_2 denote the column matrix which is to contain the contribution of this harmonic to the absolute displacement components at the locations of the diaphragm redundants. (Δ_2 is the same size as both Δ_1 and P_D). By considering combined complementary and particular solutions of the differential equation systems of each folded shell element, a matrix E_2 can be assembled such that

$$\Delta_2 = E_2 \cdot P_D \qquad \ldots (106)$$

In order to obtain the net contribution of this harmonic, the matrices Δ_1 and Δ_2 are to be added. Hence

$$\begin{aligned} \Delta &= \Delta_1 + \Delta_2 \\ &= [E_1 \cdot K_S^{-1} \cdot L_3 + E_2] \cdot P_D \\ &= E_3 \cdot P_D \end{aligned} \qquad \ldots (107)$$

Diaphragm flexibility matrix

The contributions Δ for each harmonic must be accumulated as indicated by equation (108).

$$\left[\sum_{m=1}^{\infty} \Delta \right] = \left[\sum_{m=1}^{\infty} E_3 \right] \cdot P_D \qquad \ldots (108)$$

This equation may be written as follows.

$$\Delta_D = F_D \cdot P_D \qquad \ldots (109)$$

Equation (109) defines the direct relationship between the absolute diaphragm displacement components and the values of the diaphragm redundants, and therefore the square matrix F_D is the true diaphragm flexibility matrix.

Displacement components at the locations of all diaphragm redundants, due to the action of external loads on the primary structure

The general method for solving the problem of external loads on a primary structure is outlined in Section 3.3.4. For each Fourier harmonic, the absolute values of the displacement components at the locations of the diaphragm redundants are calculated. These values are then accumulated for all harmonics. Δ_{m_o} is chosen to denote the column matrix which contains the final values associated with all moveable diaphragms, and Δ_{u_o} is chosen to denote the column matrix which contains the final values associated with all unmoveable diaphragms.

Diaphragm compatibility equation

Let the column matrices of diaphragm redundants which correspond to Δ_{m_o} and Δ_{u_o} be P_m and P_u

respectively, where P_m and P_u together constitute the column matrix P_D. Since each diaphragm is assumed to be infinitely rigid in its own plane, then for each moveable diaphragm, only three absolute displacement components at any location on the diaphragm are necessary to define the final in-plane rigid body movements. For convenience, displacement components (two linear; one rotational) at the same curved joint are chosen for all moveable diaphragms. Let δ_R denote the column matrix which is to contain the total number of these rigid body displacements. Then a matrix B can be assembled in such a way that if δ_R is premultiplied by B, the resulting column matrix will contain the rigid body displacement components at all redundant locations associated with moveable diaphragms. The general compatibility equation can therefore be written as follows, where partitions are used to indicate the contributions of both moveable and unmoveable diaphragms.

$$\begin{bmatrix} \Delta_{u_o} \\ \hline \Delta_{m_o} \end{bmatrix} + \left[\begin{array}{c|c} F_{D_{uu}} & F_{D_{um}} \\ \hline F_{D_{mu}} & F_{D_{mm}} \end{array}\right] \cdot \begin{bmatrix} P_u \\ \hline P_m \end{bmatrix} = - \begin{bmatrix} 0 \\ \hline B \end{bmatrix} \cdot \delta_R \qquad \ldots (110)$$

Equilibrium equation for moveable diaphragms

All moveable diaphragms are supported solely by the folded shell structure, and so equilibrium is expressed by the equation

$$B^T \cdot P_m = 0 \qquad \ldots (111)$$

where B^T is the transpose of matrix B.

Diaphragm redundants

Equations (110) and (111) are combined and solved as indicated by equation (112).

$$\left[\begin{array}{c} P_u \\ \hline P_m \\ \hline \delta_R \end{array}\right] = -\left[\begin{array}{c|c|c} F_{D_{uu}} & F_{D_{um}} & 0 \\ \hline F_{D_{mu}} & F_{D_{mm}} & B \\ \hline 0 & B^T & 0 \end{array}\right]^{-1} \cdot \left[\begin{array}{c} \Delta_{u_o} \\ \hline \Delta_{m_o} \\ \hline 0 \end{array}\right] \qquad \ldots (112)$$

The actual values of the diaphragm redundants can be calculated from this equation. Should all diaphragms be moveable, then $F_{D_{uu}}$, $F_{D_{um}}$, $F_{D_{mu}}$ are all (0 × 0) matrices. Should all diaphragms be unmoveable, then $F_{D_{um}}$, $F_{D_{mu}}$, $F_{D_{mm}}$, B, B^T are all (0 × 0) matrices. Once the redundants are known, their influence on the primary structure can be evaluated by using the equations developed earlier.

Final results, in member coordinates, at selected points on each element

For every Fourier harmonic, due to the presence of the diaphragm loads P_D, equation (83) must be modified to include additional particular solutions on the right hand side. It then becomes

$$R_{(b)} = H_1 \cdot C + H_2 \cdot P_{ext} + H_3 \cdot P_{diaph} \qquad \ldots (113)$$

where P_{diaph} is the column matrix which contains the actual values of all distributed diaphragm redundants acting on this element. (There are four such redundants per diaphragm).

Similarly, equation (84a) must be modified to include additional particular solutions on the right hand side. Therefore

$$\delta_M = G \cdot C + G_1 \cdot P_{ext} + G_2 \cdot P_{diaph} = 0 \qquad \ldots (114)$$

From equation (114), it follows that

$$C = -G^{-1} \cdot [G_1 \cdot P_{ext} + G_2 \cdot P_{diaph}] \qquad \ldots (115)$$

and so equation (113) can be written

$$R_{(b)} = [H_2 - H_1 \cdot G^{-1} \cdot G_1] \cdot P_{ext} + [H_3 - H_1 \cdot G^{-1} \cdot G_2] \cdot P_{diaph} \qquad \ldots (116)$$

The solution for this harmonic is the sum of $R_{(a)}$ and $R_{(b)}$. Hence

$$R_{(a)} + R_{(b)} = [H_1 \cdot G^{-1}] \cdot \delta_M + [H_2 - H_1 \cdot G^{-1} \cdot G_1] \cdot P_{ext} + [H_3 - H_1 \cdot G^{-1} \cdot G_2] \cdot P_{diaph} \qquad \ldots (117)$$

Appropriate sine and cosine factors are then applied to these amplitudes, and the final solution is obtained by accumulating the absolute results for all harmonics.

3.5 Summary

In the preceding description of the folded shell method of analysis, extensive use is made of direct matrix

algebra. With the exceptions of the two component matrices (G and H) required in the formation of the element stiffness matrices, for the sake of brevity the detailed assembly of the various matrices is not discussed. However, all of the fundamental information necessary for their assembly is given, and in each case, only simple substitutions and manipulations are necessary. (Further details of the assembly of these matrices are given in Appendix C, where a simple three-element folded shell structure with a single diaphragm is considered as an illustrative example). It is for this reason that the whole procedure is suitable for programming on a large - capacity, high-speed digital computer. Consequently, a general program known as FOLSHEL has been prepared, to analyse folded shell structures with or without internal diaphragms. Approximately 3,000 separate FORTRAN IV statements are involved, and this fact emphasizes the extremely large number of calculation steps in the complete solution. However, in spite of its length, the program is very simple to use. The exact format of all required input data is carefully specified, and the computed results are printed in tables with appropriate headings. (Further comment on the FOLSHEL program is given in Appendix D).

At first sight, it would appear that separate treatment of the flat plate and cylindrical elements is unnecessary, as these could perhaps be considered as particular cases of a general conical shell element. The reason for maintaining the three element types is that the solution of a conical shell

requires much more computational effort than the solution of either of the other two types, due to the presence of infinite series which must be evaluated for every Fourier harmonic. However, since the chosen flat plate particular solutions cannot be used when $\beta = 1, 2, 3, 4,$ or 5, then for these particular harmonics only, each flat plate is analysed automatically as a degenerate conical shell by the FOLSHEL program. This technique is considered preferable to the alternative of deducing and programming special particular solutions.

Throughout all of the calculations, the key to the method is the simple matrix formulation of the eighth order differential equations, as detailed in Section 3.3.1. This procedure is an extension of an original suggestion by JENKINS[114] in 1947, followed up by SCORDELIS and LO[115] in 1964, concerning the matrix analysis of cylindrical shell segments supported along their straight (generator) edges.

4. EXPERIMENTAL INVESTIGATION

4.1 Introduction

No matter how sophisticated an analysis may be, its true worth cannot be evaluated until it has been checked against experimental values obtained from the real structures which the theory attempts to represent. As part of the present study, two plastic models of curved box beams were constructed and tested to check the predictions of the folded shell theory.

For any curved box beam structure with internal diaphragms, the FOLSHEL program includes an analysis of the primary structure. A model of a typical twin-cell primary structure was built to check the accuracy of this portion of the calculation procedure. Another model was then constructed similar to the first, except for the inclusion of a single moveable diaphragm at quarter span. In this chapter, the fabrication, instrumentation, and testing of these models are described.

4.2 Selection of Materials

In the folded shell analysis, it is assumed that each shell element is isotropic, homogeneous, and linearly elastic. Some commercial plastics closely approximate these requirements, and since they also have low moduli of elasticity and are simple to machine and fabricate into curved shapes, they are ideal for modelling curved box beam bridges.

WALLACE[116] conducted an extensive investigation into the elastic properties of a few commercial thermoplastics

which have previously been used for structural model analyses[117, 118,119]. Special attention was given to the effects of creep, temperature, and relative humidity. He concluded that the P.V.C. plastic known as Vybak was a superior modelling material. Accordingly, models for the current investigation were fabricated from flat sheets of rigid grey Vybak, nominally $\frac{1}{4}$" thick.

During a series of tests conducted at the University of Adelaide concerning the bonding of plastics, it was discovered that Vybak could be efficiently 'cold-welded' by using a commercial dental repair material known as Prothoplast Subiton. This is supplied in the form of a clear liquid and a fine white powder. When mixed, a chemical reaction occurs, ultimately resulting in the formation of a transparent solid. Almost full strength is achieved only a few minutes after the mixing. Preliminary bending and tensile tests on a number of joint types indicated that the weld strength was well in excess of that required to ensure perfectly rigid connections between Vybak members loaded to the limit of the elastic range, claimed by Wallace[116] to be approximately 3,200 p.s.i. Since cured Prothoplast Subiton is essentially an acrylic plastic, its modulus of elasticity is considered to be sufficiently close to that of Vybak for it to be used as a suitable gap-filling weld material. No special joint preparation is necessary to achieve excellent bonding.

4.3 Construction and Testing of Primary Structure

4.3.1 Dimensions

Middle-surface dimensions of the chosen cross

section are shown in Figure 4.1. The cross section was symmetrical about the vertical centre-line, and all elements were $\frac{1}{4}$" thick. (These proportions are similar to those of typical modern prestressed concrete elevated roadway bridges). The curved beam subtended an angle of 60° at the axis of rotation, and superelevation was taken to be zero. For future reference, joints are numbered 1, 2, ... 8 and folded shell elements are numbered (1), (2) ... (9) as shown in Figure 4.2. Joint 8 represents the inner radius (36") of the curved box beam, and joint 1 represents the outer radius (49"). Preliminary runs with the FOLSHEL program indicated that a Vybak model with these dimensions would give suitable elastic deflections and strains when loaded with a concentrated load of approximately 150 lb. at midspan.

The method of supporting the beam is schematically shown in Figure 4.3. (Details of end diaphragms are omitted from this sketch). Slender columns ($\frac{1}{4}$" Vybak) were clamped at their bases, and were rigidly connected (welded) to the box beam ends. Two factors governed the choice of the free column length. When the bridge was loaded:

(a) Bending moments induced about the beam-column intersections should be as small as possible in order to simulate the desired simple support condition

(b) The columns should not buckle

As a compromise, 15" was chosen.

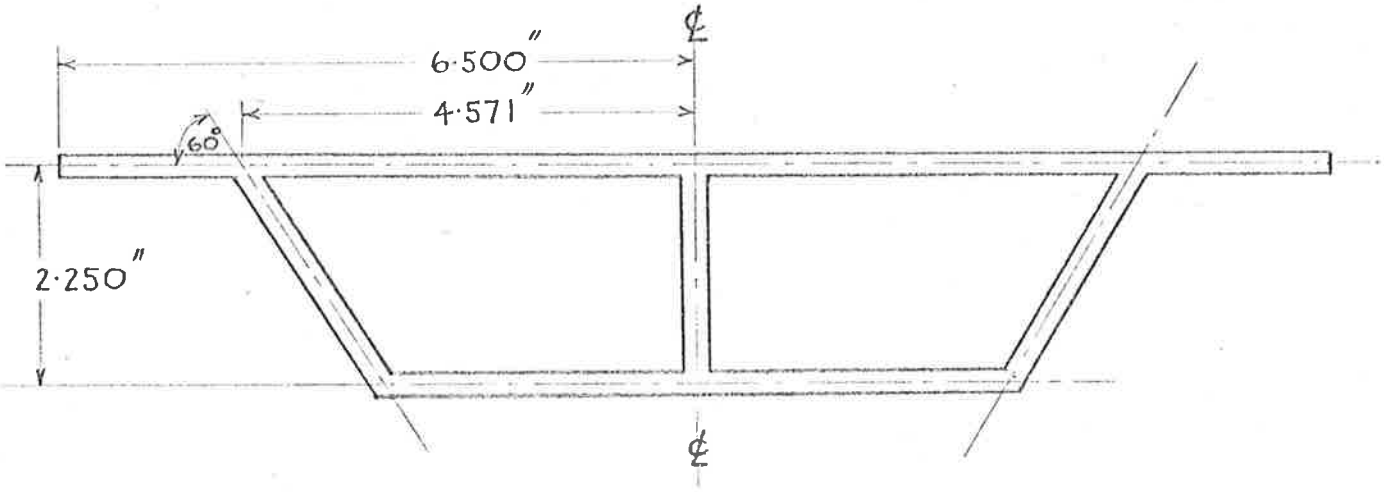

Figure 4.1 Middle-surface dimensions of model cross section

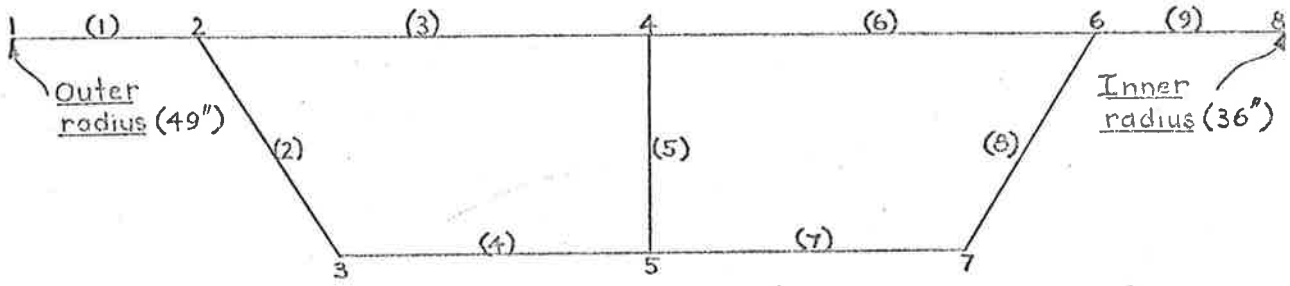

Figure 4.2 Joint and element numbering systems

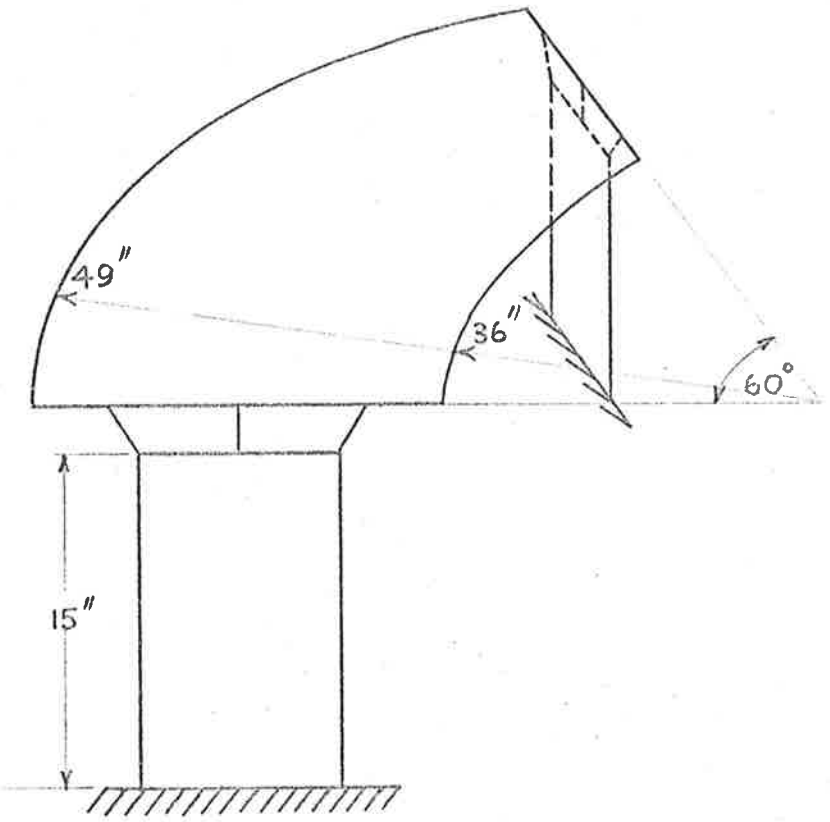

Figure 4.3 Model support conditions

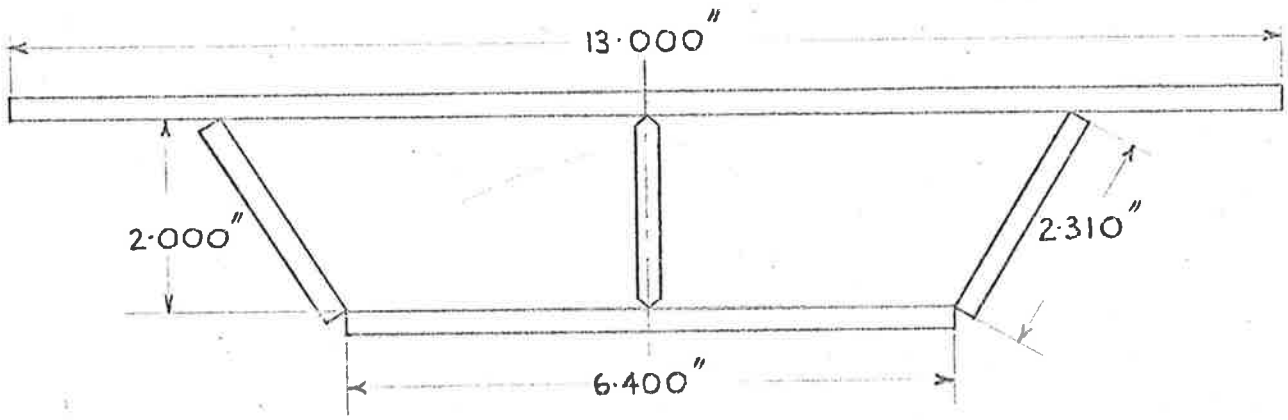

Figure 4.4 Lateral dimensions of constituent pieces

4.3.2 Construction

The beam was constructed as an assembly of two flat plates (top and bottom flanges), one cylindrical shell (central web), and two conical shells (inner and outer webs). These five pieces were first developed on a plane sheet of $\frac{1}{4}$" Vybak. Their lateral dimensions are shown in Figure 4.4. Radial lines corresponding to 5° increments on the final structure were scribed on both sides of each piece. In addition, circular arcs were scribed to indicate lateral division of elements (3) and (6) into four equal parts, and lateral division of the remaining seven elements into three equal parts. (Division was based on the middle-surface dimensions of Figure 4.1).

Each piece was then cut from the plane sheet, and machined to its correct lateral dimensions. However, several inches were left in excess of the circumferential dimensions. There were two important reasons for this excess.

(a) During the welding sequence, the extra length of the three web pieces would enable their desired constant curvature to be maintained even at the extreme ends of the beam.

(b) After all five pieces had been welded together, a single vertical cut at each end of the beam would automatically ensure a perfectly planar finish.

Edges of the central web were machined at 45° as shown in Figure 4.4, in preparation for the double-vee butt welds which were to eventually connect them to the top and bottom flanges. At

this stage, those strain gauges which had to finish on the inside of the completed box beam were applied to each piece. (Details of all instrumentation are given in Section 4.3.3).

The chosen welding sequence is shown in Figure 4.5

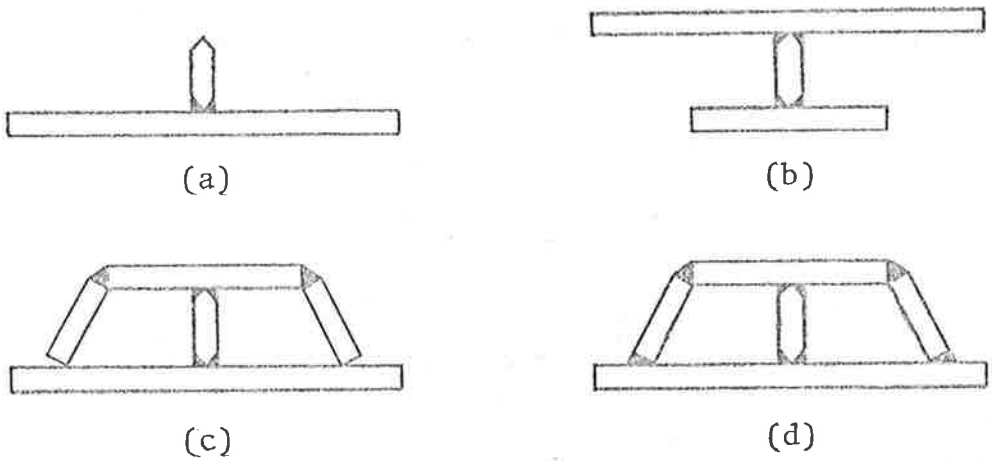

Figure 4.5 Welding sequence

Figure 4.5(a) indicates the connection of the vertical web to the inverted top flange. The web was cold-bent into its correct lateral position by clamping it so that the concave surface was held vertical and flush against a template of appropriate radius (42.375"). Gaps were provided in the template to avoid interference with the strain gauges previously affixed to the top flange and the concave surface of the web. The outer half of the connecting butt weld was completed along the full beam length, and after removal of the template, the inner half was completed. The 'T'-shaped structure thus formed was then inverted and clamped in position on the bottom flange as indicated in

Figure 4.5(b). Several spacers were used to maintain the required 2" distance between the top and bottom flanges. Plate 4.1 shows a view of the clamped structure in convenient angular position for completing the outer half of the required connecting butt weld. By reversing the inclination of the supporting table, the inner half was also completed. At this stage, the model appeared as shown in Plate 4.2. Figures 4.5(c) and 4.5(d) indicate the external fillet weld connections of the inclined webs to the top and bottom flanges. Each web was cold-bent and positioned so that for every cross section along the structure, point to point contact was established between it and the bottom flange. A series of stitch welds was used to maintain this condition. Plate 4.3 shows one of the inclined webs after being stitch-welded to the bottom flange. Since the lateral dimension of each web had been accurately maintained during the fabrication, several templates cut to exactly 120° were used to establish the correct contact arc between the web and the top flange. The exact nature and use of these templates are shown in Figure 4.6. Stitch welds were again used to maintain this condition throughout the full length of the beam. Finally, all four fillet welds were completed, and the beam was cut to length at the 0° and 60° cross sections. Plate 4.4 shows the model just prior to being cut to length.

End diaphragms and supporting columns were to be made from $\frac{1}{4}$" Vybak. Holes were drilled in each diaphragm to ensure uniform temperature conditions inside and outside of

PLATE 4.1 Model in position for welding vertical web to bottom flange.

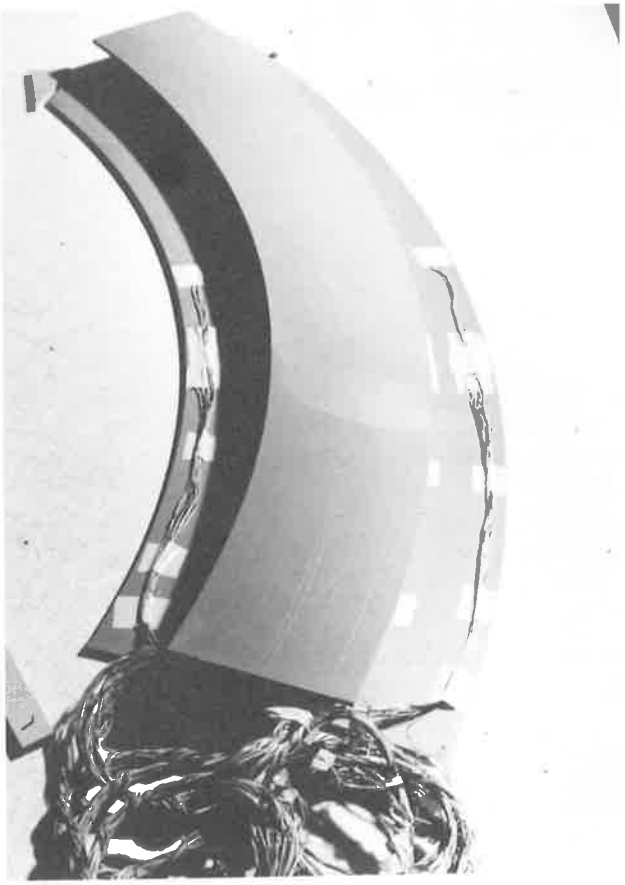

PLATE 4.2 Model after completion of vertical web butt welds.

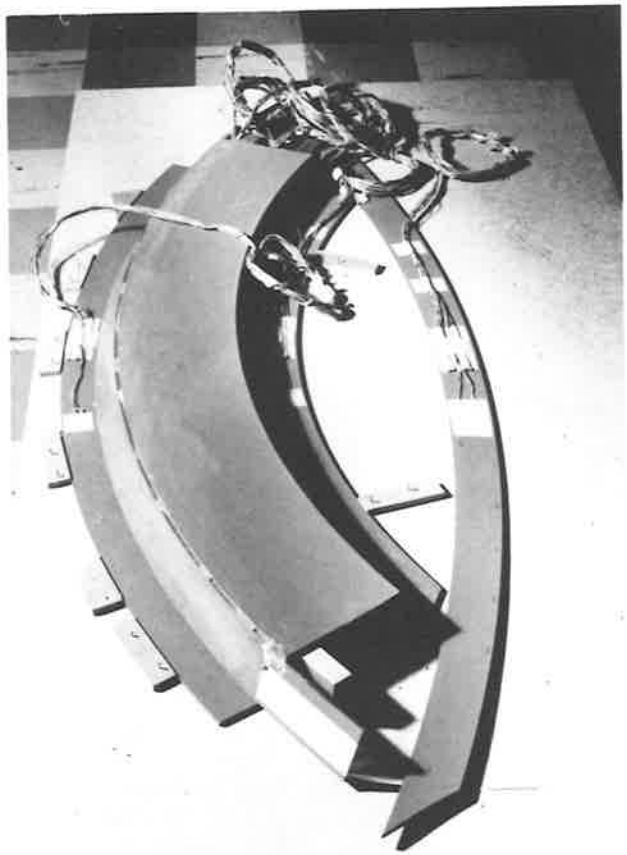

PLATE 4.3 Model after stitch-welding one inclined web to bottom flange.

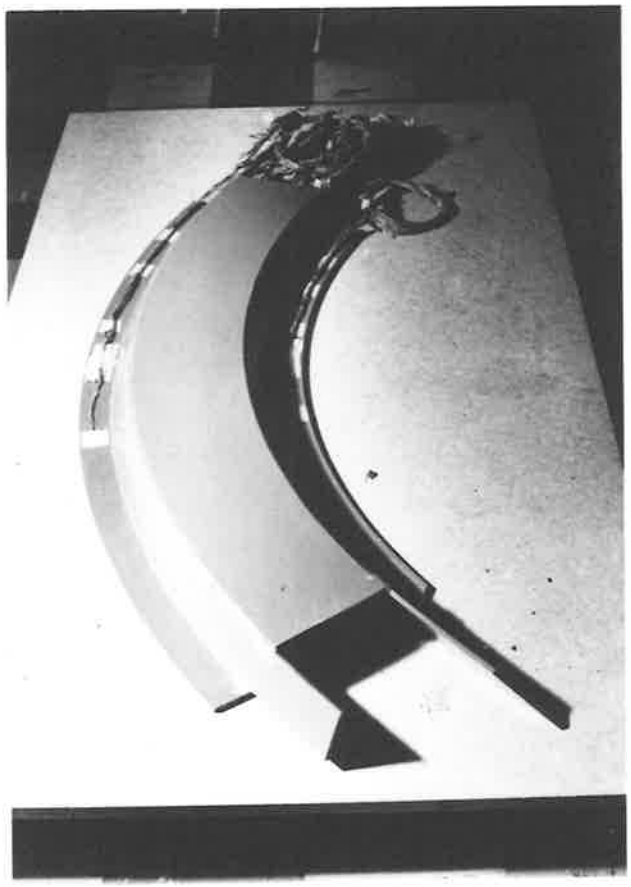

PLATE 4.4 Model after completing all inclined web fillet welds.

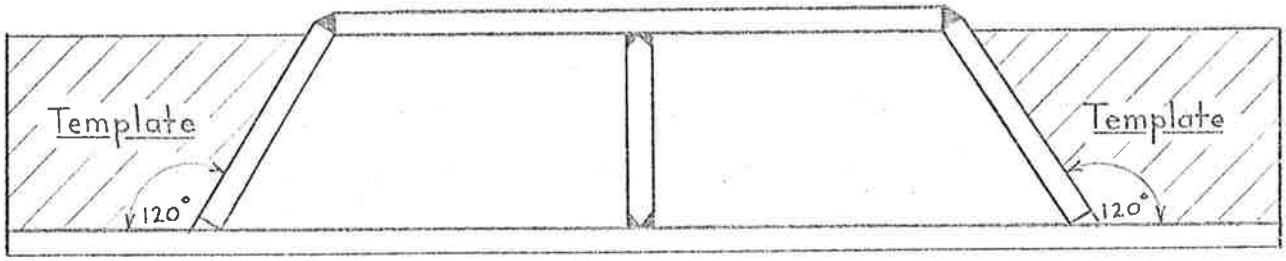

Figure 4.6 Templates used to establish location of inclined web-top flange connection

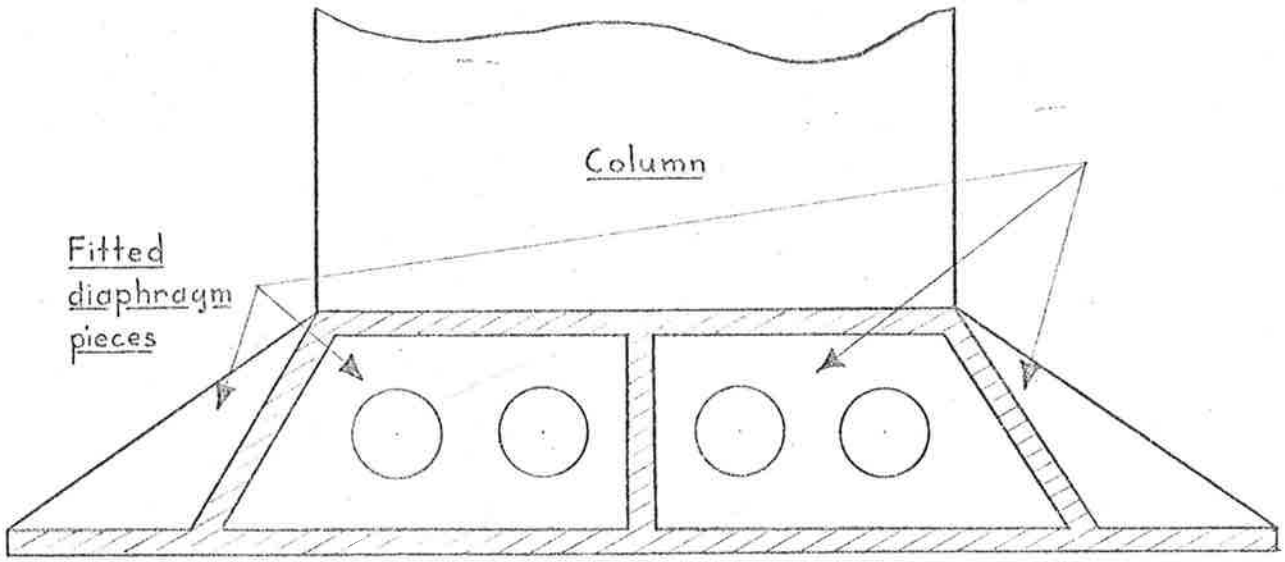

Figure 4.7 End view of completed model

the beam, and to enable the internal strain gauge leads to be brought to the outside. Each portion of the diaphragm was fitted to the shape of the end cross section, and was positioned so that half of its thickness projected beyond the end of the beam. Similarly, each column was positioned so that half of its thickness also projected beyond the end of the beam. Sufficient weld material was then applied to connect the curved beam elements to the protruding pieces. In the end view of the completed model shown in Figure 4.7, this weld material is indicated by the hatched areas. Plate 4.5 shows a view of the model at this stage. The total length of the columns was 21" so that 6" could be used for bolting them to steel supporting frames, leaving the desired 15" unsupported. A general view of the completed model mounted in position on the steel frames is shown in Plate 4.6.

4.3.3 Instrumentation

Deflections and strains were measured at selected points on the beam by means of dial gauges and electrical resistance strain gauges respectively.

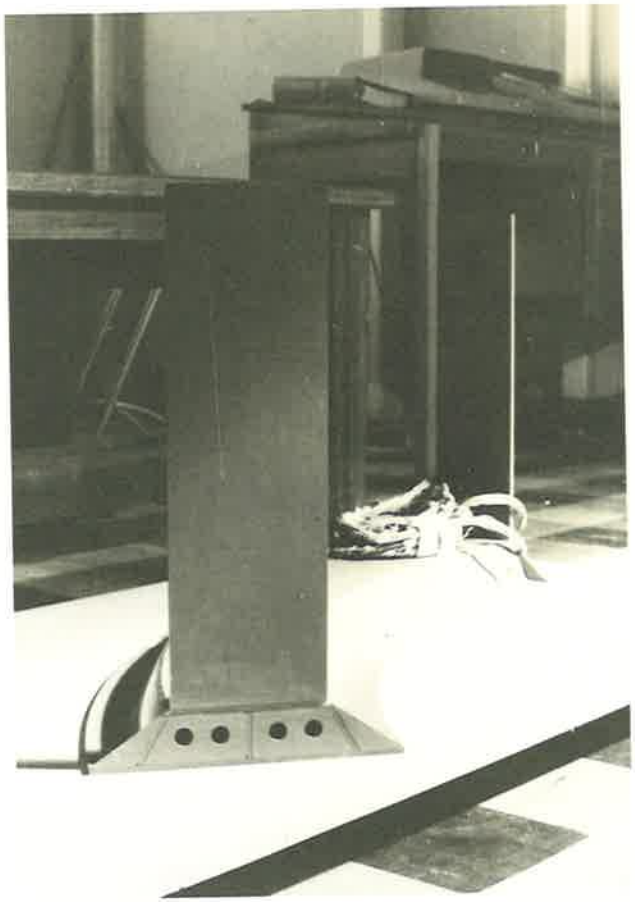

PLATE 4.5 Completed model before bolting in position for testing.

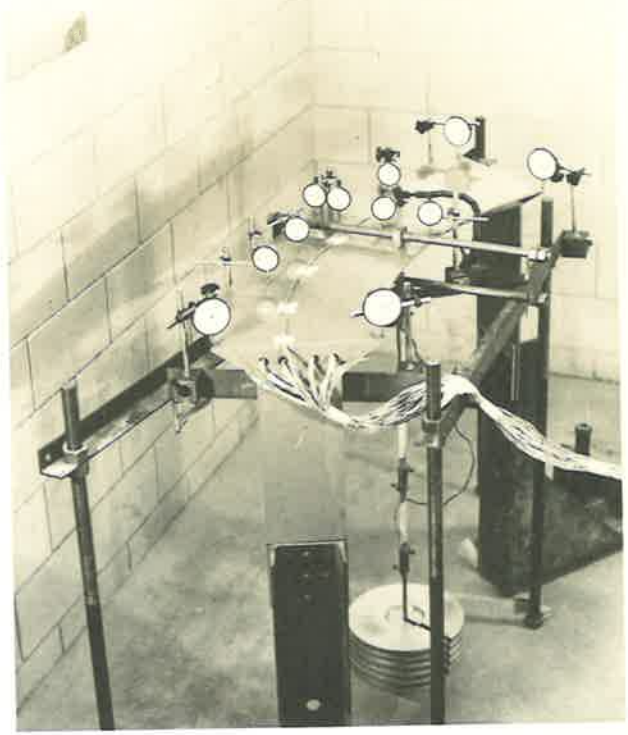

PLATE 4.6 Model during load test.

Measurement of deflections

Figure 4.8 shows a plan view of the top flange of the beam.

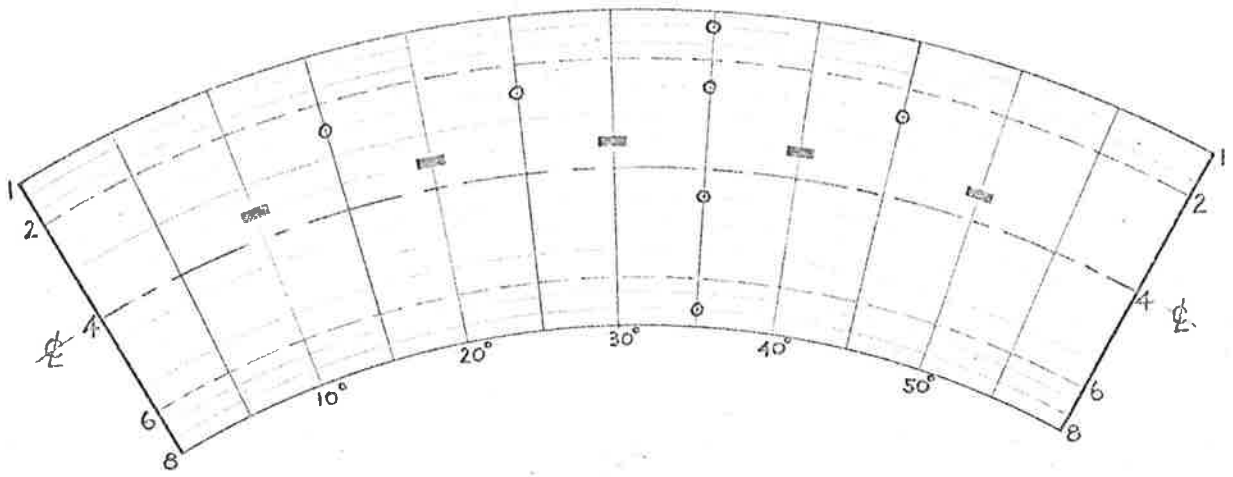

Figure 4.8 Locations of dial gauges and strain gauges on upper surface of top flange

Joints 1, 2, 4, 6 and 8 are clearly marked, together with the surface grid lines described in Section 4.3.2. Seven dial gauges were mounted vertically at the locations marked by small circles. In addition to these, an extra dial gauge graduated in ten-thousandths of an inch was placed at each of the four corners of the top flange in order to measure vertical movements induced by compression and in-plane rotation of the end columns. (The latter measurements were extremely important, since the effects of any rigid body in-plane movements of the end diaphragms had

to be subtracted from the total deflections measured by the seven internal gauges, before any direct comparisons could be made between the experimental results at these points and the corresponding theoretical folded shell predictions. A simple linear interpolation and extrapolation procedure based on the measured corner deflections was used in order to deduce the appropriate quantities to be subtracted). All eleven dial gauges were supported by independent steel frames as shown in Plate 4.6.

Measurement of strains

Figure 4.9 indicates the strain gauges which were used throughout the experimental investigation of both the primary and diaphragm structural models.

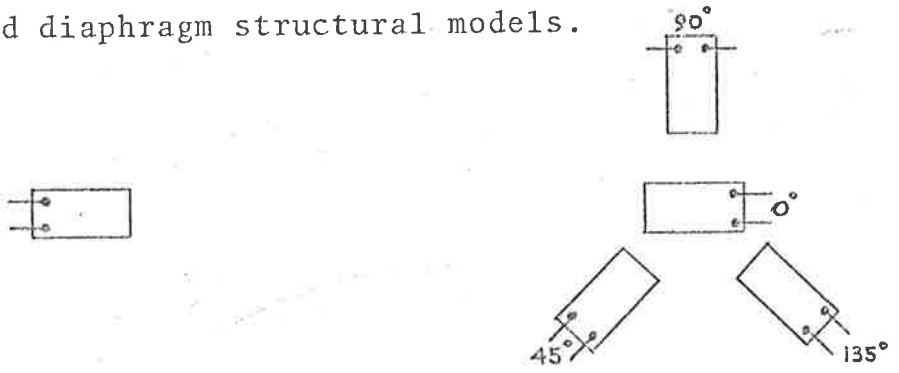

(a) Ordinary strain gauge (b) Strain gauge rosette

Figure 4.9 Strain gauges

All gauge lengths were 2 mm. For the primary structure model, these gauges were used to measure strains at selected points on the 25° cross section and also at selected points on the upper

surface of the top flange. Since only three gauges are necessary to define the complete surface strain condition at the location of a rosette, the fourth gauge is redundant and can therefore be used as a useful check. In this work, the gauge marked 0° (Figure 4.9) was chosen as the redundant gauge.

Figure 4.10 shows the strain gauge instrumentation at the 25° cross section. Most gauges were placed on the interior surfaces of the box beam so that transient changes in temperature due to the movement of air in the vicinity of the model would be reduced to a minimum. As described in Section 4.3.2, when the five component pieces of the model were initially developed, circular arcs were scribed on both sides to indicate lateral division of elements (3) and (6) into four equal parts, and lateral division of the remaining elements into three equal parts. These arcs were used to locate the strain gauges so that after the pieces were welded together, the gauges finished in the positions shown in Figure 4.10. Ordinary gauges are represented by small dark rectangles. They were orientated to record lateral strains. Rosettes are represented by small dark circles. They were orientated so that the gauges marked 45° (Figure 4.9) always pointed in the positive x-directions of the appropriate member coordinate systems. In Figure 4.10, the positive x-direction of each element is indicated by an arrow.

In addition to the strain gauges at the 25° cross section, five ordinary gauges were positioned to measure circumferential strains on the upper surface of the top flange.

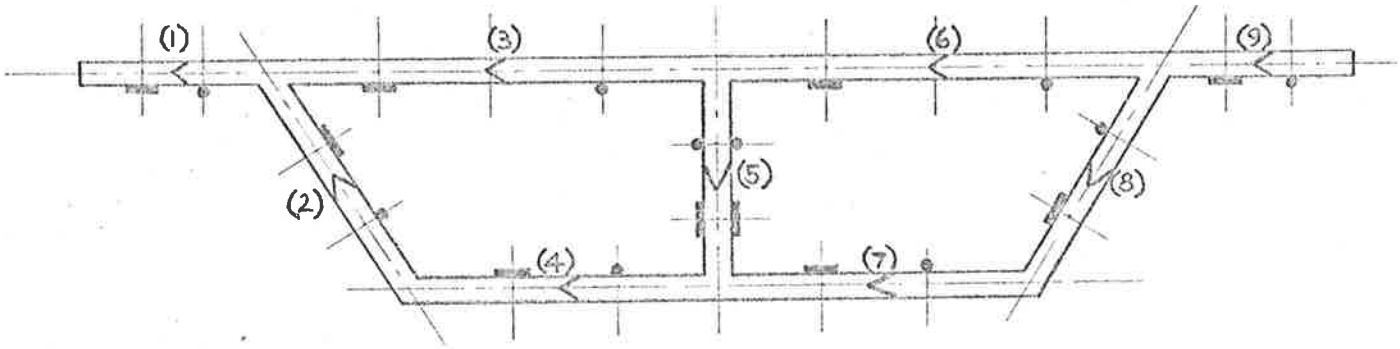

Figure 4.10 Instrumented 25° cross section of primary structure

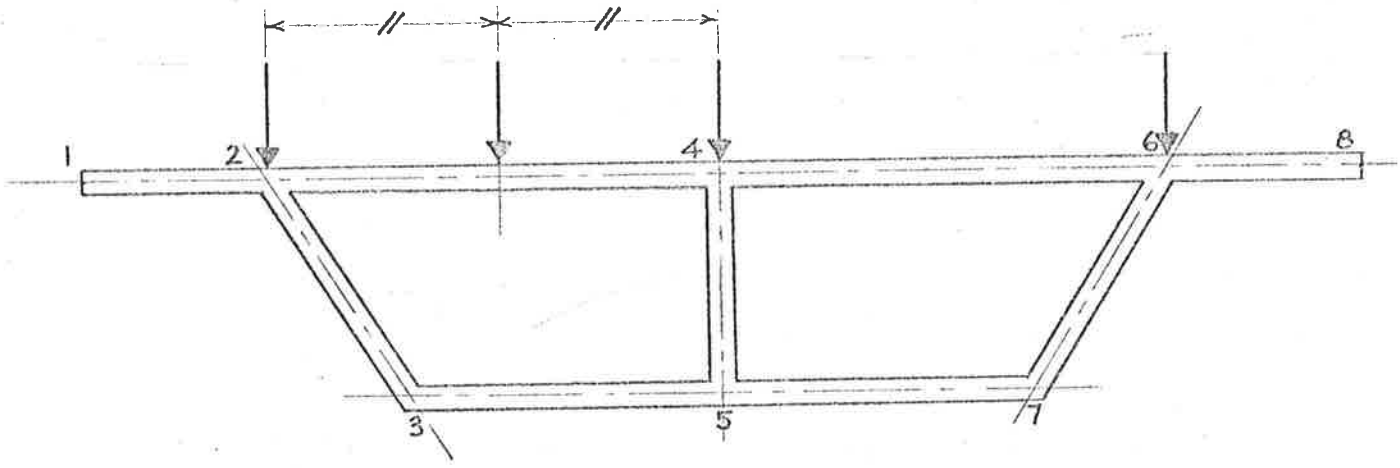

Figure 4.11 Four lateral load positions at 30° cross section

Actual locations of these gauges are shown in Figure 4.8.

All strain gauges were connected to an automatic strain gauge logger capable of reading up to 99 gauges in approximately three minutes. Short reading times were necessary to reduce the effects of creep to a minimum. Throughout any load test, constant current was maintained through every gauge to reduce errors caused by transient heating. As each gauge was read, a value was automatically printed by an electronic typewriter. Typed values were later reduced to actual strains by applying multipliers which incorporated gauge resistances and gauge factors. A view of the strain gauge logger is shown in Plate 4.7.

4.3.4 Application of loads and determination of elastic properties

Weights were used to apply constant vertical loads to the beam via a short knife edge aligned parallel to the circumferential direction. (The actual length of the knife edge was 1.33", which corresponded to a subtended angle of 2° at the axis of rotation when the load was positioned immediately above joint 6). A close-up view of the knife-edge arrangement is shown in Plate 4.8.

In order to obtain the values of Young's modulus (E) and Poisson's ratio (ν) under exactly the same conditions as for the loaded beam, three rectangular specimens were suspended serially between the knife edge and the load hanger.

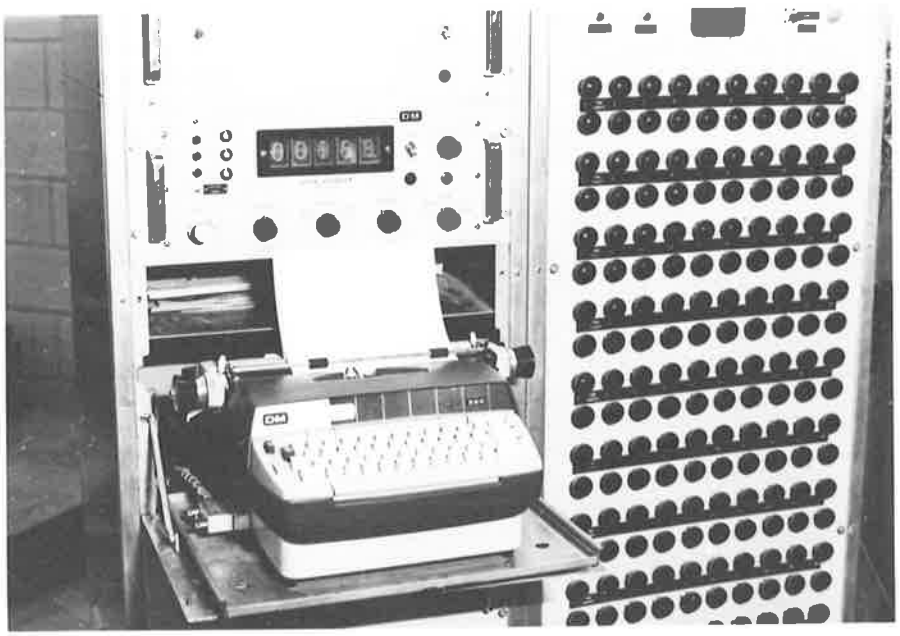

PLATE 4.7 Strain gauge logger with automatic typewriter display unit.

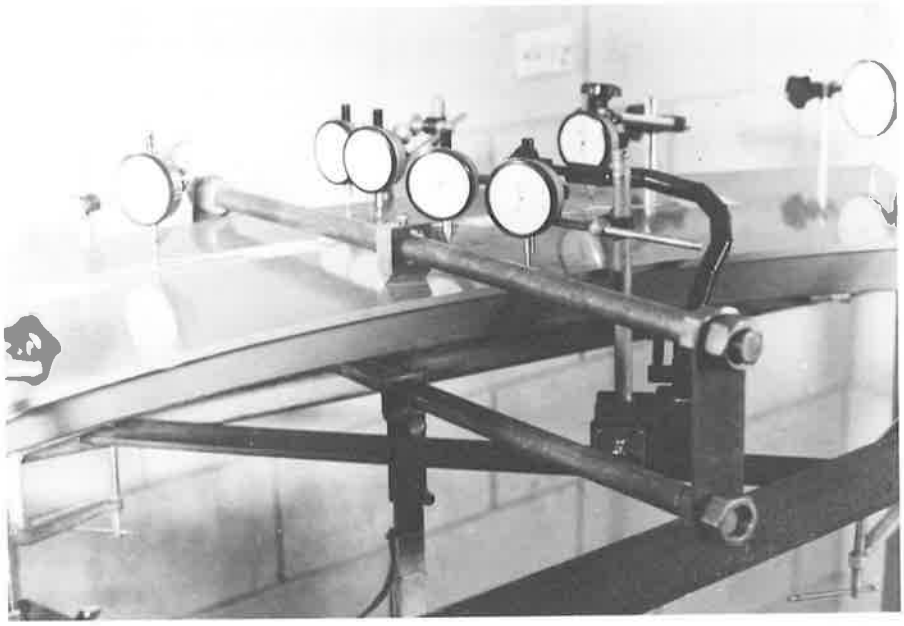

PLATE 4.8 Close-up view of knife edge arrangement.

These specimens were machined from the same sheet of Vybak as was used to fabricate both the primary structure model and (later) the diaphragm structure model. The first specimen was taken parallel to one edge of the original sheet. The second was taken at an angle of 45° to this edge, and the third was taken normal to the edge. Opposite pairs of longitudinal and lateral strain gauges were applied to the faces of each rectangular specimen in order to determine the values of E and ν for every individual load test. During any one test, a comparison of the values indicated by each specimen would give a measure of the degree of isotropy for the original Vybak sheet. Since the variation was subsequently found to be always less than 3%, a simple average of the values indicated by the three specimens was used in the theoretical calculations.

4.3.5 Test procedure

Four separate load tests were conducted, corresponding to four different lateral positions of the knife edge load across the central (30°) cross section of the beam. These positions are indicated in Figure 4.11. The experimental procedure was identical for all four tests, and the various steps are described below.

(a) With zero weights on the hanger, the knife edge was placed in position. A single weight (20 lb.) was then applied.

(b) The strain gauge logger was switched on for some

thirty minutes to allow all strain gauges, including those on the elastic property specimens, to reach steady temperature conditions.

(c) Zero readings were taken for all dial gauges and strain gauges. Five weights of 20 lb. each were then simultaneously applied to the hanger, and after five minutes, all dial gauge and strain gauge readings were again taken*.

(d) The 100 lb. load was removed.

Steps (c) and (d) together constituted one zero-full load cycle. They were executed twice more, each time allowing five minutes for creep recovery upon removal of the load.

4.3.6 Processing experimental results

(a) Since each of the four load tests was executed three times, the first step in processing the experimental results was to obtain averages for the increments in measured deflections and strains due to the applied 100 lb. load.

(b) Simple linear interpolation and extrapolation was used to correct the measured vertical deflections for rigid body movements of the end diaphragms.

---

* Preliminary tests showed that after 5 minutes, there was no measurable change in any of the readings as a result of creep.

(c) Inspection of the rosette in Figure 4.9 indicates clearly that apart from the gauge marked 0°, all three other gauges were a finite distance from the centre of the rosette. Due to the presence of high lateral strain gradients, this shift had to be taken into account before a comparison could be made between the measured strains and the strains predicted by the folded shell analysis. Consequently, by using the predicted theoretical strain gradients at the rosette centre, the experimental values of the three gauges were modified to allow for their eccentricity.

Since the predicted gradients in the circumferential direction were comparatively small, for the purpose of these calculations they were taken to be zero. Once the experimental strains had been transferred to the centre of the rosette, the 'experimental' value of the shear strain could be found from Mohr's circle considerations in the usual way. Details of the calculations for eccentric rosette gauges are presented in Appendix E.

4.4 Construction and Testing of Diaphragm Structure

4.4.1 Dimensions

Dimensions of the diaphragm structure were identical to those of the primary structure, except that the thickness of the end diaphragms (and of the additional internal diaphragm) was only $\frac{1}{8}$". The thickness was reduced so that the

resistance of the diaphragms to curved beam warping displacements would also be reduced.

4.4.2 Construction

The same general method of construction was used for the diaphragm structure as for the primary structure. (Details of the strain gauge instrumentation required before the assembly of the five developed pieces are given in Section 4.4.3). However, when the model had reached the stage indicated in Figure 4.5(b), the internal diaphragm was welded into position at the 45° cross section. Figure 4.12 shows a view of the two halves of the diaphragm in their correct positions ready for welding. This particular view is towards the 0° cross section. Edges in contact with the I-shaped structure were machined on both sides, in preparation for double-vee butt welds. The two inclined edges were machined from one side only, in preparation for fillet welds which were later to be applied from the nearer open end of the beam (60°) after the stage indicated in Figure 4.5(d) had been reached. Plates 4.9 and 4.10 show two views of the I-shaped structure with the internal diaphragm welded in position.

The method of fixing the end diaphragms and supporting columns in position was identical to that of the primary structure. However, since the diaphragms were only $\frac{1}{8}$" thick, each portion (Figure 4.7) was positioned so that only $\frac{1}{16}$" projected beyond the beam end.

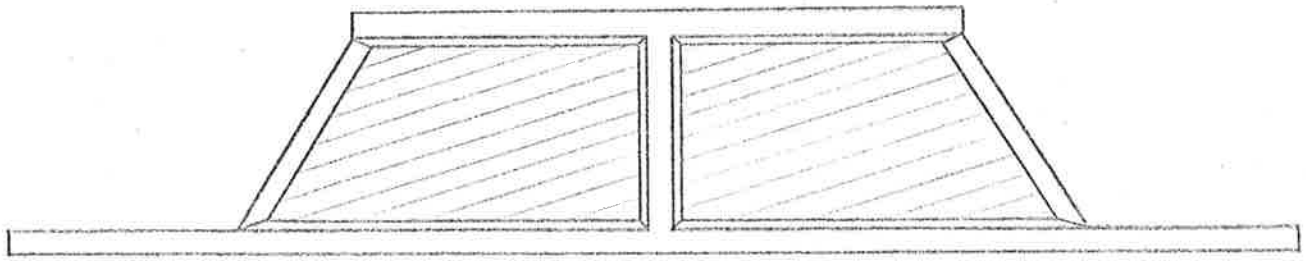

Figure 4.12 Internal diaphragm ready for welding

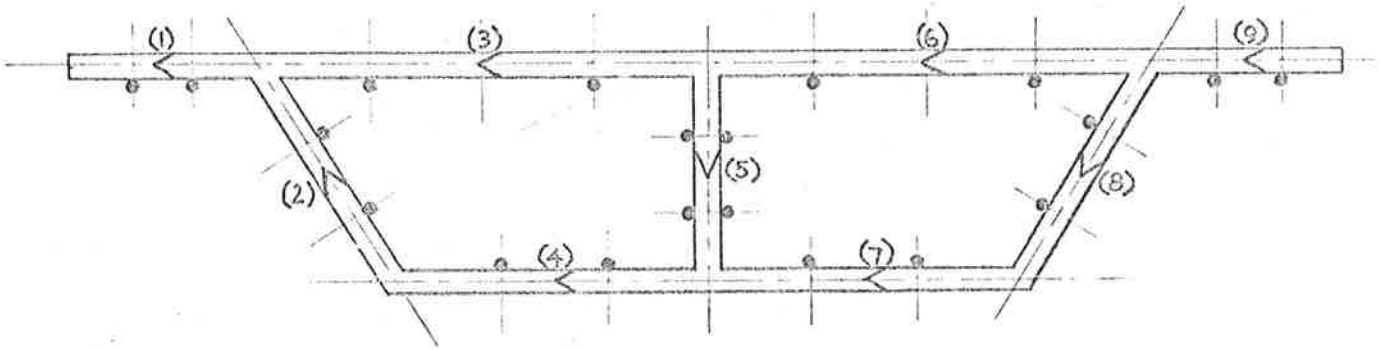

Figure 4.13 Instrumented 25° cross section of diaphragm structure

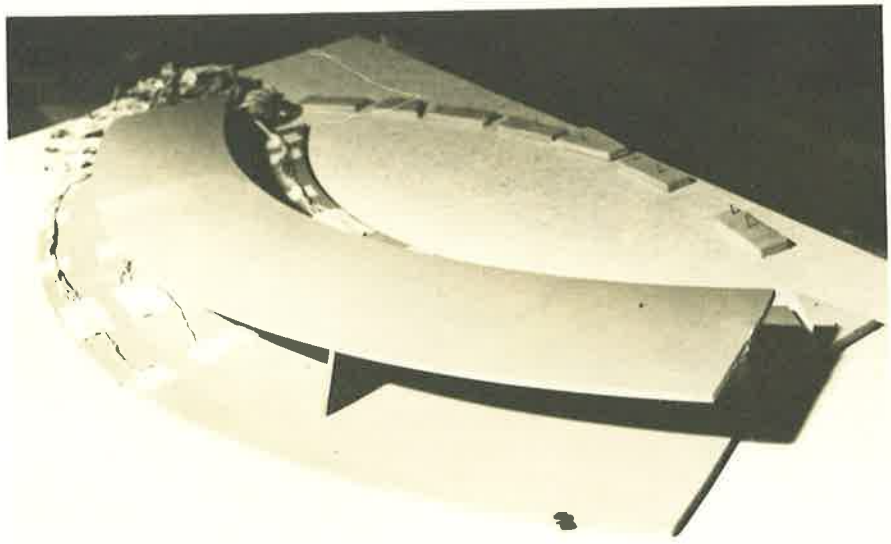

PLATE 4.9 I-shaped model with internal diaphragm in position.

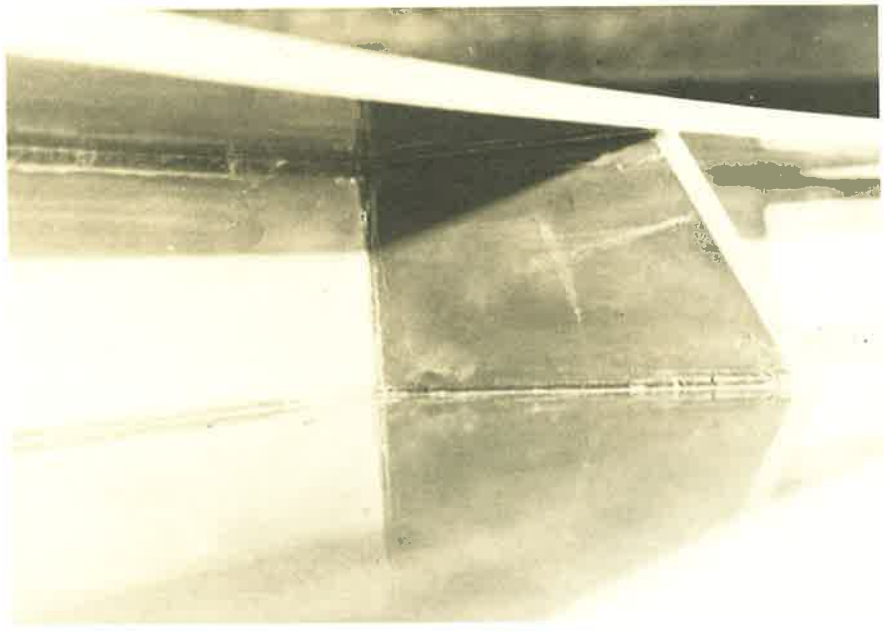

PLATE 4.10 Close-up view of internal diaphragm.

4.4.3 Instrumentation

In order to measure any different effects caused by the internal diaphragm, the diaphragm structure was instrumented for stresses and strains at the same selected points as for the primary structure. However, some additional strain gauge instrumentation was also provided. Instrumentation of the upper surface of the top flange was identical to that shown in Figure 4.8.

The instrumented 25° cross section of the diaphragm structure is shown in Figure 4.13. (Comparison with Figure 4.10 reveals that instead of using ordinary gauges at half of the chosen points, rosettes were used throughout). Orientation of all rosettes was the same for both models.

Figure 4.14 shows the 35° cross section of the diaphragm structure and its associated strain gauge instrumentation. Once again, most of the gauges were placed on the interior surfaces of the box beam in order to reduce the transient changes in temperature caused by movement of air in the vicinity of the model. All gauges were ordinary, and were orientated to measure circumferential strains. Unfortunately, the two gauges on element (1) were damaged during construction of the model, and failed to operate during the load tests. These gauges were not replaced because they could not be removed easily from the plastic without damaging the smooth surface. Sufficient experimental evidence was obtained without them.

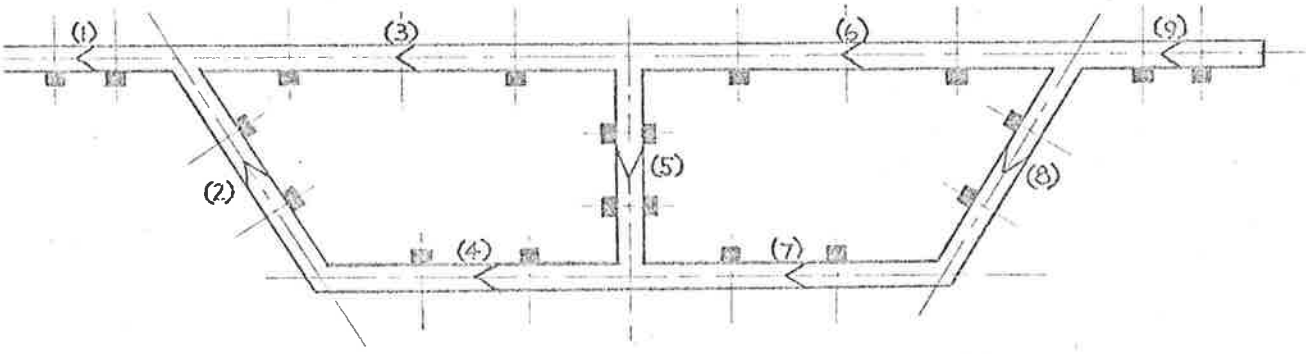

Figure 4.14 Instrumented 35° cross section of diaphragm structure

	PRIMARY STRUCTURE		DIAPHRAGM STRUCTURE	
LOAD TEST	E(p.s.i.)	ν	E(p.s.i.)	ν
1 (Joint 6)	4.34×10^5	0.36	4.35×10^5	0.36
2 (Joint 4)	4.34×10^5	0.36	4.35×10^5	0.36
3 (Joint 2)	4.38×10^5	0.36	4.37×10^5	0.37
4 (Plate (3))	4.38×10^5	0.36	4.35×10^5	0.36

Table 4.1 Values of E and ν

The application of loads and determination of elastic properties, test procedure, and processing of experimental results were all exactly as described in Sections 4.3.4, 4.3.5, and 4.3.6 respectively.

4.5 Summary

For each of the four load tests conducted on both models, values of E and ν determined by the suspended specimens are tabulated in Table 4.1. These values were used in the FOLSHEL program to obtain theoretical predictions for all quantities measured experimentally. (21 Fourier harmonics were used in these analyses). Final experimental and theoretical results for deflections and actual-surface lateral, circumferential, and shear strains are presented graphically in Figures 4.15-4.34. The experimental results are indicated by discrete points, whereas the theoretical predictions are indicated by uniformly dashed lines. In Figures 4.15, 4.16, and 4.21-4.34, the various lateral positions of the knife-edge load are indicated by bold arrowheads. However, it should be remembered that in every case, the load was applied at the midspan cross section (30°) and not at the instrumented cross sections (25° and 35°).

Where the strain results are shown for a particular cross section (Figures 4.21-4.34), only the middle-surfaces of the elements which comprise that section are drawn, and all strains are plotted normal to these. Consequently, when interpreting the strain results, Figures 4.10, 4.13, and 4.14

should be considered in order to avoid any possible confusion as to which actual-surfaces of the cross section are associated with the plotted values. Due to the fact that the vertical web was always instrumented on both the concave and convex surfaces, then in this case only are the corresponding strain results specifically identified in each figure. Tensile and compressive strains are indicated by plus and minus signs respectively. Since all of the strains in Figures 4.21-4.34 are plotted to the same small scale, the actual values obtained from both the theoretical and experimental analyses are given, and the magnitude of any discrepancy is therefore clearly evident. It is the experimental values which are written in brackets.

Discussion of the correlation between all theoretical and experimental results is given in Section 5, together with some general comments concerning the observed structural behaviour of the two bridge models.

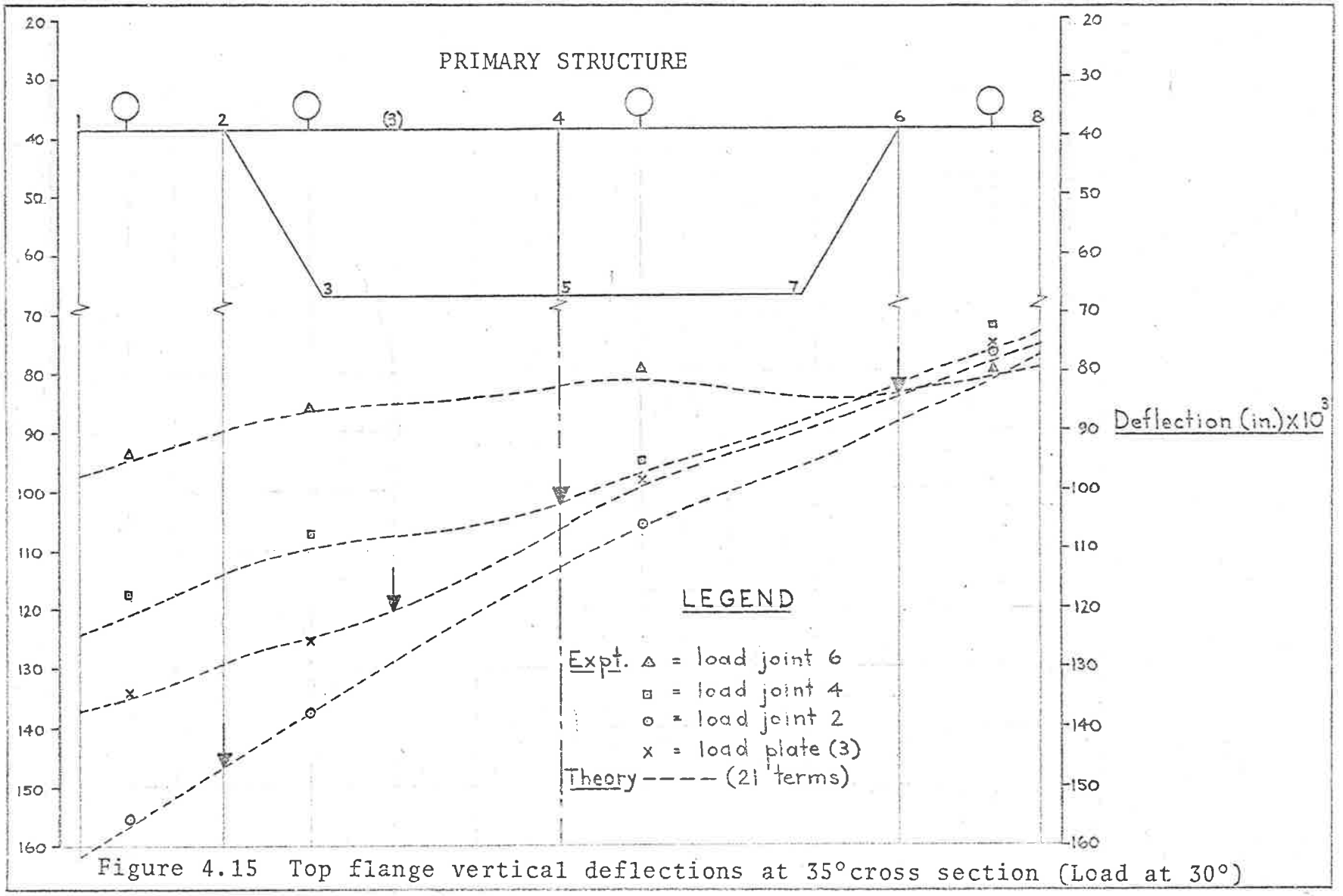

Figure 4.15 Top flange vertical deflections at 35°cross section (Load at 30°)

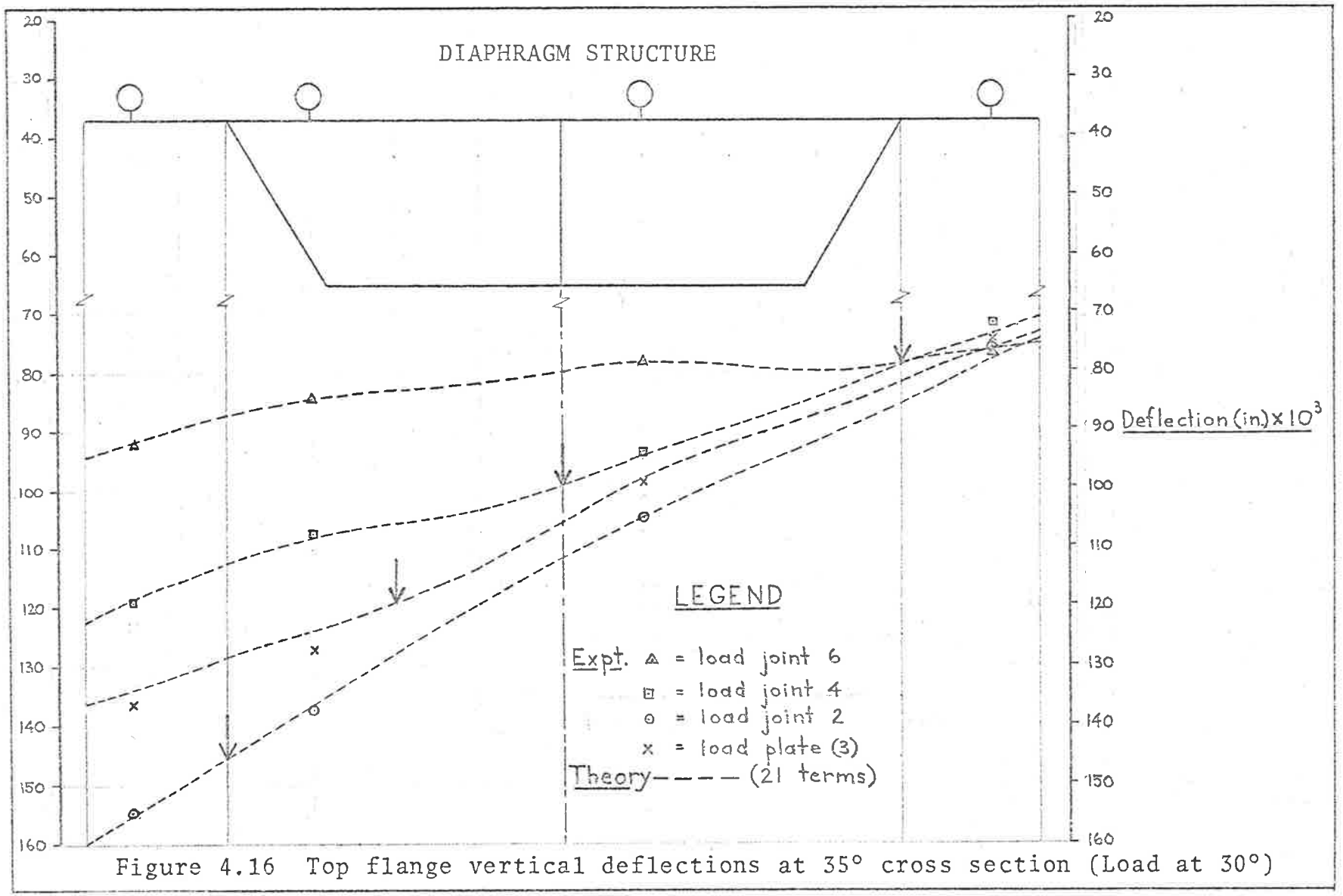

Figure 4.16 Top flange vertical deflections at 35° cross section (Load at 30°)

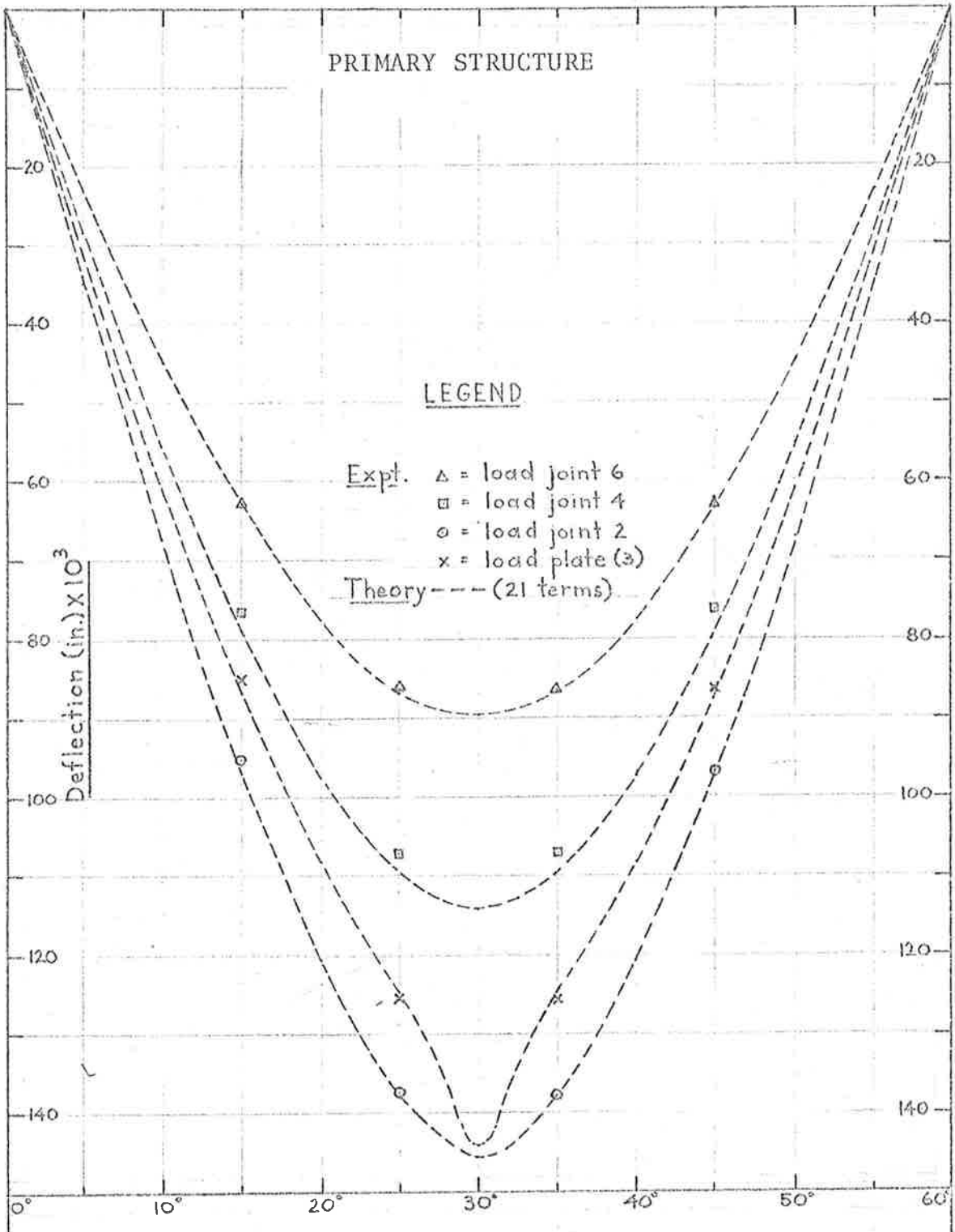

Figure 4.17 Top flange vertical deflections at R = 45.93" (Load at 30°)

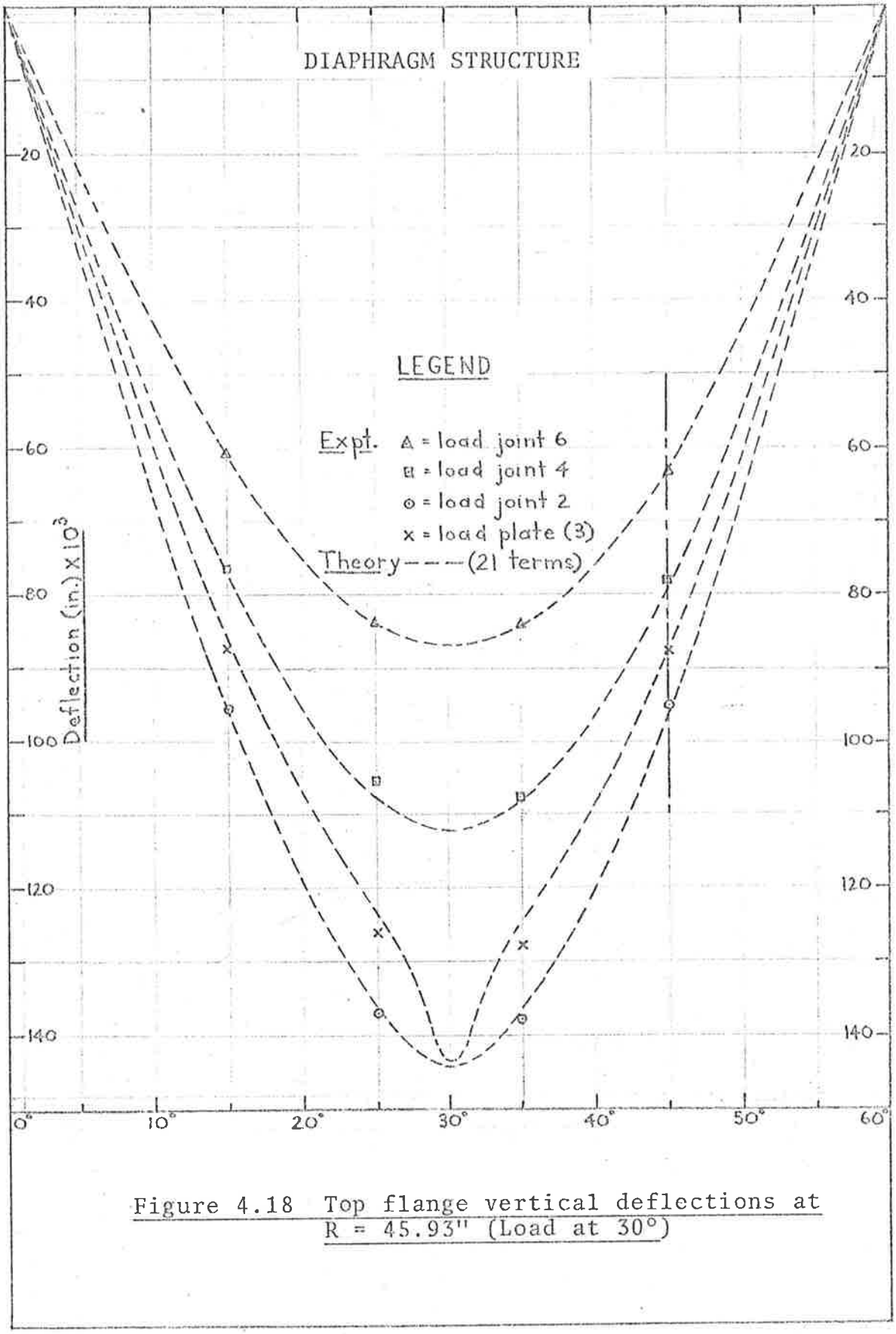

Figure 4.18 Top flange vertical deflections at R = 45.93" (Load at 30°)

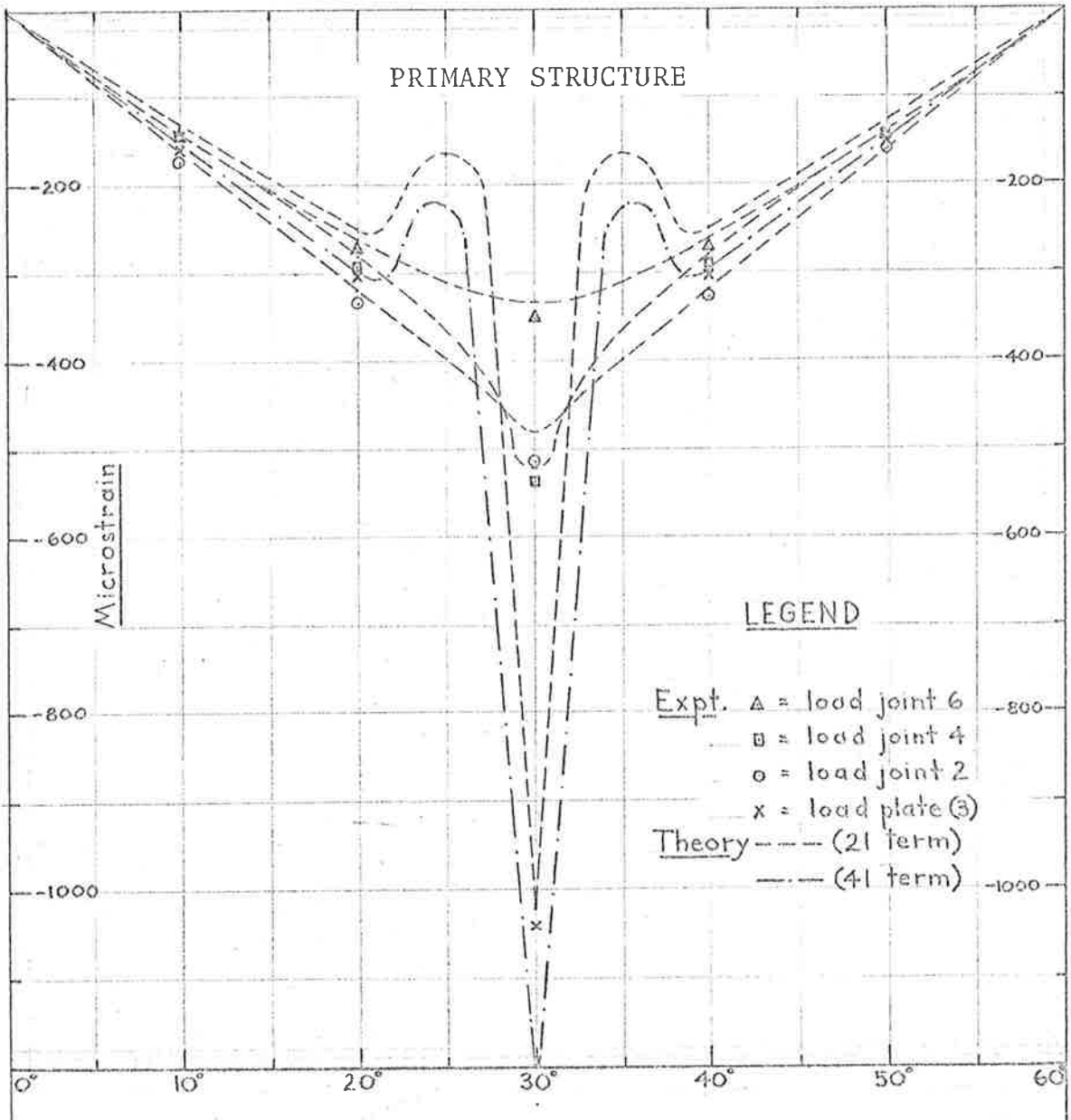

Figure 4.19 Top flange upper surface circumferential strains (Load at 30°) at R = 43.64"

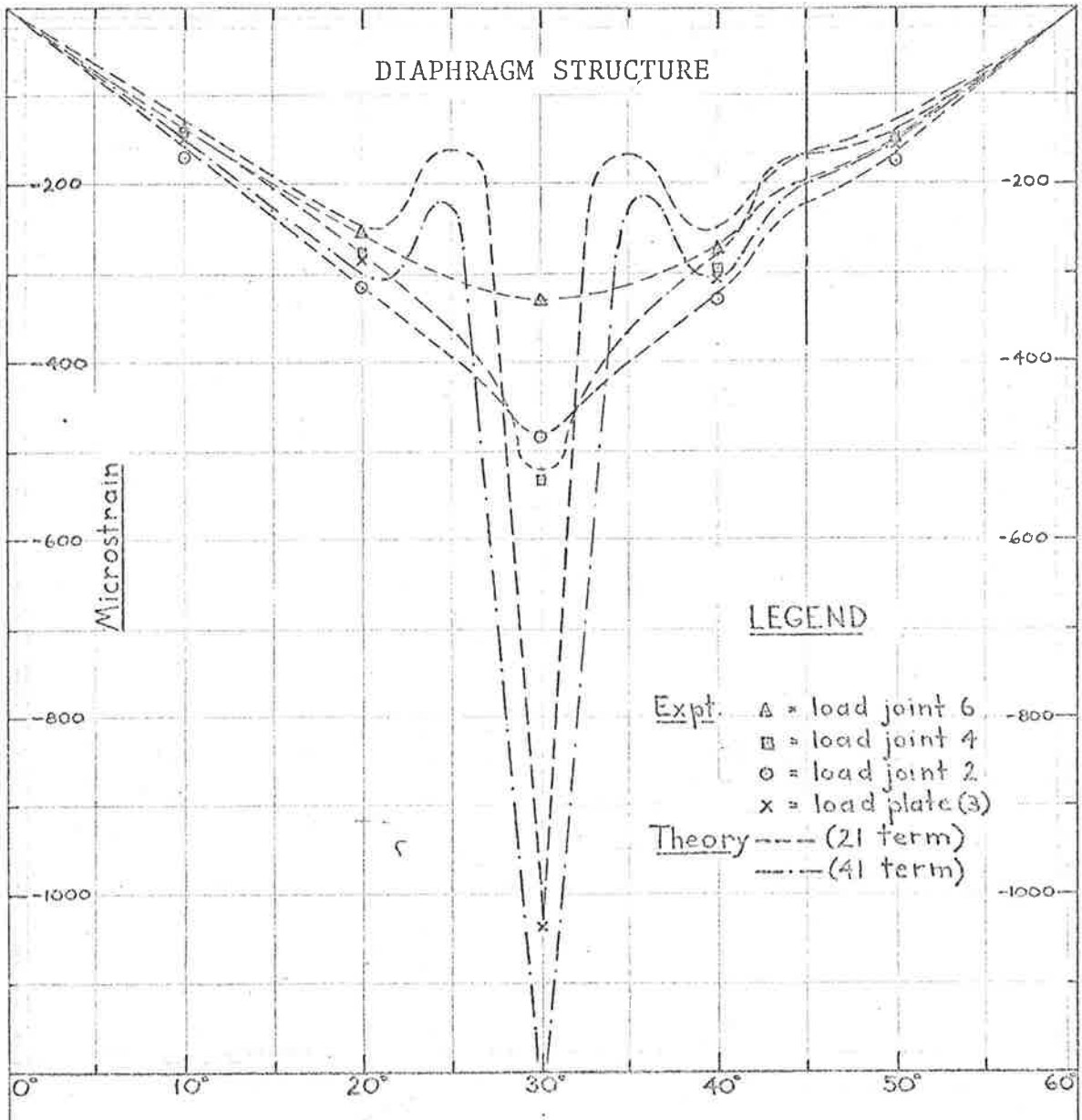

Figure 4.20 Top flange upper surface circumferential strains (Load at 30°) at R = 43.64"

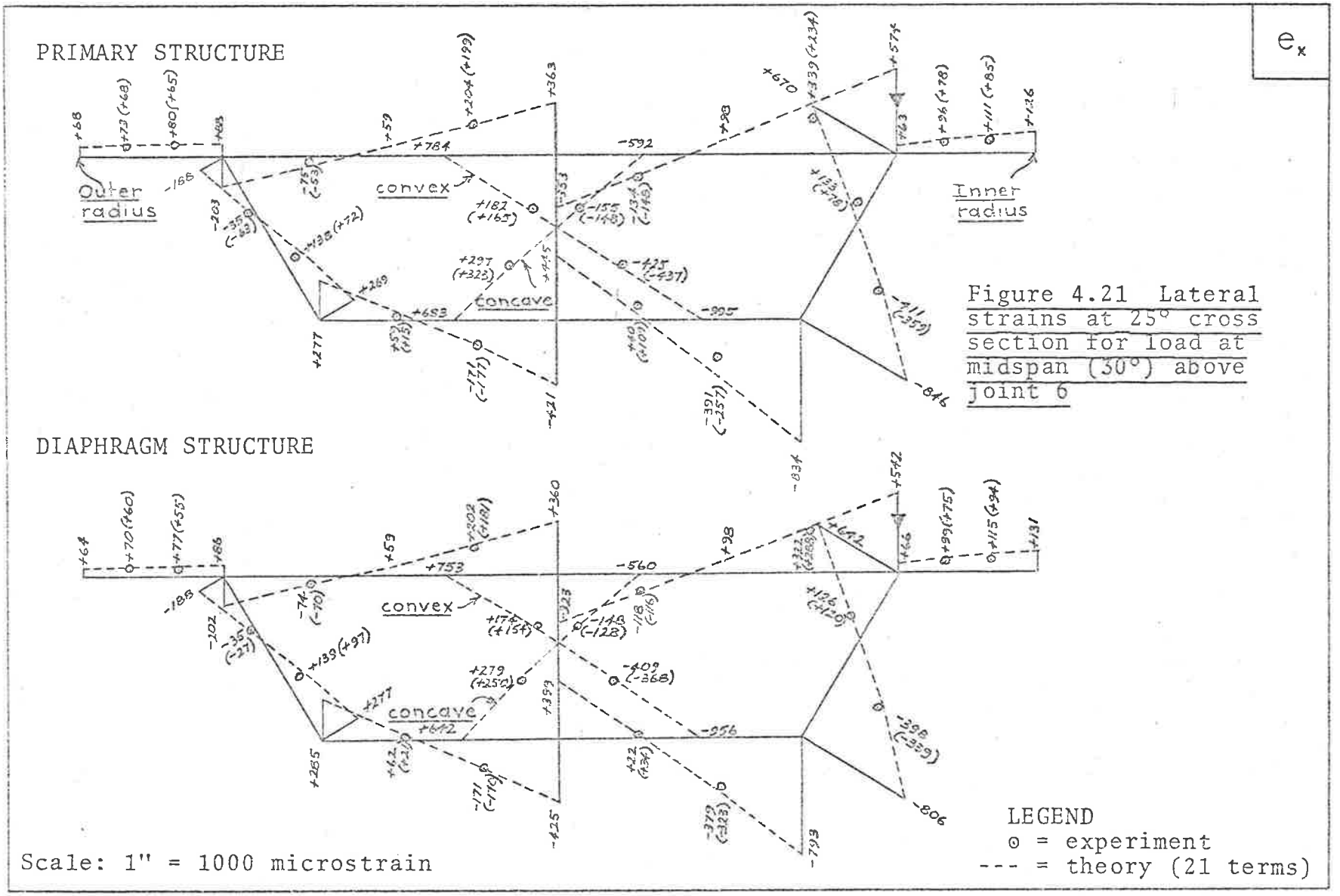

Figure 4.21 Lateral strains at 25° cross section for load at midspan (30°) above joint 6

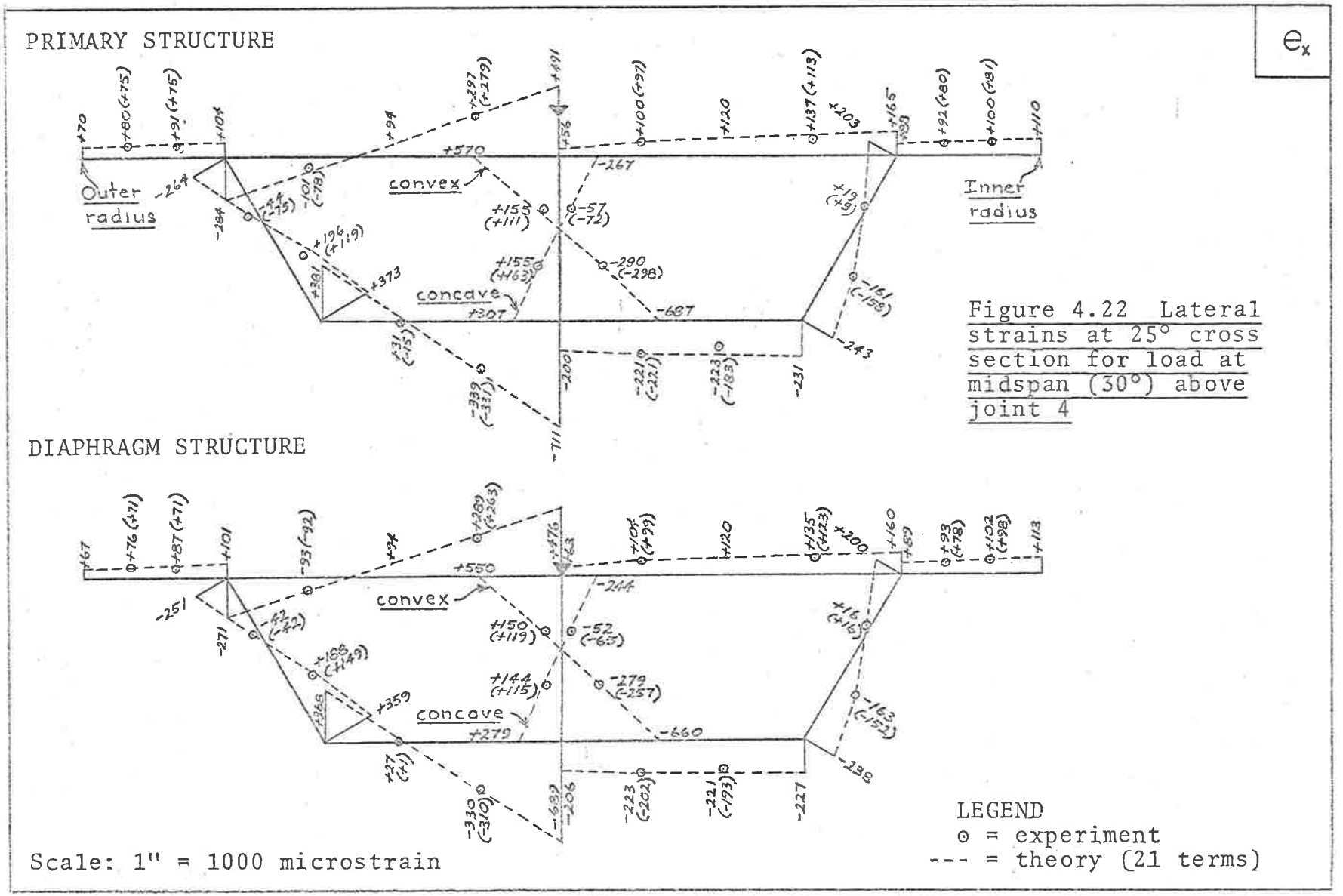

Figure 4.22 Lateral strains at 25° cross section for load at midspan (30°) above joint 4

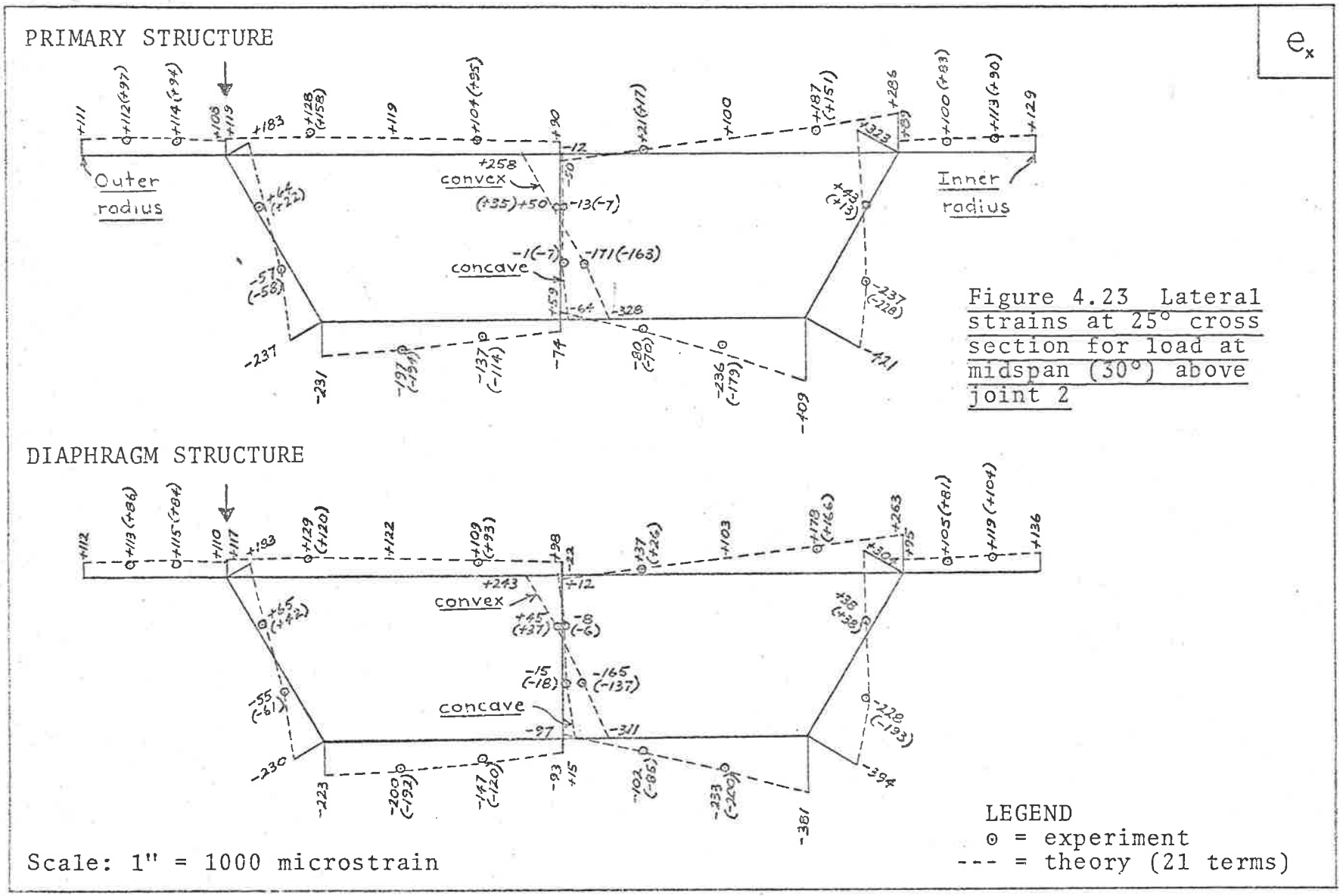

Figure 4.23 Lateral strains at 25° cross section for load at midspan (30°) above joint 2

PRIMARY STRUCTURE

e_x

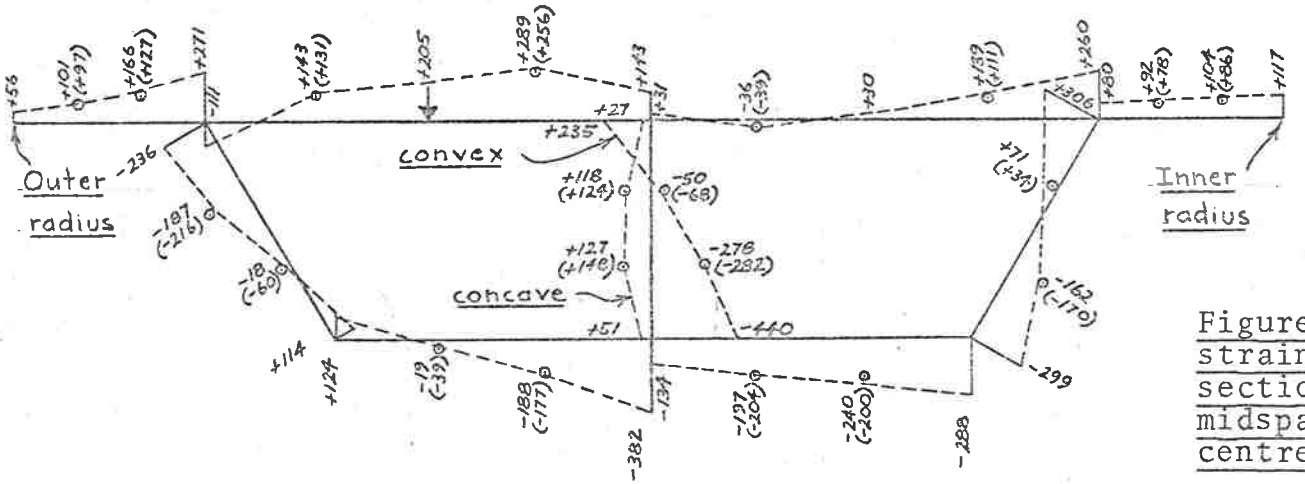

Figure 4.24 Lateral strains at 25° cross section for load at midspan (30°) above centre of plate (3)

DIAPHRAGM STRUCTURE

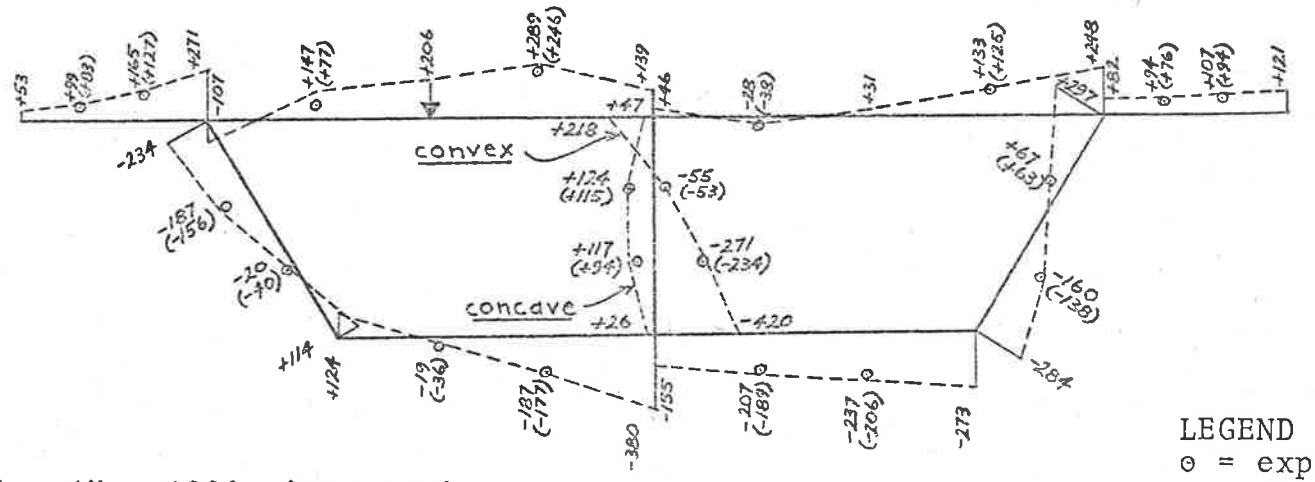

Scale: 1" = 1000 microstrain

LEGEND
⊙ = experiment
--- = theory (21 terms)

PRIMARY STRUCTURE

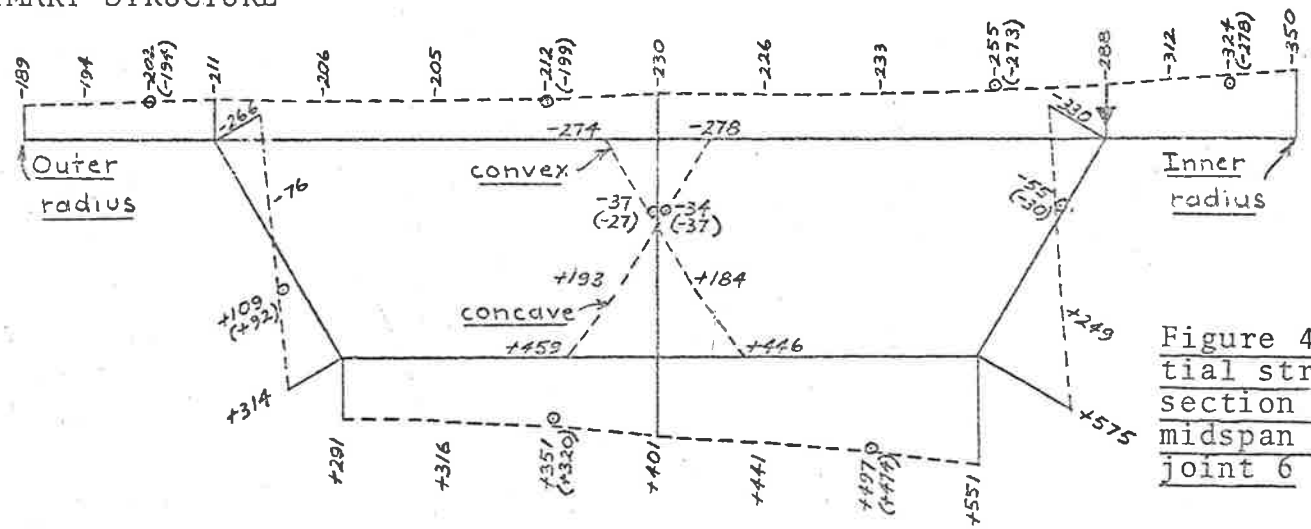

Figure 4.25 Circumferential strains at 25° cross section for load at midspan (30°) above joint 6

DIAPHRAGM STRUCTURE

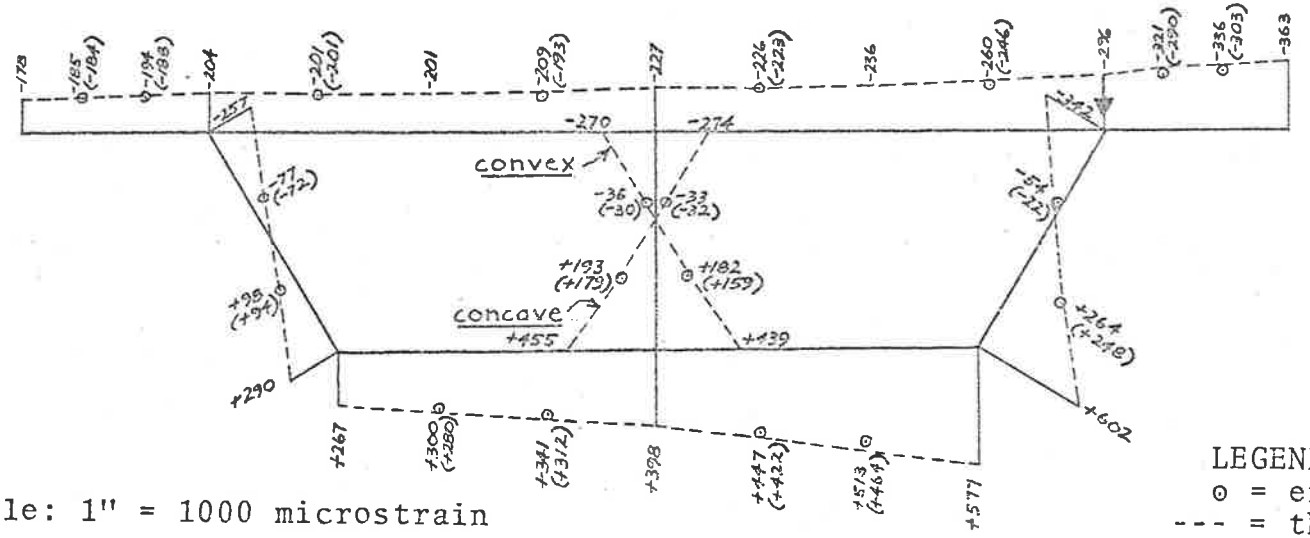

Scale: 1" = 1000 microstrain

LEGEND
⊙ = experiment
--- = theory (21 terms)

PRIMARY STRUCTURE

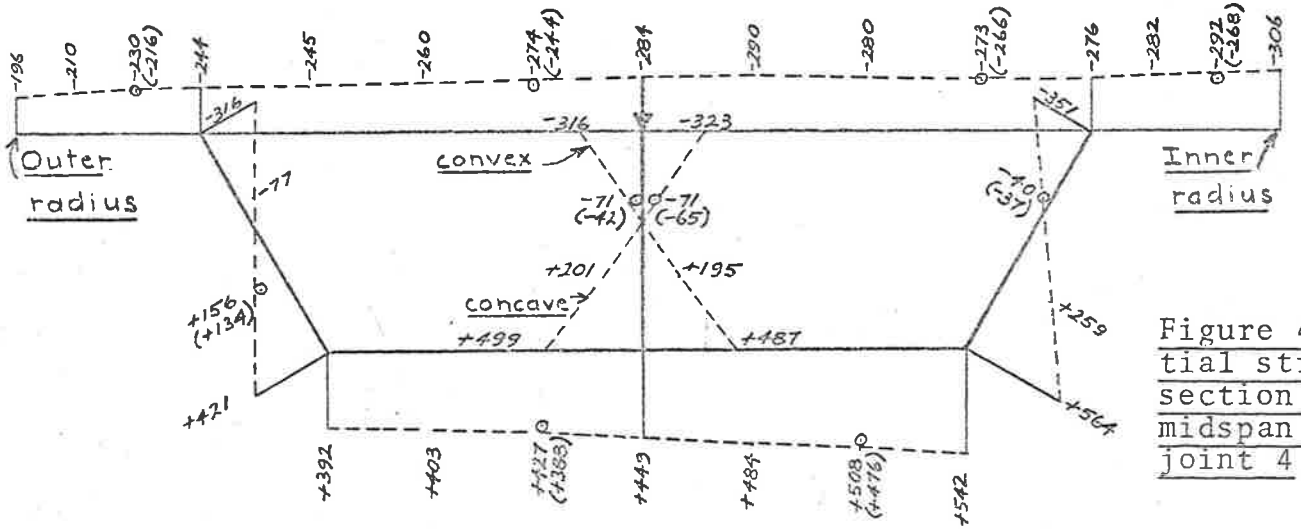

Figure 4.26 Circumferential strains at 25° cross section for load at midspan (30°) above joint 4

DIAPHRAGM STRUCTURE

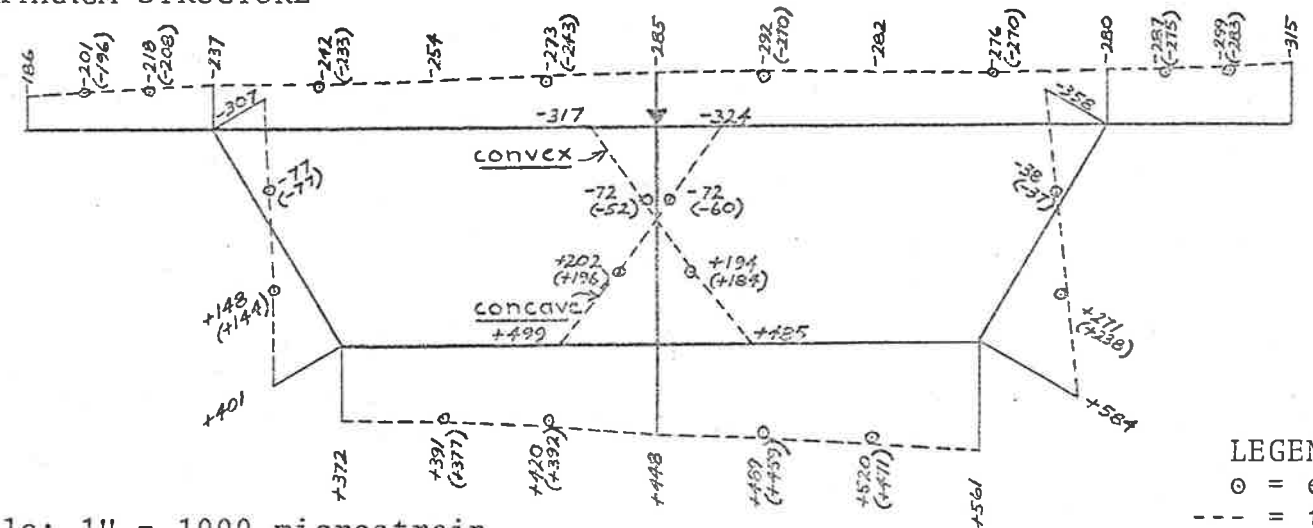

LEGEND
⊙ = experiment
--- = theory (21 terms)

Scale: 1" = 1000 microstrain

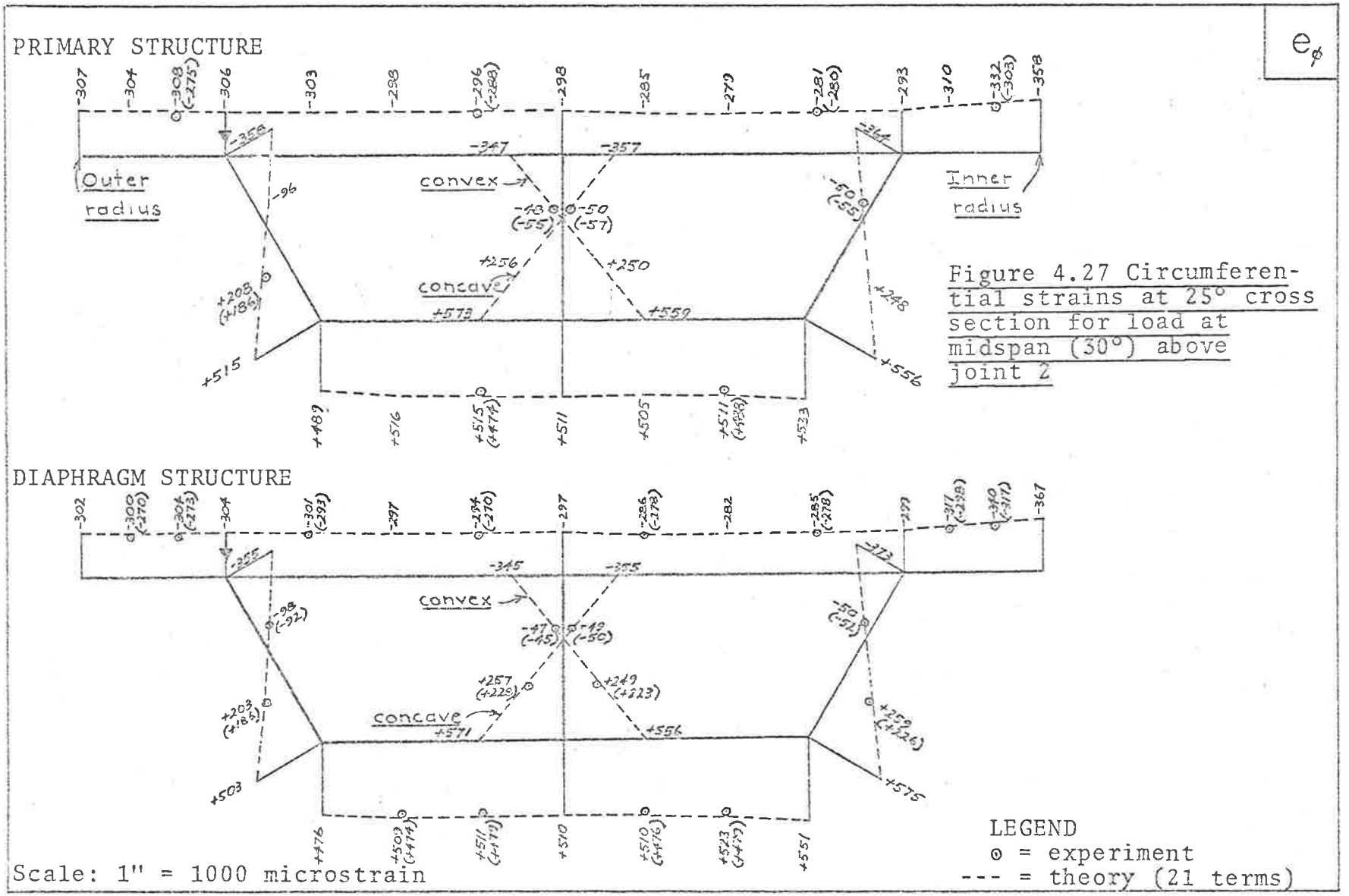

Figure 4.27 Circumferential strains at 25° cross section for load at midspan (30°) above joint 2

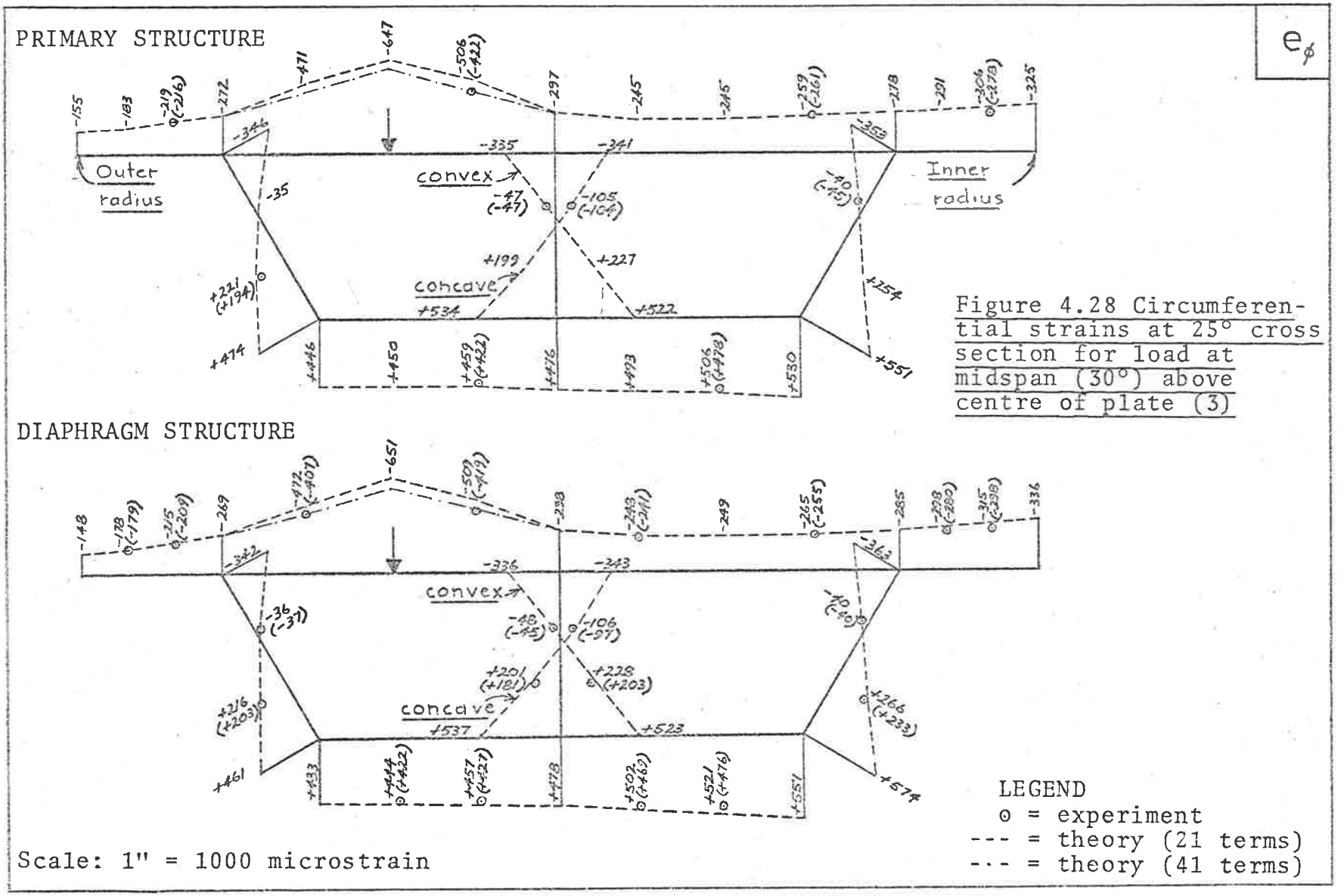

Figure 4.28 Circumferential strains at 25° cross section for load at midspan (30°) above centre of plate (3)

$e_{x\phi}$

PRIMARY STRUCTURE

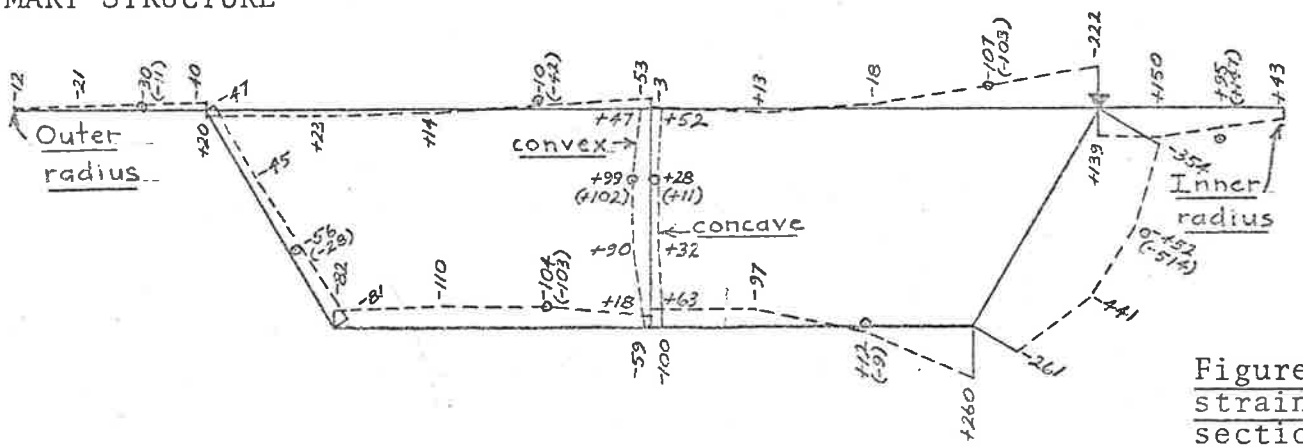

Figure 4.29 Shear strains at 25° cross section for load at midspan (30°) above joint 6

DIAPHRAGM STRUCTURE

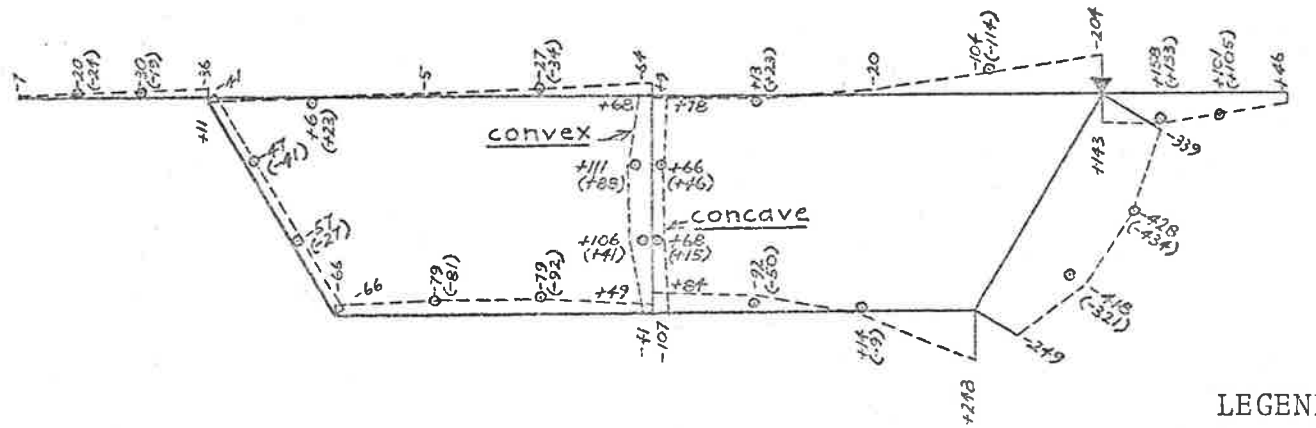

LEGEND
o = experiment
--- = theory (21 terms)

Scale: 1" = 1000 microstrain

$\epsilon_{x\phi}$

PRIMARY STRUCTURE

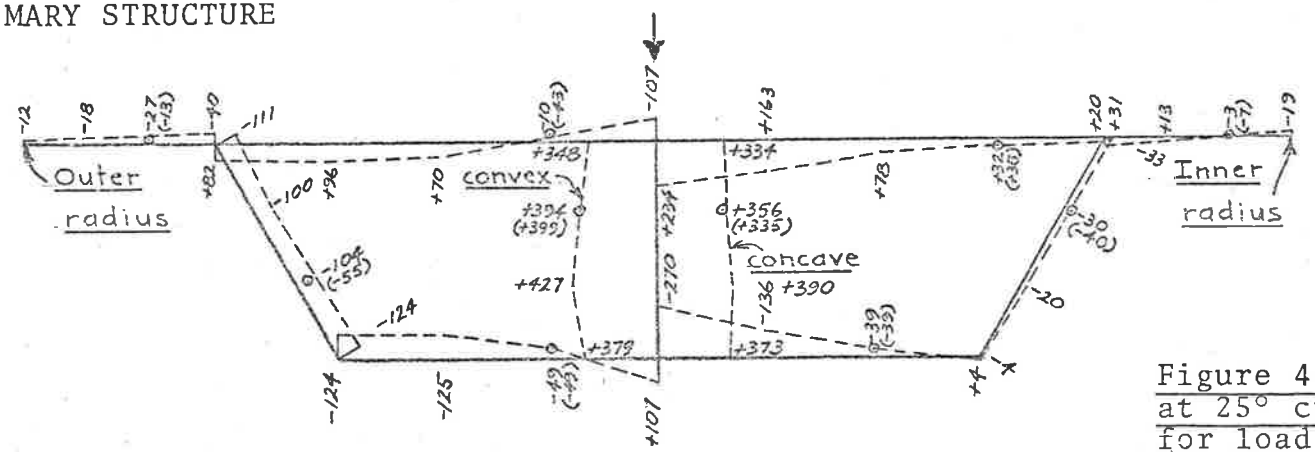

Figure 4.30 Shear strains at 25° cross section for load at midspan (30°) above joint 4

DIAPHRAGM STRUCTURE

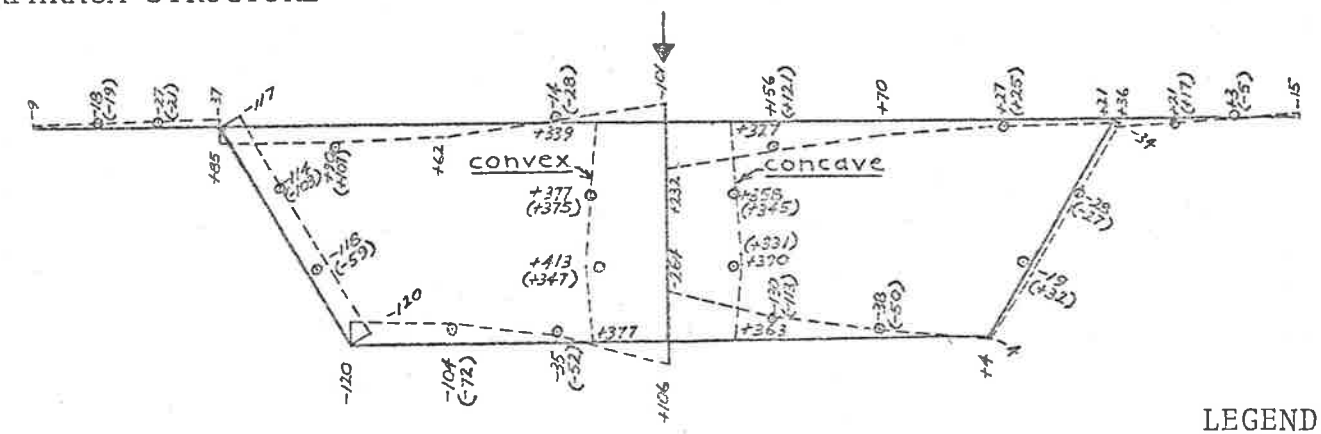

LEGEND
⊙ = experiment
--- = theory (21 terms)

Scale: 1" = 1000 microstrain

$e_{x\phi}$

PRIMARY STRUCTURE

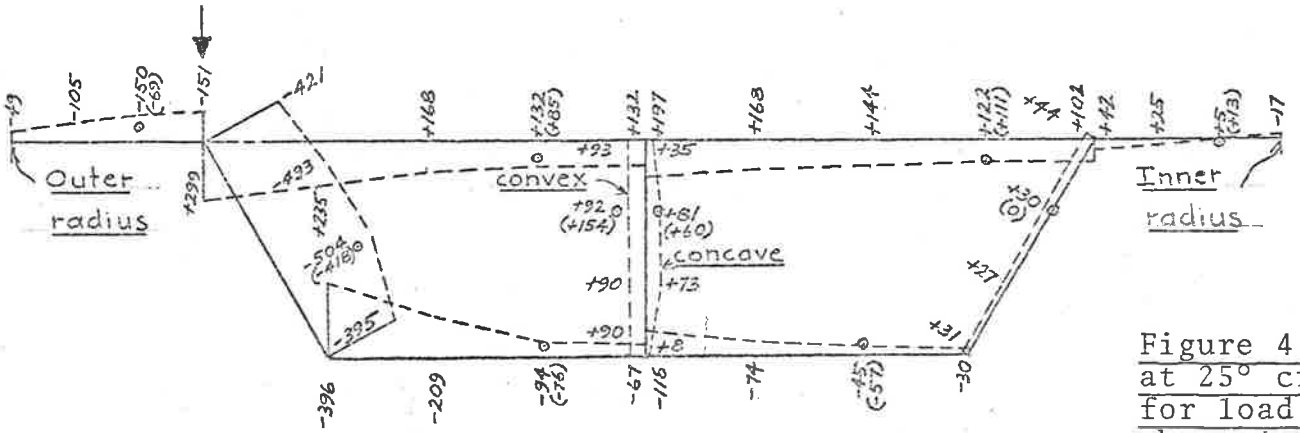

Figure 4.31 Shear strains at 25° cross section for load at midspan (30°) above joint 2

DIAPHRAGM STRUCTURE

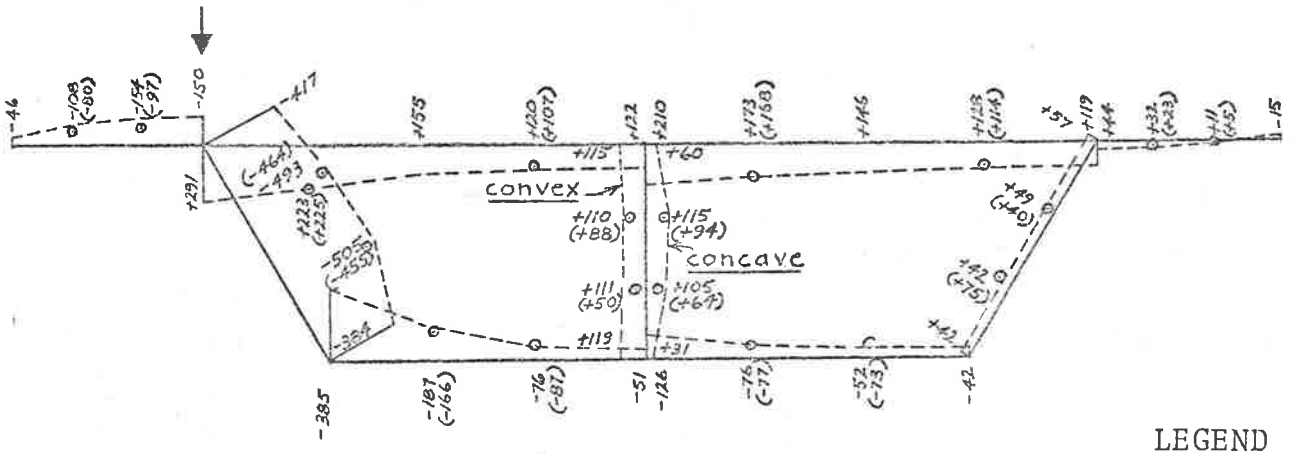

Scale: 1" = 1000 microstrain

LEGEND
o = experiment
--- = theory (21 terms)

$e_{x\phi}$

PRIMARY STRUCTURE

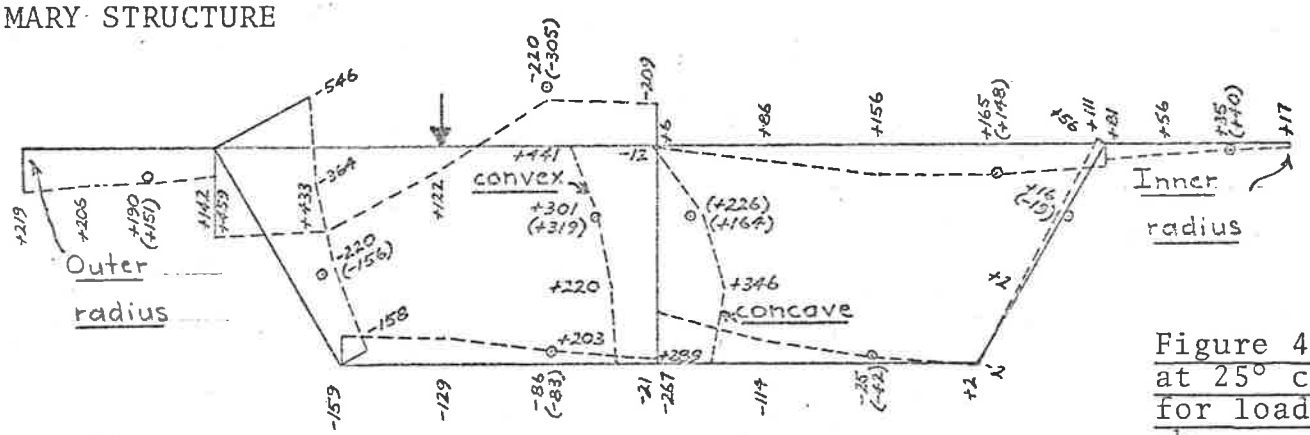

Figure 4.32 Shear strains at 25° cross section for load at midspan (30°) above centre of plate (3)

DIAPHRAGM STRUCTURE

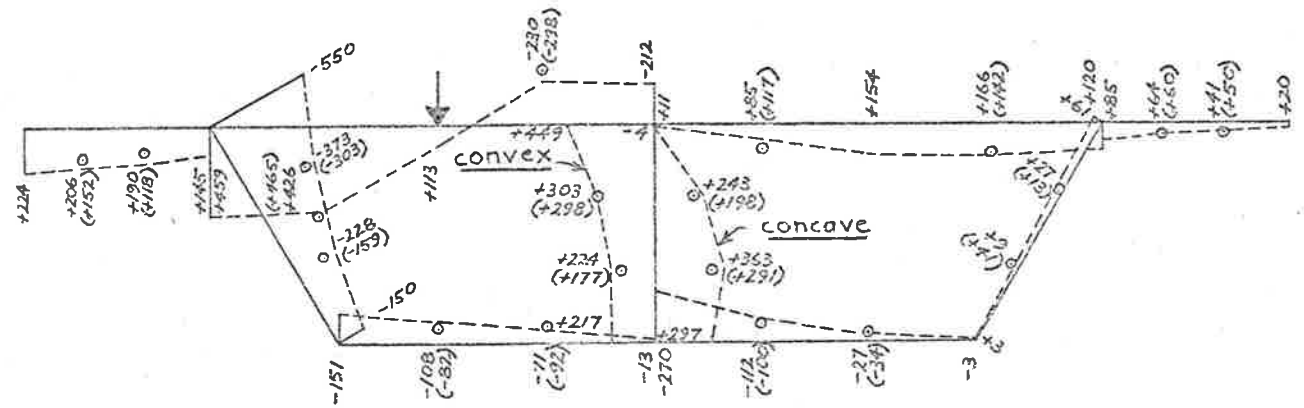

LEGEND
⊙ = experiment
--- = theory (21 terms)

Scale: 1" = 1000 microstrain

DIAPHRAGM STRUCTURE

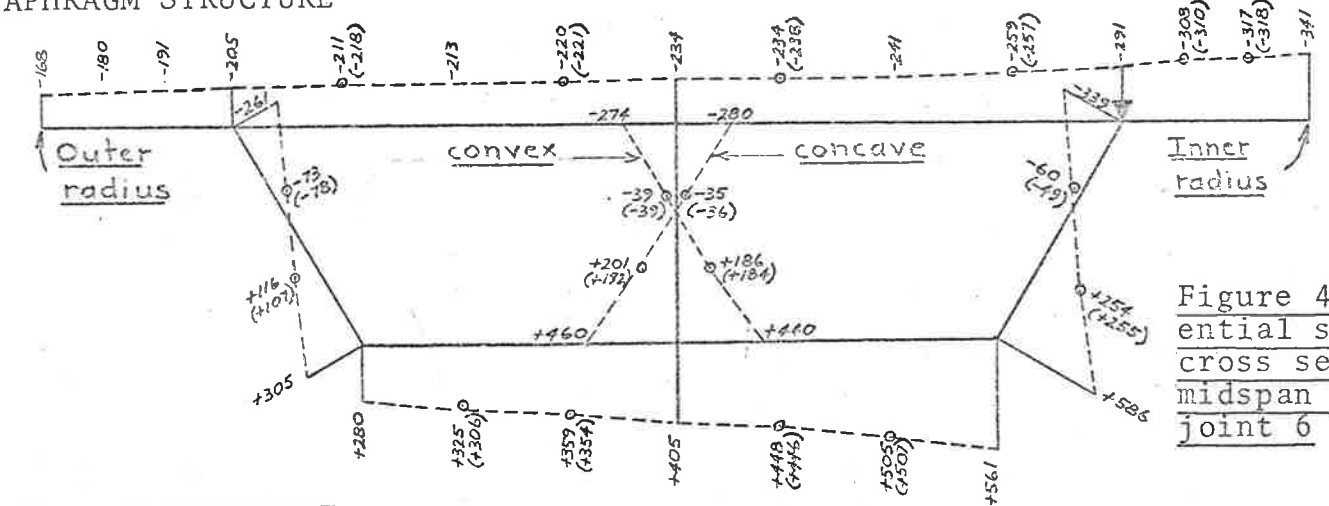

Figure 4.33(a) Circumferential strains at 35° cross section for load at midspan (30°) above joint 6

DIAPHRAGM STRUCTURE

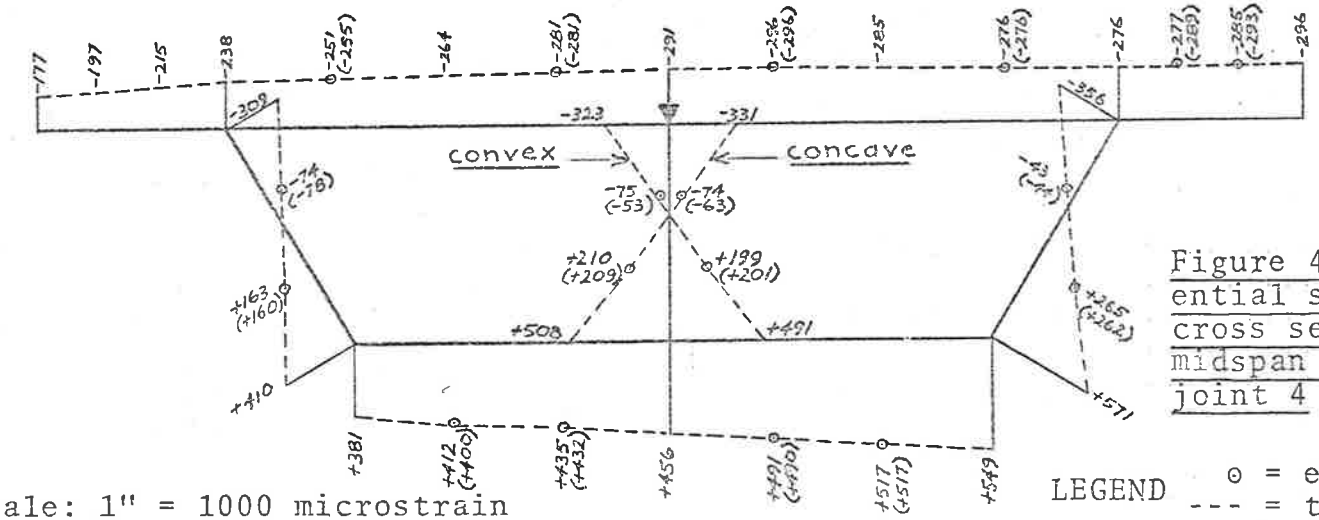

Figure 4.33(b) Circumferential strains at 35° cross section for load at midspan (30°) above joint 4

Scale: 1" = 1000 microstrain

LEGEND ⊙ = experiment
--- = theory (21 terms)

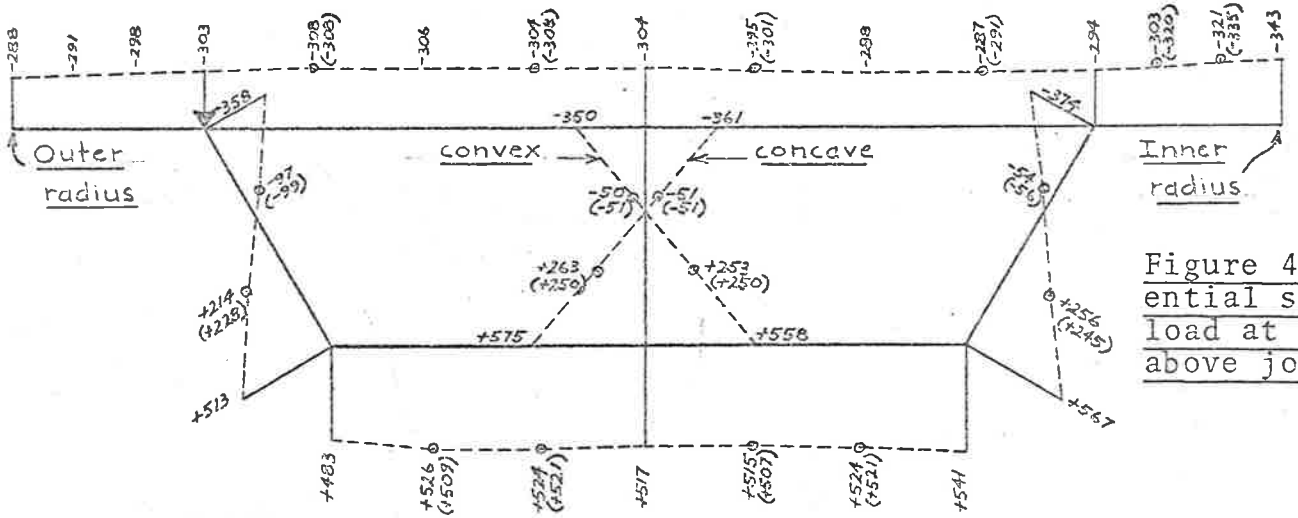

Figure 4.34(a) Circumferential strains at 35° for load at midspan (30°) above joint 2

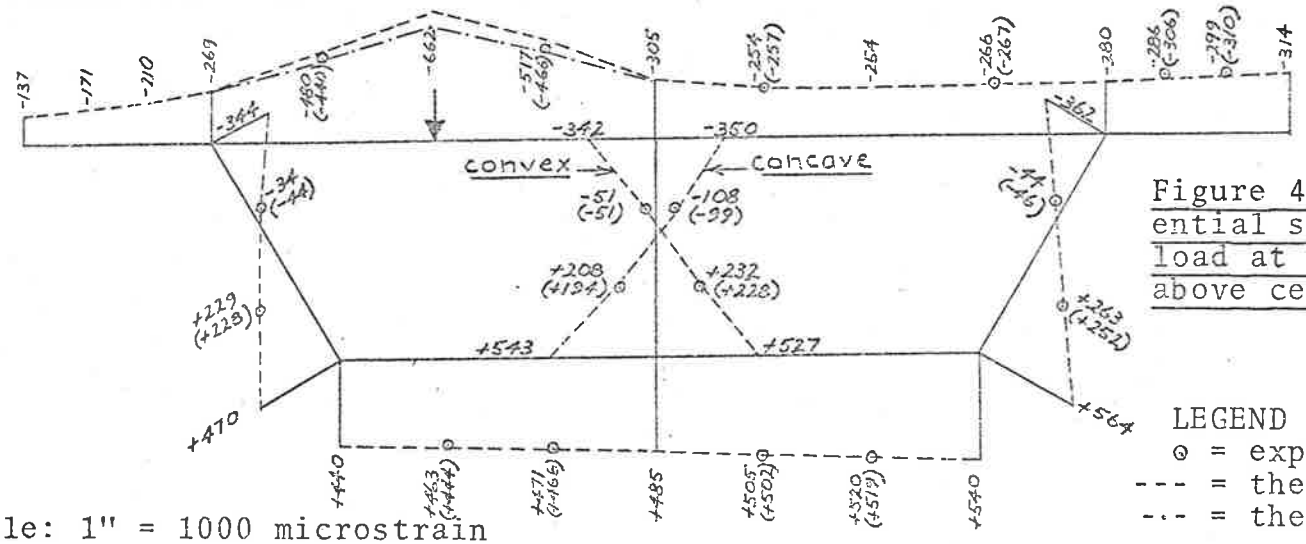

Figure 4.34(b) Circumferential strains at 35° for load at midspan (30°) above centre of plate (3)

LEGEND
⊙ = experiment
--- = theory (21 terms)
-·- = theory (41 terms)

Scale: 1" = 1000 microstrain

5. DISCUSSION OF EXPERIMENTAL AND THEORETICAL RESULTS

5.1 Introduction

Experimental results for deflections and actual-surface strains, together with corresponding folded shell predictions are shown graphically in Figures 4.15-4.34. The figures are arranged so that not only can the experimental and theoretical values be directly compared, but the structural effects caused by the addition of a moveable diaphragm at quarter span can be readily assessed. (Elementary calculations suggested that the structural effects caused by the reduction of end diaphragm thickness from $\frac{1}{4}$" (primary structure) to $\frac{1}{8}$" (diaphragm structure) would be negligible in comparison with the effects due to the presence of the extra internal diaphragm).

5.2 Comparison Between Theory and Experiment

5.2.1 Lateral and circumferential profiles of top flange vertical deflections (Figures 4.15-4.18)

Inspection of the top flange vertical deflection profiles indicates that for all four load tests conducted on each model, there is very good agreement between any experimental value and its corresponding theoretical prediction. (For every profile, the maximum discrepancy is within 4% of the maximum deflection predicted anywhere on that profile).

5.2.2 Circumferential profiles of top flange upper surface circumferential strains (Figures 4.19 and 4.20)

For each folded shell model, reference to

the appropriate circumferential profiles reveals that the agreement between theory and experiment is again very good for the first three of the four load cases. (For each of these profiles, the maximum discrepancy is within 8% of the maximum predicted value). However, with the load positioned above the centre of plate (3), the 21 term FOLSHEL solution was obviously insufficient to completely resolve the high strains and high strain gradients which existed in both models. Consequently, this particular load case was re-analysed by considering 41 Fourier harmonics, and the corresponding circumferential strain results are plotted in Figures 4.19 and 4.20 as compound dashed lines*. The latter curves then agree very well with the experimental results except at the midspan locations. Discrepancies at these points are largely due to the fact that in the immediate vicinity of concentrated loads, a large number of Fourier harmonics must be considered before proper convergence is assured. In addition, the actual positioning of a gauge becomes very critical where such extremely large strain gradients occur.

---

* In most of the theoretical profiles plotted in other figures for this load case, only the 21 term solution is presented as this was usually adequate to provide reliable predictions of the observed behaviour of both models. However, in those few areas (near the load) where the 21 term solution was not sufficiently accurate to resolve the high strains and high strain gradients, the 41 term solution is also given.

5.2.3 Lateral profiles of actual-surface lateral, circumferential, and shear strains (Figures 4.21-4.34)

For the profiles of lateral and circumferential strains (Figures 4.21-4.28, 4.33 and 4.34), there is good general agreement between theory and experiment. (For every profile, the discrepancies at 90% of all instrumented locations are always less than 9% of the maximum predicted value). As could be expected, however, general agreement for the dependent shear strains (Figures 4.29-4.32) is not quite as good. (For each of these profiles, the discrepancies at 90% of all instrumented locations are always less than 16% of the maximum predicted value). Nevertheless, it is evident that the folded shell analysis still gives a close estimate of the true lateral distribution of surface shear strains.

5.2.4 Possible sources of error

The following is a list of some possible causes of discrepancy between the theoretical and experimental results presented in Figures 4.15-4.34.

(a) It is assumed in the folded shell analysis that at every cross section along a structure, all joints are formed ideally as the point intersection of two or more element centroidal axes. In the models, all joints were a finite size.

(b) There may have been imperfect bonding between some of the electrical resistance strain

gauges and the Vybak surfaces to which they were affixed.

(c) Additional local stiffness is always induced due to the presence of any cemented strain gauges. However, since both models were constructed from $\frac{1}{4}$" Vybak, the magnitude of any such additional stiffness was minute.

(d) Small errors of up to $\frac{1}{16}$" were detected in the cross sectional dimensions of the completed models.

(e) The thickness of Vybak was not constant throughout the length and breadth of each element. (Values varying from 0.22" to 0.27" were recorded). A constant value of $\frac{1}{4}$" was assumed in all theoretical calculations.

(f) Experimental strains were measured by the strain gauge logger to an accuracy of ±3 microstrain.

(g) In areas of high local strain gradients, any slight errors made in the translational or rotational positioning of a strain gauge would have caused apparent errors in the results.

(h) A number of preliminary tests on the completed models indicated that any errors made in the lateral positioning of the knife-edge load would induce corresponding significant changes in the experimental results, particularly for lateral strains and shear strains.

(i) The finite bending stiffness of the slender supporting columns induced corresponding small bending moments about the ends of the two models. However, further preliminary tests on the completed models indicated that all experimental results were relatively insensitive to the application of end bending moments of this order.

(j) All model diaphragms had finite out-of-plane resistance to beam warping displacements.

(k) All model diaphragms were not infinitely rigid in their own plane.

(l) At the ends of the models, the diaphragms were not physically 'hinged' to the constituent beam elements as is ideally assumed in the folded shell analysis.

(m) Small errors were induced during the processing of experimental results when it was assumed that strain gradients in the circumferential direction were negligible compared with strain gradients in other directions.

(n) Infinite series associated with the folded shell analysis were truncated after a finite number of terms had been considered.

Unfortunately, it is extremely difficult, if not impossible, to determine the magnitudes of the errors induced

by all of the various causes listed above. However, in order to obtain at least some estimate of the net absolute accuracy which could be expected from the strain gauge techniques used, a model plane frame was constructed having the same shape as the cross sections of the two folded shell models. Each frame member was machined from $\frac{1}{4}$" Vybak, and all joints were welded with Prothoplast Subiton. The method of supporting the model is indicated in the pictorial sketch of Figure 5.1, together with the location of a suspended knife-edge load. The load and support conditions were chosen so that most of the induced actual-surface lateral strains would be of the same order of magnitude as those measured during the folded shell model tests. Ordinary strain gauges orientated to measure these lateral strains were positioned as shown in Figure 5.2, and the load test was conducted according to the same general procedure as described in Section 4.3.5 for the folded shell models. A value of Young's modulus (E) was then determined from the two statically determinate members of the loaded plane frame. Based on this value and on the measured mean thicknesses of each frame member, the complete redundant frame was analysed in detail by the well known 'STRESS' structural analysis program system[120,121]. (This analysis was chosen because all secondary effects due to shear deformation and axial shortening of members are automatically included). From the bending moments and axial forces thus obtained, the theoretical actual-surface strains which corresponded to the measured values were calculated. It was

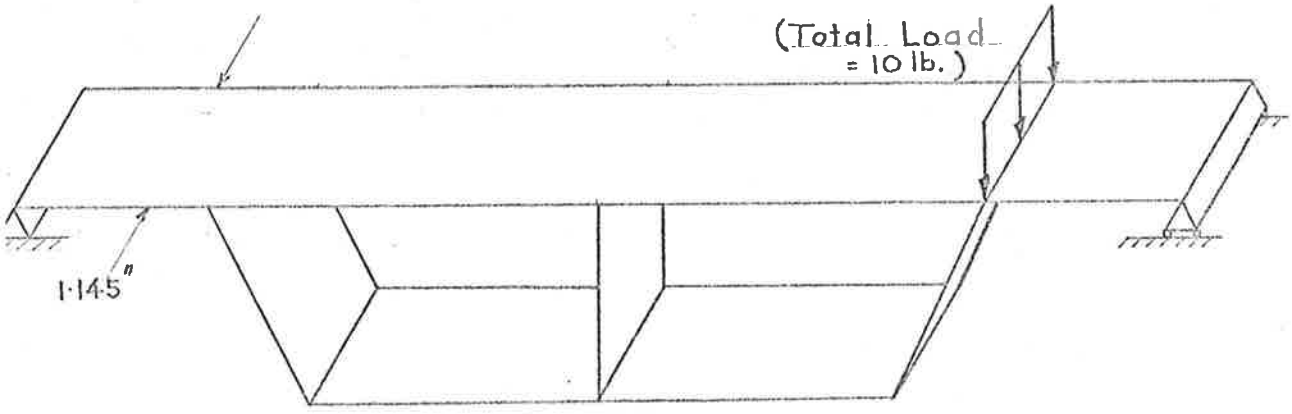

Figure 5.1 Plane frame model support conditions

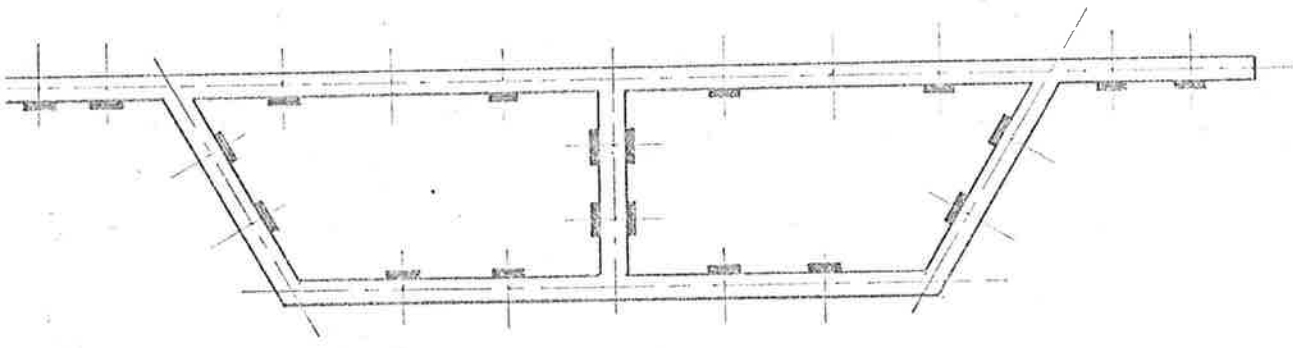

Figure 5.2 Locations of lateral strain gauges on plane frame model

subsequently found that absolute discrepancies of approximately 50 microstrain occurred at four of the instrumented locations, whereas at the other sixteen locations, agreement between the theoretical and experimental strain values was much closer. The maximum discrepancy of 58 microstrain was 4% of the maximum predicted strain which occurred anywhere on the instrumented surfaces of the members comprising the two closed cells of the frame.

Although the list of possible causes of discrepancy given at the beginning of this section refers specifically to the folded shell models, the first eight comments, (a)-(h), could also be considered to apply to the plane frame model. Therefore, the conclusion to be drawn from the simple plane frame test is that absolute discrepancies even greater than 50 microstrain might be expected at a few of the strain gauge locations on the folded shell models. Whilst it is emphasized here that this conclusion is far from categorical, detailed examination of Figures 4.21-4.34 reveals that occasional discrepancies of this order were in fact obtained.

5.3 Model Structural Action

5.3.1 Lateral and circumferential profiles of top flange vertical deflections (Figures 4.15-4.18)

(a) Influence of diaphragm:

These profiles indicate that the vertical deflections of the diaphragm structure are generally less than

those of the primary structure, thereby suggesting that the presence of the diaphragm causes a slight increase in overall structural bending stiffness. No significant changes occur in the shape of any of the plotted deflection profiles, although some asymmetry can be detected in the circumferential profiles for the diaphragm structure (Figure 4.18).

(b) General response:

For each of the four load cases, the lateral profiles of Figures 4.15 and 4.16 show clearly the significant lateral distortion of the top flange on both models, particularly when the load is placed above joint 6. As expected, the largest deflections occur at the outer radius of the flange when the load is above joint 2.

In the circumferential profiles of Figures 4.17 and 4.18, there is evidence of severe local bending distortion of the top flange when the load is above the centre of plate (3). Large variations in the values of circumferential bending strain would occur in this area.

5.3.2 Circumferential profiles of top flange upper surface circumferential strains (Figures 4.19 and 4.20)

(a) Influence of diaphragm:

Comparison of these profiles for the two models indicates that the influence of the diaphragm extends over only a very short length of the beam. Although the diaphragm has little effect on the shape of the strain profiles

which correspond to each separate load case, points of inflection are apparent at the actual diaphragm location (45°).

(b) General response:

With the load above the centre of plate (3), a comparatively large value of compressive strain is induced on the top surface of each model, due to severe local bending distortion similar to that illustrated in Figures 4.17 and 4.18. The large strain value thus corresponds to a large local value of circumferential curvature.

5.3.3 Lateral profiles of actual-surface lateral, circumferential, and shear strains (Figures 4.21-4.34)

(a) Influence of diaphragm:

As could perhaps be deduced from the results shown in Figures 4.19 and 4.20, only very small differences exist between all of the corresponding strain profiles for the primary and diaphragm structures at the instrumented 25° cross sections. Even the sensitive shear strain profiles fail to expose any significant differences. It may be of interest to note, however, that for each of the four load cases, detailed examination of Figures 4.25-4.28 reveals that the mean lateral gradient of the circumferential strain distribution across the bottom flange actually increases in magnitude due to the influence of the diaphragm.

For the diaphragm structure only, since the load is at 30° the differences between the actual-surface

circumferential strain results at the 35° cross section (Figures 4.33 and 4.34) and the corresponding strain results at the 25° cross section (Figures 4.25-4.28) are due solely to the presence of the diaphragm at 45°. The differences are obviously very small, and this fact provides further proof that the influence of the diaphragm extends for only a very short length along the beam.

(b) General response:

For each of the four load cases, the lateral bending strains shown in Figures 4.21-4.24 are a manifestation of the complex distortional actions which occur at the 25° cross sections of both models. As the load is moved radially outwards, so the lateral bending distortion of the cross section is reduced until finally, with the load above joint 2, the distortion is at a minimum.

The profiles of circumferential strain at the 25° cross sections for both models (Figures 4.25-4.28) and at the 35° cross section for the diaphragm model only (Figures 4.33 and 4.34) illustrate the essential beam-like action of the folded shell structures, although superimposed local bending effects are clearly evident when the load is above the centre of plate (3). The magnitudes of the mean strain gradients across the top and bottom flanges are at a minimum when the load is above joint 2, and this result is consistent with the simultaneous condition of minimum cross sectional distortion. Perhaps the most striking feature of all the circumferential strain

results is that no strain value is as large as some of the lateral strains induced at the 25° cross section with the load above joint 6 (Figure 4.21). This fact emphasizes the need for careful consideration of cross sectional distortion when designing any box beam member, because, as detailed in Section 6, the stresses induced by lateral bending can combine with the normal circumferential bending stresses and the surface shear stresses to produce potentially dangerous stress conditions which would not otherwise be recognised by conventional analysis.

As expected, the actual-surface shear strain profiles of Figures 4.29-4.32 reveal that the largest shear strains occur in those elements of the cross section which are closest to the load.

5.4 Summary

Experimental results obtained from a number of different load configurations confirm the validity of the folded shell method for predicting the true structural response of the two Vybak models. It is evident that induced structural effects caused by the addition of the moveable diaphragm were extremely local, and thus the overall structural performance was largely unaffected. The results obtained for lateral and circumferential strains on both models emphasize the fact that there is always a vital need for adequate consideration of cross sectional distortion when designing box beam structures.

6. CONCLUSION

The major part of this dissertation is concerned with the presentation of the basic theory for folded shell analysis of continuous box beams with simply-supported ends, constant curvatures in plan, and non-varying cross sections. Effects caused by the action of any additional interior transverse stiffening diaphragms are considered. The theory is derived from classical equations of elasticity which describe the detailed structural behaviour of thin cylindrical, flat plate, and conical shell elements rigidly connected along their curved (circumferential) edges. Fourier series expansions in the circumferential direction facilitate the solution of these equations, and direct matrix algebra is used extensively in formulating the net response of the complete structure. Due to the complexity of the calculations, a large-capacity high-speed digital computer is essential to perform the analysis, and a general computer program known as FOLSHEL has therefore been written to accommodate a wide variety of folded shell structures subjected to most of the common load configurations encountered in normal civil engineering bridge design practice. In order to check the validity of results produced by this program, a number of independent tests were devised.

(a) Two single-span models were constructed and then subjected to various load conditions. The experimental results for deflections and strains obtained from these tests were found to agree very well with

the theoretical predictions. Although the models were essentially similar, one model incorporated an internal transverse diaphragm at quarter span.

(b) By specifying a very large mean radius and a correspondingly small subtended angle at the axis of rotation, a curved folded shell structure can closely approximate a straight folded plate structure. For a number of continuous straight box beams, results thus obtained from the FOLSHEL program were compared with those obtained from the general program known as MUPDI[104,105] for the analysis of folded plate structures. Excellent agreement was noted in all cases. (The folded plate solution is, of course, much more direct for this type of structure).

(c) Simple isolated static checks of equilibrium and compatibility were applied at selected points along each analysed structure, and these checks always confirmed the internal consistency of the folded shell solutions.

From the results of all of these tests, it is concluded that the folded shell method does give reliable predictions of the true elastic structural behaviour of continuous box beams curved in plan. However, there are three main areas where further development and research would be of benefit in improving the current version of the FOLSHEL program.

(a) Although large amounts of computing time would be required, the convergence properties of the various infinite solutions incorporated in the analysis could perhaps be investigated. In particular, since the cost of running the program is approximately proportional to the number of terms taken for the infinite Fourier series expansions, it would be useful to know in advance the minimum number of harmonics that are necessary for the adequate solution of each problem.

(b) In the FOLSHEL program, most common load configurations can be specified by the user, including a simple form of frictionless circumferential post-tension prestress applied along the full length of any selected folded shell joint(s). However, in its present form, the program does not allow for the more realistic case of draped prestress cable profiles which are arbitrarily positioned within any shell element(s). This problem is one which warrants further detailed study, since draped profiles are often used in the construction of concrete curved box beam structures.

(c) Throughout the whole of the folded shell analysis as presented herein, no allowance is made for elastic instability of any of the elements. The possible onset of local buckling must always be a significant factor for consideration during the design of any box beam structure.

The most important conclusion to be drawn from the folded shell research described in this dissertation is that it is unquestionably dangerous to assume that the design of any curved (or straight) box beam can be based solely on estimates of the circumferential (longitudinal) stresses caused by simple beam action and on estimates of the lateral stresses induced by local bending of the loaded top flange. Experimental and theoretical results obtained for each of the two models showed conclusively that under particular load conditions, some values of lateral strain which existed on the surfaces of the various box beam elements were much larger than any values of surface circumferential strain which existed . Furthermore, the largest lateral strains did not necessarily occur on those elements which were closest to the load. Although these facts illustrate the importance of calculating the effects due to lateral distortion of box beam cross sections, it is emphasized here that estimates of even both the circumferential and lateral stresses at each chosen point on the structure may still be insufficient because it is the values of the principal stresses which should really govern the design. In order to predict these, the surface shear stress associated with the circumferential and lateral directions must first be calculated and combined with the direct stresses by using the familiar Mohr's circle considerations. Irrespective of which failure criterion is then chosen for the materials used, the principal stresses will be sufficient for checking the stress safety of the structure.

At present, the folded shell method is one of the very few analyses available which is in fact capable of accurately predicting the principal stresses which exist on the elements of loaded continuous curved box beams.

APPENDIX A. Fourier Series

Fourier series expansions in the circumferential (ϕ) direction for the various loads associated with the folded shell analysis are given in this appendix. In the first section, loads applied to joints are considered. Circumferential loads are expressed by cosine half-range Fourier series, whereas all other joint loads are expressed by sine half-range Fourier series. In the second section, loads applied to shell surfaces are considered. Since none of these is a circumferential load, no cosine half-range Fourier series are required.

A.1 Loads applied to joints

(a) Sine series

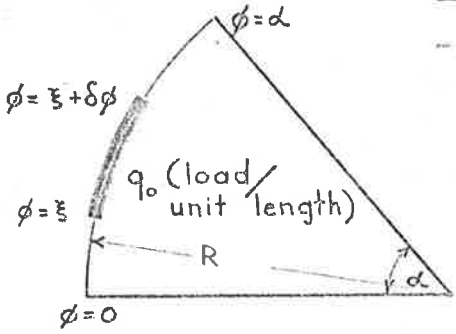

Figure A.1 Partial uniform load

$$q = \frac{4q_o}{\Pi} \sum_{m=1}^{\infty} \frac{1}{m} \sin\frac{m\Pi(2\xi+\delta\phi)}{2\alpha} \sin\frac{m\Pi\delta\phi}{2\alpha} \sin\frac{m\Pi\phi}{\alpha} \qquad \ldots(A.1)$$

If $\delta\phi << 2\xi$, as is usually the case with joint loads induced by internal diaphragm action (Section 3.2), then equation (A.1) becomes

$$q = \frac{4q_o}{\Pi} \sum_{m=1}^{\infty} \frac{1}{m} \sin\frac{m\Pi\xi}{\alpha} \sin\frac{m\Pi\delta\phi}{2\alpha} \sin\frac{m\Pi\phi}{\alpha} \qquad \ldots(A.2)$$

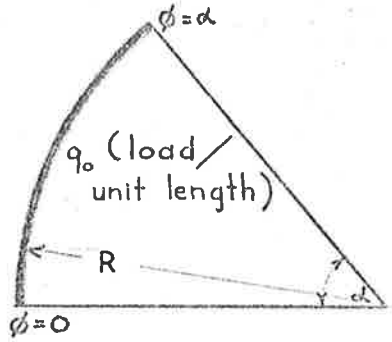

Figure A.2 Uniform load

$$q = \frac{4q_o}{\Pi} \sum_{m=1,3,5\ldots}^{\infty} \frac{1}{m} \sin\frac{m\Pi\phi}{\alpha} \qquad \ldots(A.3)$$

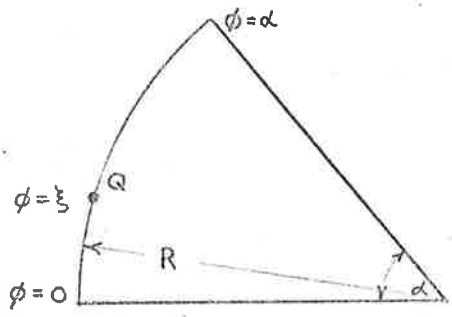

Figure A.3 Point load

$$q = \frac{2Q}{R\alpha} \sum_{m=1}^{\infty} \sin\frac{m\Pi\xi}{\alpha} \sin\frac{m\Pi\phi}{\alpha} \qquad \ldots(A.4)$$

(b) Cosine series

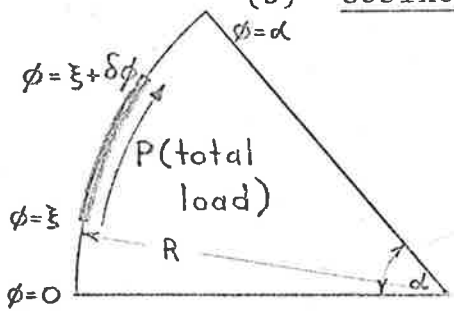

Figure A.4 Partial uniform load

$$p = \frac{P}{R\alpha} + \frac{4P}{R\Pi\delta\phi} \sum_{m=1}^{\infty} \frac{1}{m} \cos\frac{m\Pi(2\xi+\delta\phi)}{2\alpha} \sin\frac{m\Pi\delta\phi}{2\alpha} \cos\frac{m\Pi\phi}{\alpha} \qquad \ldots(A.5)$$

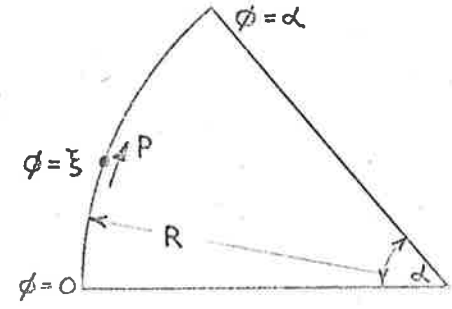

Figure A.5 Point load

$$p = \frac{P}{R\alpha} + \frac{2P}{R\alpha} \sum_{m=1}^{\infty} \cos\frac{m\Pi\xi}{\alpha} \cos\frac{m\Pi\phi}{\alpha} \qquad \ldots(A.6)$$

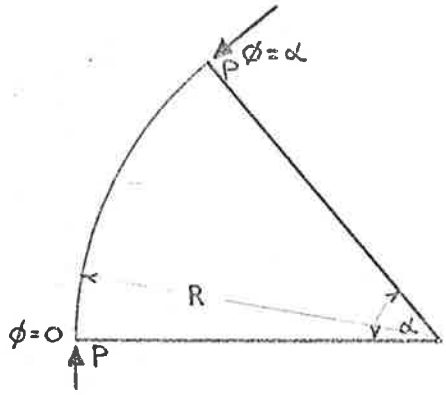

Figure A.6 Prestress load (post-tension)

$$p = \frac{4P}{R\alpha} \sum_{m=1,3,5\ldots}^{\infty} \cos\frac{m\Pi\phi}{\alpha} \qquad \ldots(A.7)$$

A.2 Loads applied to shell surfaces

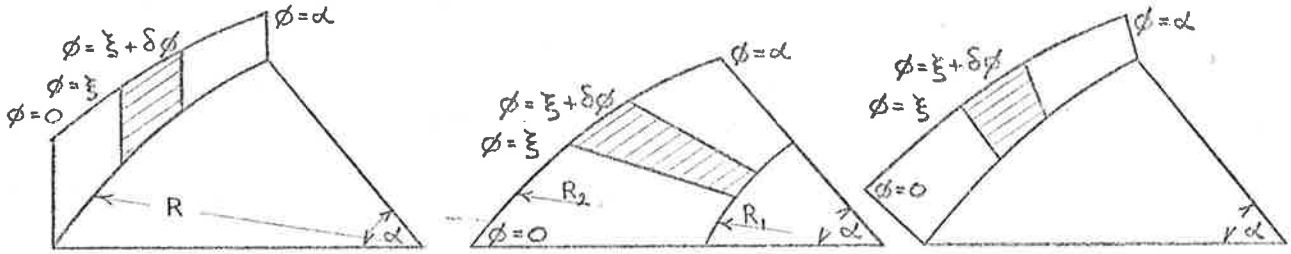

Figure A.7 Partial uniform load q_o (load/unit surface area)

$$q = \frac{4q_o}{\Pi} \sum_{m=1}^{\infty} \frac{1}{m}\sin\frac{m\Pi(2\xi+\delta\phi)}{2\alpha}\sin\frac{m\Pi\delta\phi}{2\alpha}\sin\frac{m\Pi\phi}{\alpha} \qquad \ldots(A.8)$$

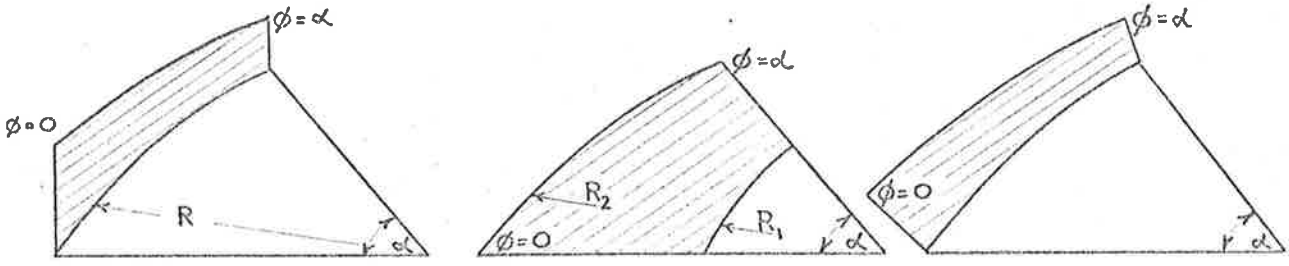

Figure A.8 Uniform load q_o (load/unit surface area)

$$q = \frac{4q_o}{\Pi} \sum_{m=1,3,5\ldots}^{\infty} \frac{1}{m}\sin\frac{m\Pi\phi}{\alpha} \qquad \ldots(A.9)$$

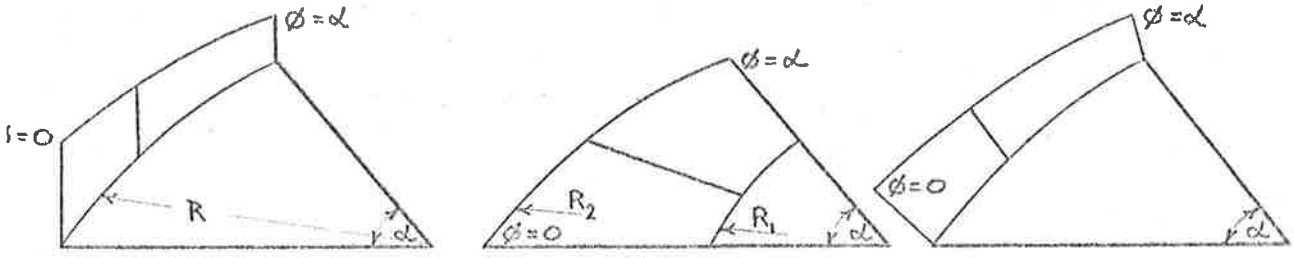

Figure A.9 Uniform line load (total load Q)

For the cylindrical shell element,

$$q = \frac{2Q}{LR\alpha} \sum_{m=1}^{\infty} \sin\frac{m\Pi\xi}{\alpha}\sin\frac{m\Pi\phi}{\alpha} \qquad \ldots(A.10)$$

For the flat plate element,

$$q = \frac{4Q}{(R_2^2-R_1^2)\alpha} \sum_{m=1}^{\infty} \sin\frac{m\Pi\xi}{\alpha}\sin\frac{m\Pi\phi}{\alpha} \qquad \ldots(A.11)$$

For the conical shell element,

$$q = \frac{4Q}{(ah_1)^2 b(b+2)\alpha\sin\gamma} \sum_{m=1}^{\infty} \sin\frac{m\Pi\xi}{\alpha}\sin\frac{m\Pi\phi}{\alpha} \qquad \ldots(A.12)$$

Due to the action of an internal diaphragm, each shell may be subjected to in-plane (x direction) and normal (z direction) loads X_C, X_D, Z_C, Z_D as described in Section 3.2 and sketched in Figure 3.2. If the location of the diaphragm is $\phi = \xi$, and if the angular thickness of the diaphragm is $\delta\phi$ where $\delta\phi << 2\xi$, then the Fourier series expansions for these loads are as follows.

For the cylindrical shell element:

$$q = \frac{8Q(L-x)}{\Pi L^2 R\delta\phi} \sum_{m=1}^{\infty} \frac{1}{m}\sin\frac{m\Pi\xi}{\alpha}\sin\frac{m\Pi\delta\phi}{2\alpha}\sin\frac{m\Pi\phi}{\alpha} \qquad \ldots(A.13)$$

where Q may be either X_C or Z_C; and

$$q = \frac{8Qx}{\Pi L^2 R\delta\phi} \sum_{m=1}^{\infty} \frac{1}{m}\sin\frac{m\Pi\xi}{\alpha}\sin\frac{m\Pi\delta\phi}{2\alpha}\sin\frac{m\Pi\phi}{\alpha} \qquad \ldots(A.14)$$

where Q may be either X_D or Z_D.

For the flat plate element:

$$q = \frac{24Q(R_2-x)}{\Pi(R_2-R_1)^2(2R_1+R_2)\delta\phi} \sum_{m=1}^{\infty} \frac{1}{m}\sin\frac{m\Pi\xi}{\alpha}\sin\frac{m\Pi\delta\phi}{2\alpha}\sin\frac{m\Pi\phi}{\alpha} \qquad \ldots(A.15)$$

where Q may be either X_C or Z_C: and

$$q = \frac{24Q(x-R_1)}{\Pi(R_2-R_1)^2(R_1+2R_2)\delta\phi} \sum_{m=1}^{\infty} \frac{1}{m}\sin\frac{m\Pi\xi}{\alpha}\sin\frac{m\Pi\delta\phi}{2\alpha}\sin\frac{m\Pi\phi}{\alpha} \qquad \ldots(A.16)$$

where Q may be either X_D or Z_D.

For the conical shell element:

$$q = \frac{24Q(ah_1(b+1)-x)}{\Pi(ah_1)^3 b^2(b+3)\delta\phi\sin\gamma} \sum_{m=1}^{\infty} \frac{1}{m}\sin\frac{m\Pi\xi}{\alpha}\sin\frac{m\Pi\delta\phi}{2\alpha}\sin\frac{m\Pi\phi}{\alpha} \qquad \ldots(A.17)$$

where Q may be either X_C or Z_C; and

$$q = \frac{24Q(x-ah_1)}{\Pi(ah_1)^3 b^2 (2b+3)\delta\phi\sin\gamma} \sum_{m=1}^{\infty} \frac{1}{m} \sin\frac{m\Pi\xi}{\alpha} \sin\frac{m\Pi\delta\phi}{2\alpha} \sin\frac{m\Pi\phi}{\alpha} \quad \ldots(A.18)$$

where Q may be either X_D or Z_D.

APPENDIX B. Expressions and Sign Conventions for Output Quantities*

B.1 Cylindrical shell element(107)

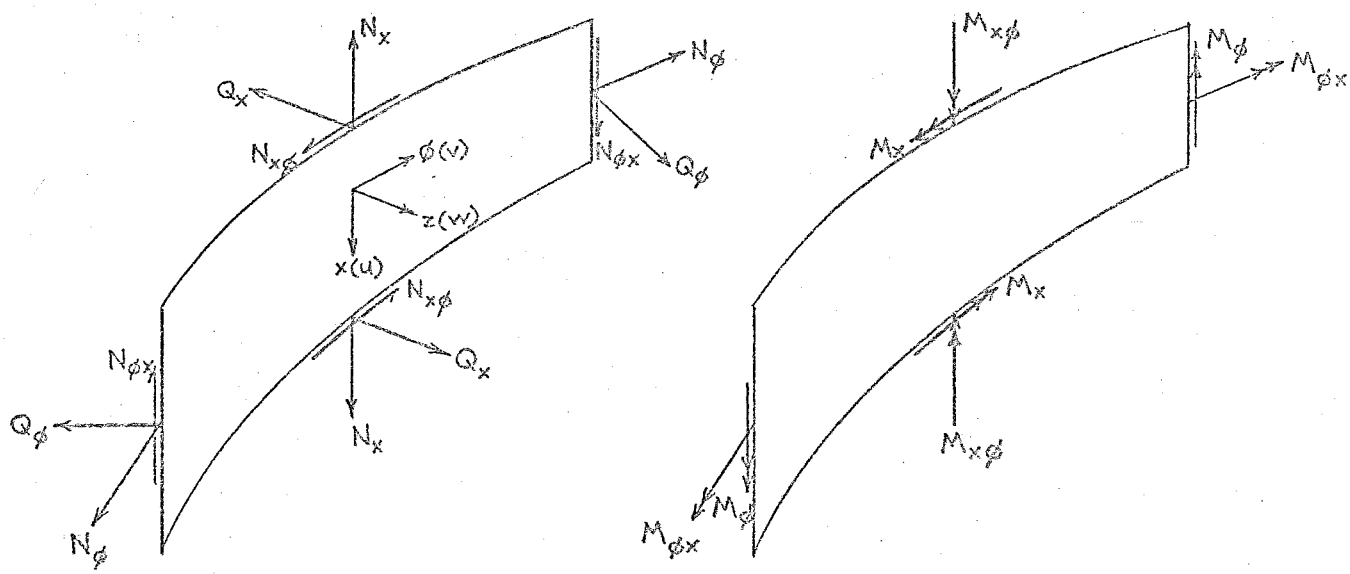

Figure B.1 Positive directions of stress resultants for cylindrical shell element

Let $K_{17} = \frac{Eh}{1-\nu^2}$, $K_{18} = \frac{Eh^3}{12(1-\nu^2)}$, $(\ )' = \frac{\partial(\ )}{\partial x}$ and $(\ )^{\cdot} = \frac{\partial(\ )}{\partial \phi}$.

Then

$\varepsilon_x = u'$ (middle surface lateral strain) ..(B.1)

$\varepsilon_\phi = \frac{v^{\cdot} - w}{R}$ (middle surface circumferential strain) .(B.2)

$\gamma_{x\phi} = \frac{u^{\cdot}}{R} + v'$ (middle surface shear strain) ..(B.3)

$\chi_x = -w''$ (lateral curvature) ..(B.4)

$\chi_\phi = -\frac{(w^{\cdot\cdot} + w)}{R^2}$ (circumferential curvature) ..(B.5)

$\chi_{x\phi} = -\left(\frac{w'^{\cdot}}{R} - \frac{u^{\cdot} - Rv'}{2R^2}\right)$ (twist) ..(B.6)

---

* The principal notation used in this appendix is defined in Section 3.3.1

$$Q_x = \frac{K_{18}}{R^2}[-R^2 w''' - \nu w'\ddot{} - Ru'' - \nu v'\dot{} + (1-\nu)(-w'\ddot{} + \frac{1}{2R}u\ddot{} - \frac{1}{2}v'\dot{})] \quad ..(B.7)$$

$$Q_\phi = -\frac{K_{18}}{R^2}[\frac{\dot{w}}{R} + \frac{\ddot{w}\dot{}}{R} + \nu R w''\dot{} + (1-\nu)R(w''\dot{} + Rv'')] \quad ..(B.8)$$

$$N_x = K_{17}(\varepsilon_x + \nu\varepsilon_\phi) - \frac{K_{18}}{R}\chi_x \quad ..(B.9)$$

$$N_\phi = K_{17}(\varepsilon_\phi + \nu\varepsilon_x) + \frac{K_{18}}{R}\chi_\phi \quad ..(B.10)$$

$$N_{x\phi} = \frac{K_{17}(1-\nu)}{2}\gamma_{x\phi} - \frac{K_{18}(1-\nu)}{2R}(\chi_{x\phi} - \frac{\gamma_{x\phi}}{2R}) \quad ..(B.11)$$

$$N_{\phi x} = \frac{K_{17}(1-\nu)}{2}\gamma_{x\phi} + \frac{K_{18}(1-\nu)}{2R}(\chi_{x\phi} + \frac{\gamma_{x\phi}}{2R}) \quad ..(B.12)$$

$$M_x = K_{18}(\chi_x + \nu\chi_\phi - \frac{\varepsilon_x + \nu\varepsilon_\phi}{R}) \quad ..(B.13)$$

$$M_\phi = K_{18}(\chi_\phi + \nu\chi_x) \quad ..(B.14)$$

$$M_{x\phi} = K_{18}(1-\nu)(\chi_{x\phi} - \frac{\gamma_{x\phi}}{2R}) \quad ..(B.15)$$

$$M_{\phi x} = K_{18}(1-\nu)\chi_{x\phi} \quad ..(B.16)$$

$z=-\frac{h}{2}$

$$e_x = \varepsilon_x - \frac{h}{2}\chi_x \qquad \text{(surface lateral strain)} \qquad ..(B.17)$$

$$e_\phi = \frac{\varepsilon_\phi - \frac{h}{2}\chi_\phi}{1+\frac{h}{2R}} \qquad \text{(surface circumferential strain)} \qquad ..(B.18)$$

$$e_{x\phi} = \frac{\varepsilon_{x\phi} - (2+\frac{h}{2R})\frac{h}{2}\chi_{x\phi}}{1+\frac{h}{2R}} \qquad \text{(surface shear strain)} \qquad ..(B.19)$$

$$\sigma_x = \frac{E}{1-\nu^2}(e_x+\nu e_\phi) \qquad \text{(surface lateral stress)} \qquad ..(B.20)$$

$$\sigma_\phi = \frac{E}{1-\nu^2}(e_\phi+\nu e_x) \qquad \text{(surface circumferential stress)} \qquad ..(B.21)$$

$$\tau_{x\phi} = \frac{E}{2(1+\nu)}e_{x\phi} \qquad \text{(surface shear stress)} \qquad ..(B.22)$$

$z=+\frac{h}{2}$

$$e_x = \varepsilon_x + \frac{h}{2}\chi_x \qquad \text{(surface lateral strain)} \qquad ..(B.23)$$

$$e_\phi = \frac{\varepsilon_\phi + \frac{h}{2}\chi_\phi}{1-\frac{h}{2R}} \qquad \text{(surface circumferential strain)} \qquad ..(B.24)$$

$$e_{x\phi} = \frac{\varepsilon_{x\phi} + (2-\frac{h}{2R})\frac{h}{2}\chi_{x\phi}}{1-\frac{h}{2R}} \qquad \text{(surface shear strain)} \qquad ..(B.25)$$

$$\sigma_x = \frac{E}{1-\nu^2}(e_x+\nu e_\phi) \qquad \text{(surface lateral stress)} \qquad ..(B.26)$$

$$\sigma_\phi = \frac{E}{1-\nu^2}(e_\phi+\nu e_x) \qquad \text{(surface circumferential stress)} \qquad ..(B.27)$$

$$\tau_{x\phi} = \frac{E}{2(1+\nu)}e_{x\phi} \qquad \text{(surface shear stress)} \qquad ..(B.28)$$

B.2 Flat plate element(109,110)

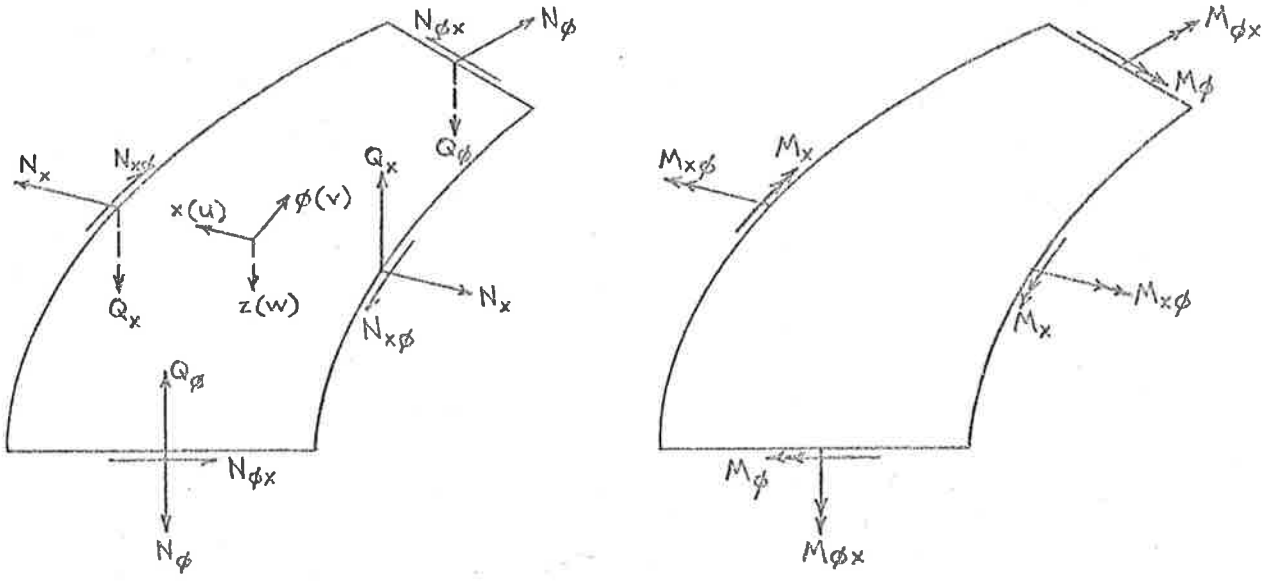

Figure B.2 Positive directions of stress resultants for flat plate element

Let $K_{17} = \frac{Eh}{1-\nu^2}$, $K_{18} = \frac{Eh^3}{12(1-\nu^2)}$, $(\ )' = \frac{\partial(\ )}{\partial x}$ and $(\ )^{\cdot} = \frac{\partial(\ )}{\partial \phi}$.

Then

$$\varepsilon_x = u' \qquad ..(B.29)$$

$$\varepsilon_\phi = \frac{u+v^{\cdot}}{x} \qquad ..(B.30)$$

$$\gamma_{x\phi} = \frac{u^{\cdot}-v}{x} + v' \qquad ..(B.31)$$

$$\chi_x = w'' \qquad ..(B.32)$$

$$\chi_{\phi} = \frac{w'}{x} + \frac{w''}{x^2} \qquad ..(B.33)$$

$$\chi_{x\phi} = \frac{w''}{x} - \frac{w'}{x^2} \qquad ..(B.34)$$

$$Q_x = -K_{18}\left(w''' + \frac{w''}{x} + \frac{w'''-w'}{x^2} - \frac{2w''}{x^3}\right) \qquad ..(B.35)$$

$$Q_{\phi} = -\frac{K_{18}}{x}\left(w''+\frac{w''}{x}+\frac{w'''}{x^2}\right) \qquad ..(B.36)$$

$$N_x = K_{17}(\varepsilon_x+\nu\varepsilon_{\phi}) \qquad ..(B.37)$$

$$N_{\phi} = K_{17}(\varepsilon_{\phi}+\nu\varepsilon_x) \qquad ..(B.38)$$

$$N_{x\phi} = N_{\phi x} = \frac{Eh}{2(1+\nu)}\gamma_{x\phi} \qquad ..(B.39)$$

$$M_x = -K_{18}(\chi_x+\nu\chi_{\phi}) \qquad ..(B.40)$$

$$M_{\phi} = -K_{18}(\chi_{\phi}+\nu\chi_x) \qquad ..(B.41)$$

$$M_{x\phi} = -M_{\phi x} = (1-\nu)K_{18}\chi_{x\phi} \qquad ..(B.42)$$

$z=-\frac{h}{2}$

$$e_x = \varepsilon_x + \frac{h}{2}\chi_x \qquad ..(B.43)$$

$$e_\phi = \varepsilon_\phi + \frac{h}{2}\chi_\phi \qquad ..(B.44)$$

$$e_{x\phi} = \varepsilon_{x\phi} + h\chi_{x\phi} \qquad ..(B.45)$$

$$\sigma_x = \frac{E}{1-\nu^2}(e_x+\nu e_\phi) \qquad ..(B.46)$$

$$\sigma_\phi = \frac{E}{1-\nu^2}(e_\phi+\nu e_x) \qquad ..(B.47)$$

$$\tau_{x\phi} = \frac{E}{2(1+\nu)} e_{x\phi} \qquad ..(B.48)$$

$z=+\frac{h}{2}$

$$e_x = \varepsilon_x - \frac{h}{2}\chi_x \qquad ..(B.49)$$

$$e_\phi = \varepsilon_\phi - \frac{h}{2}\chi_\phi \qquad ..(B.50)$$

$$e_{x\phi} = \varepsilon_{x\phi} - h\chi_{x\phi} \qquad ..(B.51)$$

$$\sigma_x = \frac{E}{1-\nu^2}(e_x+\nu e_\phi) \qquad ..(B.52)$$

$$\sigma_\phi = \frac{E}{1-\nu^2}(e_\phi+\nu e_x) \qquad ..(B.53)$$

$$\tau_{x\phi} = \frac{E}{2(1+\nu)} e_{x\phi} \qquad ..(B.54)$$

B.3 Conical shell element[108]

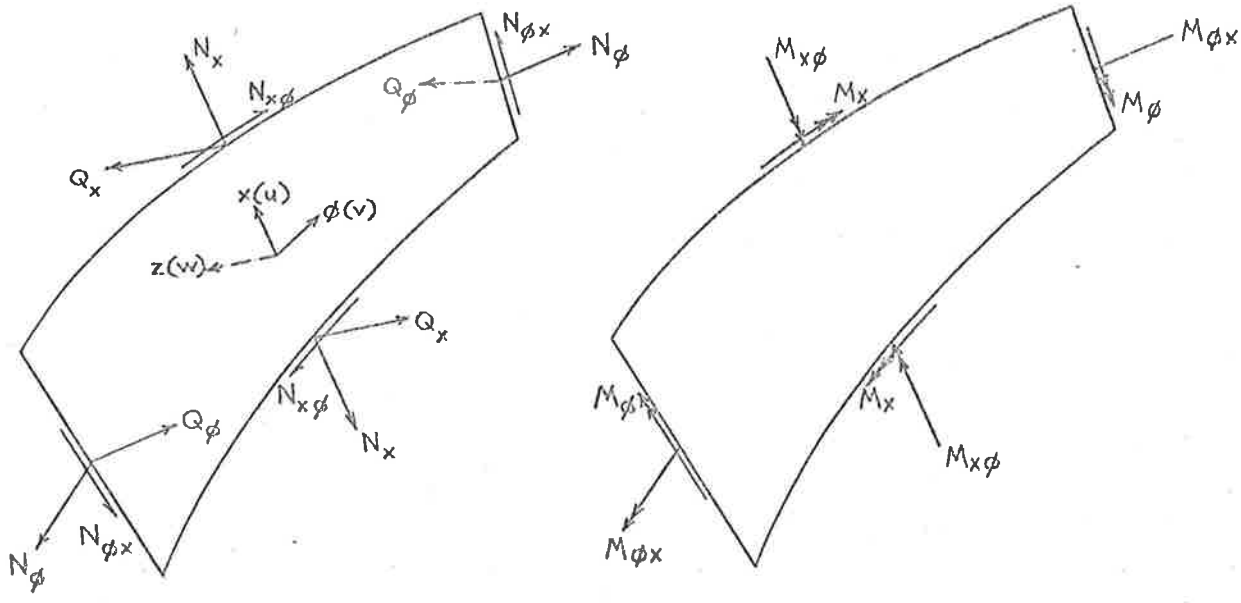

Figure B.3 Positive directions of stress resultants for conical shell element

Let $F = \frac{2Eh_1^3}{3(1-\nu^2)}$, $y = \frac{x}{ah_1} - 1$, $( )' = \frac{d( )}{dy}$, $U = \sum_{n=o}^{\infty} \alpha_n y^n$,

$V = \sum_{n=o}^{\infty} \beta_n y^n$, $W = \sum_{n=o}^{\infty} \gamma_n y^n$, and $p = \frac{\beta}{s}$. Then

$$\varepsilon_x = \frac{U'}{a} \sin\beta\phi \qquad ..(B.55)$$

$$\varepsilon_\phi = \frac{1}{a(y+1)} (U - p^2 V + \frac{W}{t}) \sin\beta\phi \qquad ..(B.56)$$

$$\gamma_{x\phi} = \frac{p}{a(y+1)} [U-V+(y+1)V']\cos\beta\phi \quad ..(B.57)$$

$$\chi_x = - \frac{W''}{a^2 h_1} \sin\beta\phi \quad ..(B.58)$$

$$\chi_\phi = \frac{1}{a^2 h_1 (y+1)^2} [(- \frac{p^2 V}{t} + p^2 W) - (y+1)W']\sin\beta\phi \quad ..(B.59)$$

$$\chi_{x\phi} = \frac{p}{a^2 h_1 (y+1)^2} [\frac{1}{t}((y+1)V'-V) + (W-(y+1)W')]\cos\beta\phi \quad ..(B.60)$$

$$Q_x = - \frac{F}{h_1^2 a^3 (y+1)^3} [(y+1)^3 W''' + (y+2)^2 W'' - (p^2+1)(y+1)W' + 2p^2 W + \frac{p^2}{t}(y+1)V' - \frac{2p^2}{t}V]\sin\beta\phi \quad ..(B.61)$$

$$Q_\phi = - \frac{Fp}{h_1^2 a^3 (y+1)^3} [(y+1)^2 W'' + (y+1)W' - p^2 W - \frac{(1-\nu)}{t}(y+1)^2 V'' + \frac{p^2}{t}V]\cos\beta\phi \quad ..(B.62)$$

$$N_x = \frac{3F}{h_1^2} (\varepsilon_x + \nu\varepsilon_\phi) \quad ..(B.63)$$

$$N_\phi = \frac{3F}{h_1^2} (\varepsilon_\phi + \nu\varepsilon_x) \quad ..(B.64)$$

$$N_{x\phi} = \frac{3F(1-\nu)}{2h_1^2} (\gamma_{x\phi} + \frac{2h_1}{3ta(y+1)} \chi_{x\phi}) \quad ..(B.65)$$

$$N_{\phi x} = \frac{3F(1-\nu)}{2h_1^2} \gamma_{x\phi} \quad ..(B.66)$$

$$M_x = F(\chi_x + \nu\chi_\phi) \quad ..(B.67)$$

$$M_\phi = F(\chi_\phi + \nu\chi_x) \quad ..(B.68)$$

$$M_{x\phi} = M_{\phi x} = F(1-\nu)\chi_{x\phi} \quad ..(B.69)$$

$z=-h_1$

$$e_x = \varepsilon_x - h_1\chi_x \quad ..(B.70)$$

$$e_\phi = \frac{\varepsilon_\phi - h_1\chi_\phi}{1-\frac{h_1}{tx}} \quad ..(B.71)$$

$$e_{x\phi} = \frac{\gamma_{x\phi} - (2-\frac{h_1}{tx})h_1\chi_{x\phi}}{1-\frac{h_1}{tx}} \quad ..(B.72)$$

$$\sigma_x = \frac{E}{1-\nu^2}(e_x+\nu e_\phi) \quad ..(B.73)$$

$$\sigma_\phi = \frac{E}{1-\nu^2}(e_\phi+\nu e_x) \quad ..(B.74)$$

$$\tau_{x\phi} = \frac{E}{2(1+\nu)} e_{x\phi} \quad ..(B.75)$$

$z=+h_1$

$$e_x = \varepsilon_x + h_1\chi_x \quad ..(B.76)$$

$$e_\phi = \frac{\varepsilon_\phi + h_1\chi_\phi}{1+\frac{h_1}{tx}} \quad ..(B.77)$$

$$e_{x\phi} = \frac{\gamma_{x\phi} + (2+\frac{h_1}{tx})h_1\chi_{x\phi}}{1+\frac{h_1}{tx}} \quad ..(B.78)$$

$$\sigma_x = \frac{E}{1-\nu^2}(e_x+\nu e_\phi) \quad ..(B.79)$$

$$\sigma_\phi = \frac{E}{1-\nu^2}(e_\phi+\nu e_x) \quad ..(B.80)$$

$$\tau_{x\phi} = \frac{E}{2(1+\nu)} e_{x\phi} \quad ..(B.81)$$

APPENDIX C. Assembly of Various Matrices Required in the Solution of a Simple Folded Shell Structure

An example of a simple 3-element box beam with a single internal diaphragm is chosen to illustrate the general methods for assembling the matrices K_S, L_1, L_2, E_1, E_2 required in the folded shell solution of any diaphragm structure (Sections 3.3.4 and 3.4.2). Only the m^{th} harmonic is considered in the ensuing discussion.

A pictorial sketch of the beam is shown in Figure C.1, together with the arbitrarily selected joint and element identification numbers. (Joint numbers are represented by plain integers whereas element numbers are represented by bracketed integers).

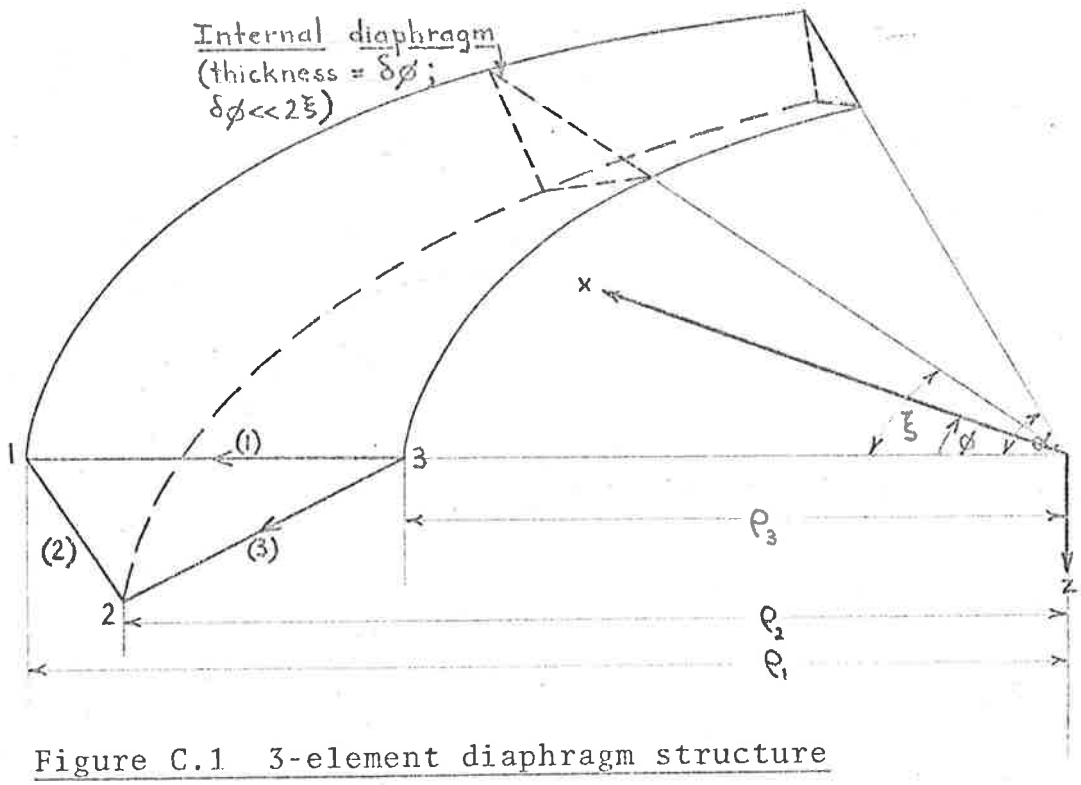

Figure C.1 3-element diaphragm structure

The arrow drawn on each element indicates the positive direction of the x-axis (member coordinate system) and hence also the direction from curved joint A to curved joint B (Section 3.3.1). During the assembly of the various matrices of interest in this appendix, a system of subscripts is used which is critically dependent upon the correct identification of joints A and B for each element. This system is therefore clearly summarized in Table C.1.

Element \ Joint	A	B
(1)	3	1
(2)	2	1
(3)	3	2

Table C.1 Key to joint subscripts

C.1 Assembly of structural stiffness matrix K_S

For each element, the (8 × 8) stiffness matrix (referred to the global coordinate system) can be partitioned according to equation (76). Hence, for the complete structure, the relationship between the joint loads (global coordinates) and the corresponding joint displacement components (global coordinates) is given by the equation

$$\begin{bmatrix} p_1 \\ \hline p_2 \\ \hline p_3 \end{bmatrix} = \left[\begin{array}{c|c|c} k_{11_{(1)}} + k_{11_{(2)}} & k_{12_{(2)}} & k_{13_{(1)}} \\ \hline k_{21_{(2)}} & k_{22_{(2)}} + k_{22_{(3)}} & k_{23_{(3)}} \\ \hline k_{31_{(1)}} & k_{32_{(3)}} & k_{33_{(1)}} + k_{33_{(3)}} \end{array}\right] \cdot \begin{bmatrix} \delta_1 \\ \hline \delta_2 \\ \hline \delta_3 \end{bmatrix}$$

(12×1) (12×12) (12×1)

... (C.1)

where the bracketed numbers indicate reference to individual shell elements. Table C.1 is used to obtain the joint subscripts. Thus, for example $k_{12_{(2)}}$ represents k_{BA} for element(2). Equation (C.1) is a partitioned form of equation (77), and the (12×12) symmetrical matrix is thus the assembled structural stiffness matrix K_S.

C.2 Assembly of diaphragm interaction matrix L_1

Figure C.2 indicates the nature of the assumed diaphragm redundants (Section 3.2) which act on the box beam cross section at the angular location $\phi = \xi$.

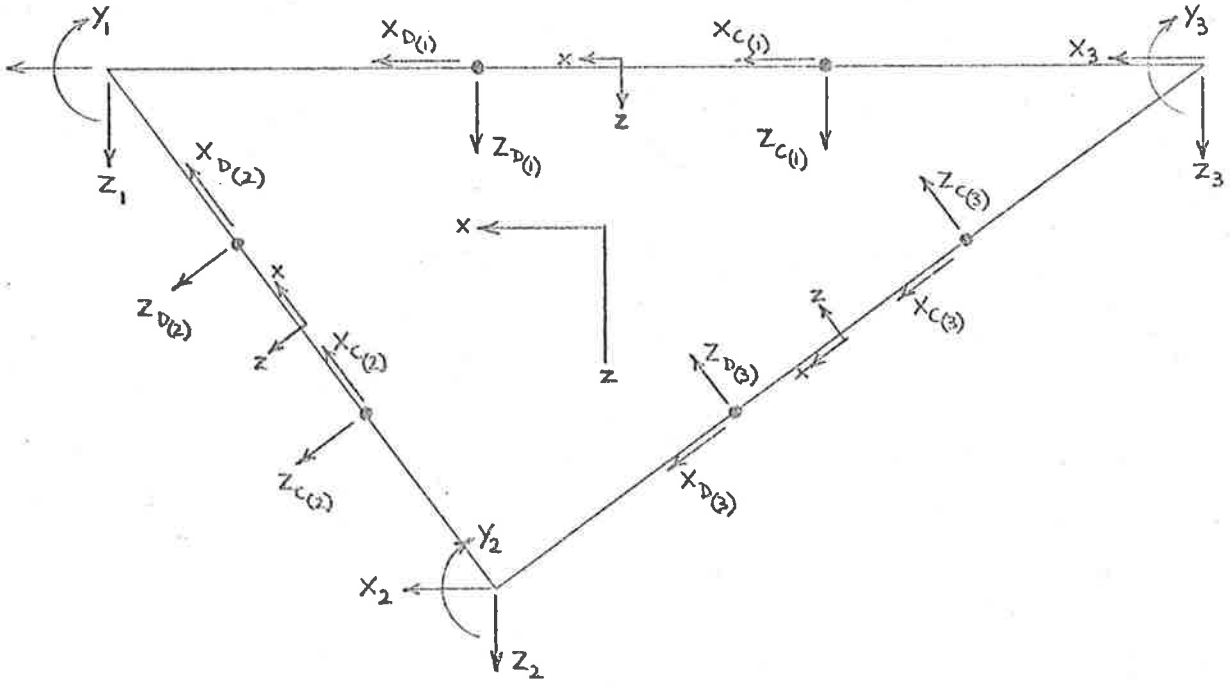

Figure C.2 Assumed diaphragm redundants

The resultants of the triangularly distributed redundants act at the one-third points across each element and are referred to the appropriate member coordinate system, whereas all joint redundants are referred to the global coordinate system. Hence the diaphragm redundant matrix P_D (Section 3.4.2) can be written

$$P_D = \underset{(21\times1)}{\begin{bmatrix} X_{C_{(1)}} \\ Z_{C_{(1)}} \\ X_{D_{(1)}} \\ Z_{D_{(1)}} \\ \hline X_{C_{(2)}} \\ Z_{C_{(2)}} \\ X_{D_{(2)}} \\ Z_{D_{(2)}} \\ \hline X_{C_{(3)}} \\ Z_{C_{(3)}} \\ X_{D_{(3)}} \\ Z_{D_{(3)}} \\ \hline X_1 \\ Z_1 \\ Y_1 \\ \hline X_2 \\ Z_2 \\ Y_2 \\ \hline X_3 \\ Z_3 \\ Y_3 \end{bmatrix}} \quad \ldots \text{ (C.2)}$$

Therefore, in accordance with equation (101), the diaphragm interaction matrix L_1 must be assembled as follows.

$$L_1 = \begin{bmatrix} 0 \ (4\times12) & \begin{matrix} q_1 & 0 & 0 \\ 0 & 0 & 0 \\ 0 & q_1 & 0 \\ 0 & 0 & q_1 \end{matrix} \ (4\times3) & 0 \ (4\times3) \\ 0 \ (4\times12) & 0 \ (4\times3) & \begin{matrix} q_2 & 0 & 0 \\ 0 & 0 & 0 \\ 0 & q_2 & 0 \\ 0 & 0 & q_2 \end{matrix} \ (4\times3) \\ 0 \ (4\times12) & 0 \ (4\times3) & 0 \ (4\times3) & \begin{matrix} q_3 & 0 & 0 \\ 0 & 0 & 0 \\ 0 & q_3 & 0 \\ 0 & 0 & q_3 \end{matrix} \end{bmatrix} \quad (12\times21) \qquad \ldots (C.3)$$

where $q_{1,2,3} = \frac{4}{m\Pi\rho_{1,2,3}\delta\phi}\sin\frac{m\Pi\xi}{\alpha}\sin\frac{m\Pi\delta\phi}{2\alpha}$

C.3 Assembly of diaphragm interaction matrix L_2

For each element, the fixed-edge stress resultants induced by the action of the triangularly distributed diaphragm redundants can be expressed as the sum of a complementary solution and a particular solution. Thus, with the established notation (Sections 3.3.1 and 3.3.2),

$$P_M = H \cdot C + H_4 \cdot P_D \qquad \text{... (C.4)}$$

$(8\times1)\quad (8\times8)\quad (8\times1)\quad (8\times21)\quad (21\times1)$

where the subscript M is included to emphasize that these fixed-edge stress resultants are referred to the member coordinate system. Matrix H_4 can be deduced from the particular solutions derived in Section 3.4.1. Similarly, the equation which describes the fixed-edge boundary conditions can be written

$$G \cdot C + G_3 \cdot P_D = 0 \qquad \text{... (C.5)}$$

$(8\times8)\quad (8\times1)\quad (8\times21)\quad (21\times1)\quad (8\times1)$

where the matrix G_3 can also be deduced from the particular solutions derived in Section 3.4.1. It is evident from equation (C.5) that

$$C = -G^{-1} \cdot G_3 \cdot P_D \qquad \text{... (C.6)}$$

and hence equation (C.4) becomes

$$P_M = [H_4 - H \cdot G^{-1} \cdot G_3] \cdot P_D \qquad \text{... (C.7)}$$

However, the product $H.G^{-1}$ is equal to the stiffness matrix k_M of the element referred to the member coordinate system (Section 3.3.1), and so

$$P_M = [H_4 - k_M \cdot G_3] \cdot P_D \qquad \text{... (C.8)}$$

By using the transpose of the element transformation matrix A (Section 3.3.3), the fixed-edge stress resultants can be referred to the global coordinate system. Hence

$$P_G = A^T \cdot [H_4 - k_M \cdot G_3] \cdot P_D \qquad \ldots (C.9)$$

where the subscript G denotes reference to the global coordinate system. After calculating the above products, this equation may be partitioned as shown in equation (C.10)

$$\underset{(8\times1)}{\begin{bmatrix} P_A \\ \hline P_B \end{bmatrix}_G} = \underset{(8\times21)}{\begin{bmatrix} \kappa_A \\ \hline \kappa_B \end{bmatrix}} \cdot \underset{(21\times1)}{P_D} \qquad \ldots (C.10)$$

where A and B are the two curved edges of the element. If the matrices κ_A and κ_B are calculated for all three elements of the complete structure, then in accordance with equation (101), the diaphragm interaction matrix L_2 must be assembled as follows.

$$\underset{(12\times21)}{L_2} = - \begin{bmatrix} \kappa_{1(1)} + \kappa_{1(2)} \\ \hline \kappa_{2(2)} + \kappa_{2(3)} \\ \hline \kappa_{3(3)} + \kappa_{3(1)} \end{bmatrix} \qquad \ldots (C.11)$$

where again the joint subscripts are obtained from Table C.1, and the bracketed numbers indicate reference to individual shell

C.4 Assembly of matrix E_1, an indirect contribution to the diaphragm flexibility matrix F_D

If each element is subjected to curved edge movements only, and no loads act on the element surface, then the complementary solutions of the governing differential equation system are sufficient to determine the net structural response. Hence the amplitudes of the four displacement components which exist at the lateral locations C and D (corresponding to the resultants of the four triangularly distributed diaphragm redundants) can be written

$$\underset{(4\times1)}{\begin{bmatrix} u_C \\ w_C \\ u_D \\ w_D \end{bmatrix}_M} = \underset{(4\times1)}{\begin{bmatrix} \delta_C \\ \hline \delta_D \end{bmatrix}} = \underset{(4\times8)}{G'} \cdot \underset{(8\times1)}{C} \qquad \ldots (C.12)$$

where the subscript M denotes reference to the member coordinate system, and the matrix G' can be calculated by using the same general procedure as described in Section 3.3.1.for the calculation of matrix G. The equation which expresses the boundary conditions is

$$\underset{(8\times1)}{\begin{bmatrix} \delta_A \\ \hline \delta_B \end{bmatrix}_M} = \underset{(8\times8)}{G} \cdot \underset{(8\times1)}{C} \qquad \ldots (C.13)$$

and so

$$\left[\frac{\delta_C}{\delta_D}\right]_M = G' \cdot G^{-1} \cdot \left[\frac{\delta_A}{\delta_B}\right]_M$$

$$= G' \cdot G^{-1} \cdot A \cdot \left[\frac{\delta_A}{\delta_B}\right]_G \qquad \ldots \text{(C.14)}$$

where the subscript G denotes reference to the global coordinate system. After calculating the above products, the matrices in this equation may be partitioned as shown in equation (C.15).

$$\left[\frac{\delta_C}{\delta_D}\right]_M = [\zeta_A | \tilde{\zeta}_B] \cdot \left[\frac{\delta_A}{\delta_B}\right]_G \qquad \ldots \text{(C.15)}$$

(4×1) (4×8) (8×1)

If the matrices ζ_A and ζ_B are calculated for all three elements of the complete structure, then in accordance with equation (104), the matrix E_1 must be assembled as follows

$$E_{1\,(21\times12)} = \left[\begin{array}{c|c|c} {}^{\zeta}1_{(1)} & \underset{(4\times4)}{0} & {}^{\zeta}3_{(1)} \\ \hline {}^{\zeta}1_{(2)} & {}^{\zeta}2_{(2)} & \underset{(4\times4)}{0} \\ \hline \underset{(4\times4)}{0} & {}^{\zeta}2_{(3)} & {}^{\zeta}3_{(3)} \\ \hline J & \underset{(3\times4)}{0} & \underset{(3\times4)}{0} \\ \hline \underset{(3\times4)}{0} & J & \underset{(3\times4)}{0} \\ \hline \underset{(3\times4)}{0} & \underset{(3\times4)}{0} & J \end{array}\right] \cdot \sin\frac{m\Pi\xi}{\alpha} \qquad \ldots \text{(C.16)}$$

where

$$J = \begin{bmatrix} 1 & 0 & 0 & 0 \\ 0 & 0 & 1 & 0 \\ 0 & 0 & 0 & 1 \end{bmatrix}$$

, and once again Table C.1 is used to obtain the appropriate joint subscripts. Bracketed numbers denote reference to individual shell elements.

C.5 Assembly of matrix E_2: a direct contribution to the diaphragm flexibility matrix F_D

For each element under fixed-edge conditions, the amplitudes of the displacement components at the one-third points C and D induced by the action of triangularly distributed diaphragm redundants can be written

$$\left[\frac{\delta_C}{\delta_D}\right]_M = G' \cdot C + G_4 \cdot P_D \qquad \ldots (C.17)$$

$(4\times1)\quad (4\times8)\quad (8\times1)\quad (4\times21)\quad (21\times1)$

where again the subscript M is used to denote reference to the member coordinate system. Matrix G_4 can be calculated directly from the particular solutions derived in Section 3.4.1. The fixed-edge boundary conditions are expressed by equation (C.5), and so equation (C.17) becomes

$$\left[\frac{\delta_C}{\delta_D}\right]_M = [G_4 - G' \cdot G^{-1} \cdot G_3] \cdot P_D \qquad \ldots (C.18)$$

This equation may be written as

$$\left[\frac{\delta_C}{\delta_D}\right]_M = \psi \cdot P_D \qquad \ldots (C.19)$$

$(4\times1)\quad (4\times21)(21\times1)$

If the matrix ψ is calculated for all three elements of the complete structure, then in accordance with equation (106), the matrix E_2 must be assembled as follows.

$$E_{2\,(21\times21)} = \begin{bmatrix} \psi_{(1)} \\ \psi_{(2)} \\ \psi_{(3)} \\ 0 \\ (9\times21) \end{bmatrix} \cdot \sin\frac{m\Pi\xi}{\alpha} \qquad \ldots \text{(C.20)}$$

where the bracketed numbers again indicate reference to individual shell elements.

APPENDIX D. Comments on Program FOLSHEL

The degree of generality which has been achieved with the FOLSHEL program is perhaps best illustrated by stating the form of the required input data. A description of this is given, followed by a flow-chart outline of the programmed folded shell solution method. Finally, brief comments are made concerning computer times and storage requirements for some of the problems analysed during this research project. A detailed list of the output quantities which are calculated by the program at any specified locations on each folded shell structure is given in Appendix B.

D.1 Form of input data

1st card: Title of problem

2nd card:
- (a) Angle subtended by shell assembly = ALPHA
- (b) Number of elements = NEL
- (c) Number of joints = NJT
- (d) Number of diaphragms (internal) = NDIAPH
  (Note: All diaphragms are assumed to be the same shape when viewed in the ϕ-direction)
- (e) Number of ϕ-coordinates at which results are desired = NPHIP
- (f) Maximum Fourier series limit = MHARM
- (g) Check on odd or even harmonics = NCHECK
  (Note: +1 for odd terms only (symmetrical)
  0 for all terms
  -1 for even terms only (anti-symmetrical))
- (h) Number of flat plate elements = NFP

(i) Number of cylindrical shell elements = NCYLSHL

(j) Number of conical shell elements = NCONSHL

(k) Number of moveable diaphragms (if any) = NMDIAPH

(l) Number of elements internally connected to diaphragms (if any) = NICEL

(m) Number of joints connected to diaphragms (if any) = NEC

(n) Identification number of the first joint connected to each diaphragm (if any) = JSTART

(Note: All joints connected to diaphragms must be numbered consecutively)

3rd card: ϕ-coordinates at which results are desired = PHIP(I)

(Note: Use more cards if necessary)

Next cards: One card for each diaphragm (No cards required if NDIAPH = 0)

(a) Diaphragm identification number = I

(Note: Input all unmoveable diaphragms first, if any)

(b) ϕ-coordinate at which diaphragm exists = DIAPHI(I)

(c) Diaphragm angular thickness = DIADEL(I)

Next cards: One card for each element

(a) Element identification number = I

(b) Joint A = JA(I)

(c) Joint B = JB(I)

(d) Type of shell element = KSHL(I)

(Note: 1 for flat plate
2 for cylindrical shell
3 for upright cone
4 for inverted cone)

(e) Number of desired evenly-spaced lateral locations for calculation of output quantities = NSEC(I)

(Note: Lateral width of each element is thus divided into NSEC(I)-1 equal parts)

(f) Dead load (force/unit surface area of element) = DL(I)

(g) Uniform horizontal load (force/unit vertical projected area) = HL(I)

(h) Uniform vertical load (force/unit horizontal projected area) = VL(I)

(i) Thickness of element = TH(I)

(j) Young's modulus = YM(I)

(k) Poisson's ratio = PR(I)

Next card: Number of partial uniform surface loads = NSURL

Next cards: One card for each partial uniform surface load (no cards required if NSURL = 0. More than one partial load may exist on an element, but each one requires a separate card)

(a) Element identification number = LEL

(b) Horizontal load, force/unit vertical projected area (force/unit vertical projected length if line load is applied) = SURHL(LEL)

(c) Vertical load, force/unit horizontal projected area (force/unit horizontal projected length if line load is applied) = SURVL(LEL)

(d) Angular location of start of partial load from left support (ϕ=0) = SURPHI(LEL)

(e) Angular width of partial load (= 0 for line load) = SURDEL(LEL)

(Note: If SURDEL $\neq$ 0, input SURHL and SURVL as force/unit area;

If SURDEL = 0, input SURHL and SURVL as force/unit length)

Next cards: One card for each joint

(a) Joint identification number = I

(b) Applied uniform horizontal joint force (force/unit length) = AJFOR(1,I)

(c) Applied uniform vertical joint force (force/unit length) = AJFOR(2,I)

(d) Applied uniform joint moment (moment/unit length) = AJFOR(3,I)

(e) Applied longitudinal joint force (post-tension prestress) = AJFOR(4,I)

(Note: For prestress P at each end, input total force at one end for AJFOR,

(f) x-coordinate (global) of joint = XC(I)

(g) z-coordinate (global) of joint = ZC(I)

Next card: Number of partial uniform joint loads = NCONL

Next cards: One card for each partial uniform joint load (No cards required if NCONL = 0. More than one partial load may exist on a joint, but each one requires a separate card)

(a) Joint identification number = LJT

(b) Total horizontal force = CONHL(LJT)

(c) Total vertical force = CONVL(LJT)

(d) Total moment = CONM(LJT)

(e) Total longitudinal force P, positive in ϕ-direction = CONS(LJT)

(Note: P must be balanced by -P somewhere along the same joint)

(f) Angular location of start of partial load from left support (ϕ=0) = CONPHI(LJT)

(g) Angular width of partial load (=0 for concentrated load) = CONDEL(LJT)

D.2 Flow-chart outline of calculation procedure

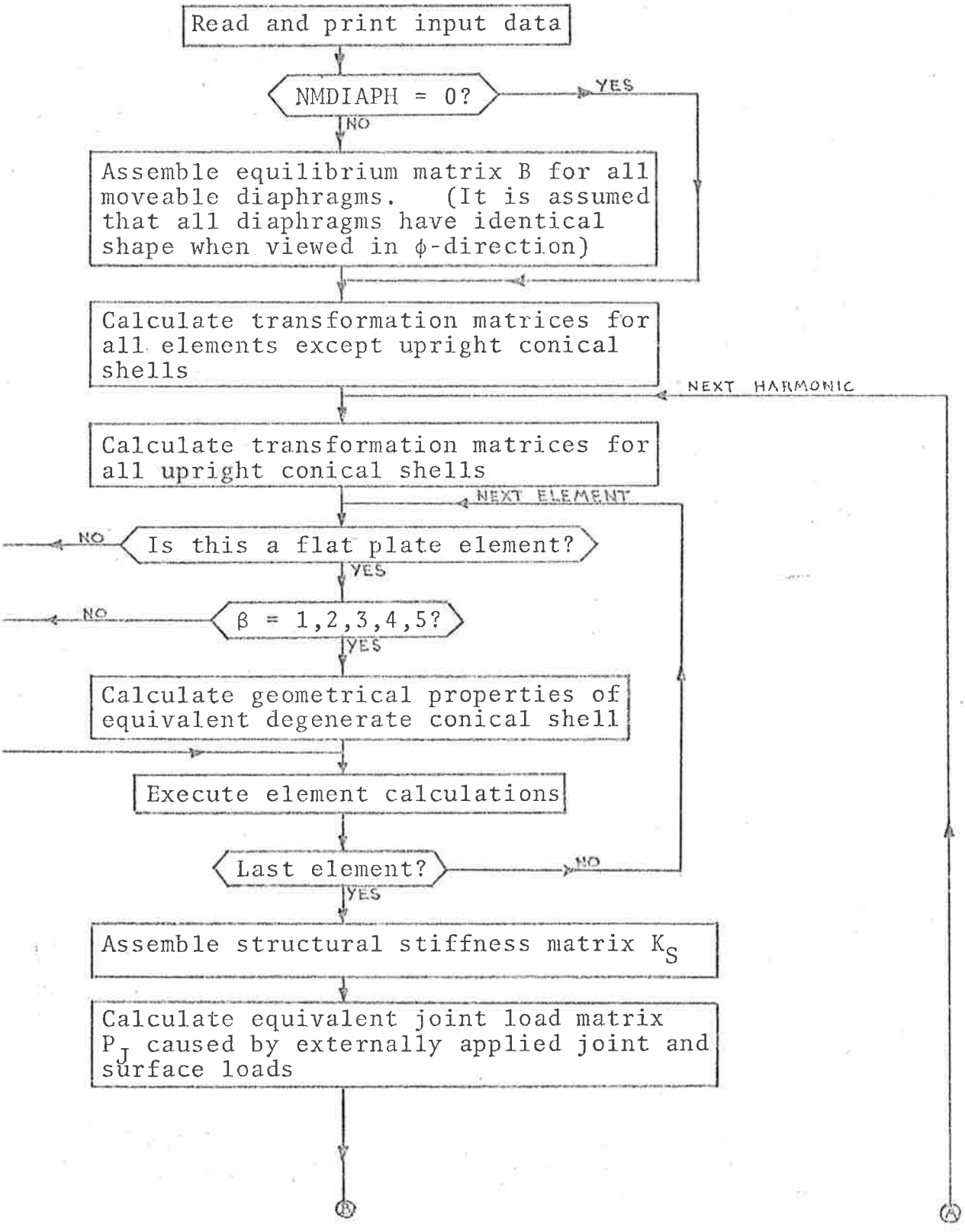

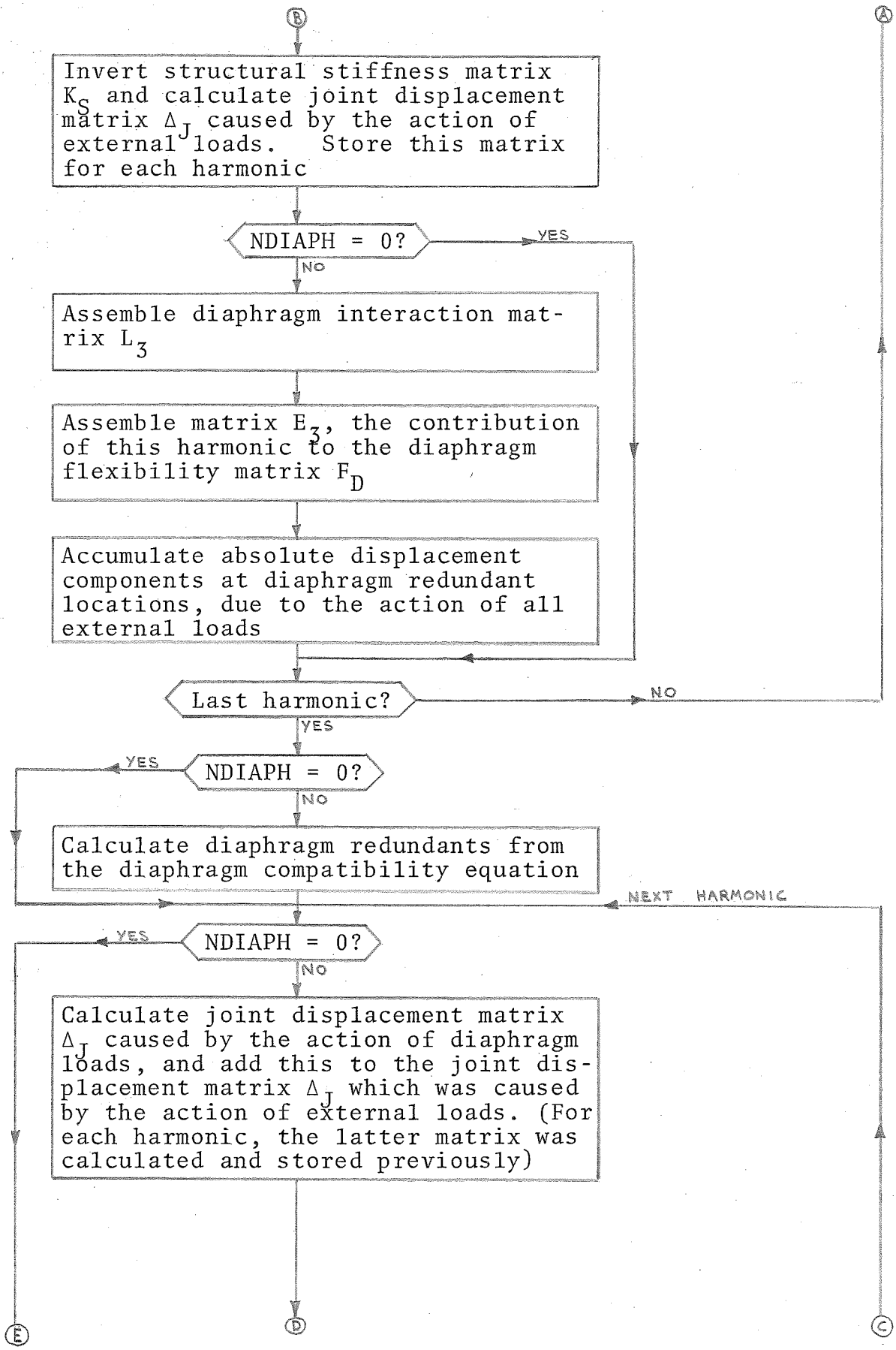
B
Invert structural stiffness matrix K_S and calculate joint displacement matrix Δ_J caused by the action of external loads. Store this matrix for each harmonic
NDIAPH = 0?
YES
NO
Assemble diaphragm interaction matrix L_3
Assemble matrix E_3, the contribution of this harmonic to the diaphragm flexibility matrix F_D
Accumulate absolute displacement components at diaphragm redundant locations, due to the action of all external loads
Last harmonic?
NO
YES
NDIAPH = 0?
YES
NO
Calculate diaphragm redundants from the diaphragm compatibility equation
NEXT HARMONIC
NDIAPH = 0?
YES
NO
Calculate joint displacement matrix Δ_J caused by the action of diaphragm loads, and add this to the joint displacement matrix Δ_J which was caused by the action of external loads. (For each harmonic, the latter matrix was calculated and stored previously)
A
C
D
E

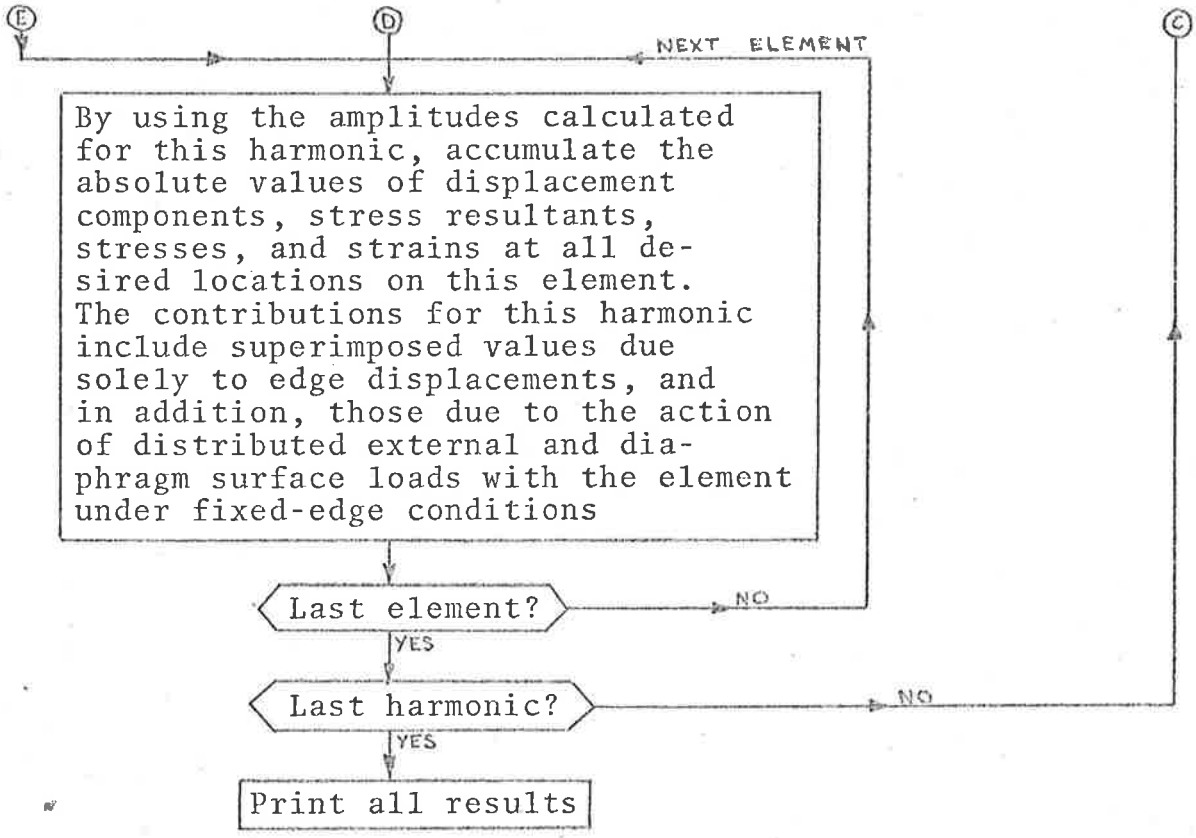

D.3 Computing time and storage requirements

In order to analyse the two folded shell models with the load positioned above the centre of plate (3), the following computing times were necessary on the C.D.C. 6400. (This particular load case is chosen to illustrate computing times, because it always required the largest amount of calculation).

(a) Primary Structure

For 11 non-zero Fourier terms (MHARM=21; NCHECK=+1),

Central Processing (C.P.) time ≒ 4 min. 0 sec.

Peripheral Processing (P.P.) time ≒ 7 min.30 sec.

For 21 non-zero Fourier terms (MHARM=41; NCHECK=+1),

C.P. time ≒ 6 min. 0 sec.

P.P. time ≒ 9 min.40 sec.

(b) Diaphragm Structure

For 21 non-zero Fourier terms (MHARM=21; NCHECK=0),

C.P. time ≒ 9 min. 0 sec.

P.P. time ≒ 27 min.10 sec.

For 41 non-zero Fourier terms (MHARM=41; NCHECK=0),

C.P. time ≒ 15 min.40 sec.

P.P. time ≒ 34 min.40 sec.

For each structure, since an extra joint had to be assumed at the lateral location of the knife-edge load, there were thus 9 folded shell joints in all, and 10 folded shell elements. Final results were evaluated at 13 cross sections along the beam, and at 3, 4, or 5 sections across each element. For the diaphragm structure, the number of redundants (excluding the three rigid body in-plane displacement components of the moveable diaphragm) was 53.

The amount of central memory computer storage required to load and execute the program is largely dependent upon the number of diaphragm redundants and the number of selected locations at which output results are desired. For every run of the FOLSHEL program, the maximum allowable field length of 140K locations was specified. By using all of

this storage, it was possible to analyse a structure with up to 145 diaphragm redundants and to evaluate the final results at up to 585 different locations on the component elements. Since the total amount of calculation is also largely dependent upon the number of diaphragm redundants, it follows that the solution of a problem of this size would require much more computing time than the examples quoted above.

APPENDIX E. Adjustment of Experimental Rosette Strain Gauge Readings due to Finite Gauge Eccentricity

A sketch of the type of quadruple-gauge rectangular strain rosette used throughout the experimental investigations is given in Figure 4.9(b). When each rosette was positioned on the surface of any folded shell element, it was always orientated as shown in Figure E.1, where the gauges marked 0°, 45°, 90°, 135° in Figure 4.9(b) are now identified as gauges 1, 2, 3, 4 respectively.

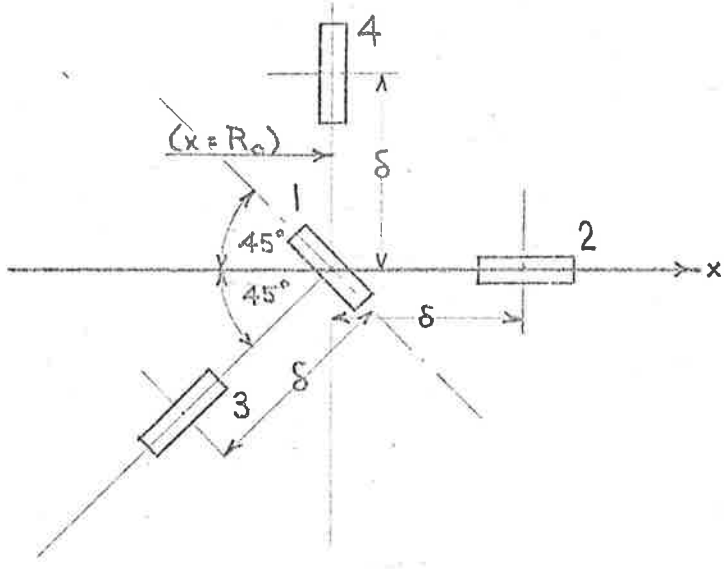

Figure E.1 Orientation of rosette with respect to x-axis of member coordinate system

Inspection of Figure E.1 indicates clearly that gauge 1 is the only one which measured strain at the centre of the rosette. The other three gauges were eccentric by the same distance δ. (For the rosettes used in the experiments, δ was approximately $\frac{1}{8}$"). Therefore, in regions of high strain gradients, the strains recorded by gauges 2, 3, 4 could not be assumed to

occur at the rosette centre. However, appropriate adjustments were made based on prior knowledge of the strain gradients in this area obtained from the folded shell theoretical calculations. With respect to the member ϕ-direction, there were two possible orientations to be considered:

(a) gauge 4 aligned with the positive ϕ-direction

Let the true strains which existed at the rosette centre and which corresponded to the directions of the four component gauges be e_{1_0}, e_{2_0}, e_{3_0}, e_{4_0}. Let the actual measured strains be e_1, e_2, e_3, e_4 respectively. From the geometry of Figure E.1, it follows that

$$e_{3_0} = e_3 + \frac{\delta}{\sqrt{2}}\left(\frac{\partial e_{3_0}}{\partial x} + \frac{\partial e_{3_0}}{R_0 \partial \phi}\right) \qquad \ldots \text{(E.1)}$$

Let the theoretical predicted values of direct strain (at the rosette centre) corresponding to the x and ϕ-directions be e_x and e_ϕ respectively, and let the corresponding theoretical value of shear strain be $e_{x\phi}$. Then consideration of Mohr's circle for strain reveals that

$$2e_{3_0} = e_x + e_\phi + e_{x\phi} \qquad \ldots \text{(E.2)}$$

Hence equation (E.1) can be written

$$e_{3_0} = e_3 + \frac{\delta}{2\sqrt{2}}\left(\frac{\partial e_x}{\partial x} + \frac{\partial e_\phi}{\partial x} + \frac{\partial e_{x\phi}}{\partial x} + \frac{\partial e_x}{R_0 \partial \phi} + \frac{\partial e_\phi}{R_0 \partial \phi} + \frac{\partial e_{x\phi}}{R_0 \partial \phi}\right) \qquad \ldots \text{(E.3a)}$$

The analogous equations for the other gauges are much simpler.

$$e_{1_0} = e_1 \qquad \ldots \text{(E.3b)}$$

$$e_{2_0} = e_2 - \delta \cdot \frac{\partial e_x}{\partial x} \qquad \ldots \text{(E.3c)}$$

$$e_{4_0} = e_4 - \delta \cdot \frac{\partial e_\phi}{R_0 \partial \phi} \qquad \ldots \text{(E.3d)}$$

The corrections to be applied to the experimental readings in order to allow for gauge eccentricity can thus be calculated from equations (E.3a-d).

(b) gauge 4 aligned with the negative ϕ-direction

For this orientation, the results can be deduced directly from equations (E.3a-d) by reversing the signs of all gradients in the ϕ-direction.

Since the folded shell analysis gave values of e_x, e_ϕ, $e_{x\phi}$ (Appendix B) at a regular grid of points on each element of the model box beams, it would have been tedious but possible to calculate all required terms for the above corrections. However, the amount of necessary calculation was considerably reduced by checking that at the instrumented locations, all strain gradients in the ϕ-direction were generally small compared with the strain gradients in the x-direction. Under these conditions

the orientation of each rosette with respect to the member ϕ-direction had no influence on the corrections to be calculated.

BIBLIOGRAPHY

1. SAINT-VENANT, B. "Memoire sur le calcul de la résistance et de la flexion des pièces solides à simple ou à double courbure, en prenant simultanément en consideration les divers efforts auxquels elles peuvent être soumises dans tous les sens". Comptes-Rendus, l'Académie des Sciences de Paris, XVII, 1843, pp. 942 and 1020-1031.

2. McMANUS, P.F., NASIR, G.A., and CULVER, C.G. "Horizontally Curved Girders - State of the Art". Proc. A.S.C.E. (Journ. Struct. Div.), 95 (ST5), 1969, pp. 853-870.

3. MAISEL, B.I. "Review of Literature Related to the Analysis and Design of Thin-walled Beams". Cement and Concrete Association, Technical Report, TRA 440, July 1970.

4. A.S.C.E. - A.A.S.H.O. COMMITTEE ON FLEXURAL MEMBERS, SUB-COMMITTEE ON BOX GIRDER BRIDGES. "Trends in the Design of Steel Box Girder Bridges. Progress Report". Proc. A.S.C.E. (Journ. Struct. Div.), 93 (ST3), 1967, pp. 165-180.

5. TIMOSHENKO, S.P. "Strength of Materials, Part II". New York, D. Van Nostrand Company, Inc., Second Edition, 1941, pp. 265-311.

6. BECHERT, H. "Zur Berechnung gekrümmter einfeldriger Brücken". Beton-und Stahlbetonbau, 58, 12, 1963, pp. 279-284 and 59, 6, 1964, pp. 143-144.

7. MELLOR, P.B. and JOHNSON, W. "Approximate Deflections in Cantilevers Curved in Plan". Journ. of Roy. Aero. Society, 62, 565, 1958, pp. 64-66.

8. MOORMAN, R.B.B. and TATE, M.B. "Influence Lines for Horizontally Curved Fixed-ended Beams of Circular Arc Plan". University of Missouri, Bulletin, Engineering Series No. 35, 1947.

9. ABBASSI, M.M. "Mathematical Analysis of Bow Girders of Any Shape". Trans. A.S.M.E. (Journ. of Applied Mech.), 23, 4, 1956, pp. 522-526.

10. ABBASSI, M.M. "Stresses in Curved Beams of Non-circular Centerline". Trans. A.S.M.E. (Journ. of Applied Mech.), 27, 3, 1960, pp. 445-454.

11. STAMPF, W. "Circularly Curved Fully Clamped Symmetrical Beams with Loads Normal to the Plane of Curvature and Twisting Moments". (in German), Bautechnik, 42, 12, 1965, pp. 404-408.

12. TERRINGTON, J.S. "Combined Bending and Torsion of Beams and Girders, Part I". British Constructional Steelwork Association Ltd, Publication 31, 1968.

13. TERRINGTON, J.S. "Combined Bending and Torsion of Beams and Girders, Part II". British Constructional Steelwork Association Ltd, Publication 31, 1970.

14. DONALD, P.T.A. and GODDEN, W.G. "Numerical Solution to Curved Beam Problems". Structural Engineer, 41, 6, 1963, pp. 179-186.

15. REDDY, M.N. and TUMA, J.J. "Analysis of Laterally Loaded Continuous Curved Beams". Proc. A.S.C.E. (Journ. Struct. Div.), 93 (ST1), 1967, pp. 495-513.

16. YOUNG, M.C. "Flexibility Influence Functions for Curved Beams". Proc. A.S.C.E. (Journ. Struct. Div.), 95 (ST7), 1969, pp. 1407-1429.

17. HALL, A.S. and WOODHEAD, R.W. "Frame Analysis". New York, John Wiley and Sons, Inc., First Edition, 1961, p. 31.

18. LIVESLEY, R.K. "Matrix Methods of Structural Analysis". Oxford, Pergamon, 1964, pp. 108-109.

19. MENN, C. "Zur Berechnung gekrümmter Brücken". Schweizerische Bauzeitung, 82, 12, 1964, pp. 185-191.

20. GARRETT, R.J. and COCHRAINE, R.A. "The Analysis of Prestressed Beams Curved in Plan with Torsional Restraint at the Supports". Structural Engineer, 48, 3, 1970, pp. 128-132.

21. WITECKI, A.A. "Simplified Method for the Analysis of Torsional Moment as an Effect of a Horizontally Curved Multispan Continuous Bridge". Paper presented at First International Symposium on Concrete Bridge Design, Toronto, 1967, A.C.I Publication SP-23, 1969, pp. 193-204.

22. BASSI, K.G., LIN, W.L., and RICHARDSON, B.S. "Continuous Post-tensioned Torsionally Stiff Concrete Bridges". Paper presented at First International Symposium on Concrete Bridge Design, Toronto, 1967, A.C.I Publication SP-23, 1969, pp. 563-577.

23. MAQUOI, R. "The Design of Curved Bridges. Application to a Three-span Highway Bridge". (in French), Ann. Travaux Publics Belgique, 3, 1967, pp. 219-237.

24. VELUTINI, B. "Analysis of Continuous Circular Curved Beams". Proc. A.C.I., 47, 3, 1950, pp. 217-228.

25. FICKEL, H.H. "Analysis of Curved Girders". Proc. A.S.C.E. (Journ. Struct. Div.), 85 (ST7), 1959, pp. 113-141.

26. COURBON, J. "Théorie des ponts courbes". Ann. des Ponts et Chaussées, 131, 5, 1961, pp. 611-648.

27. BRETTHAUER, G. and NOETZOLD, F. "Ein Beitrag zur Berechnung von gekrümmten Durchlaufträgern mit starrer und elastischer Torsionseinspannung über den Stützen". Bauingenieur, 39, 10, 1964, pp. 402-406.

28. STAMPF, W. "Zur Berechnung des im Grundiss gebogenen durchlaufenden Balkens, belastet durch Vertikalkräfte und Torsionsmomente". Bautechnik, 41, 8, 1964, pp. 253-261.

29. PETERSEN, C. "Das Verfahren der Übertragungsmatrizen für gekrümmte Trager". Bauingenieur, 41, 3, 1966, pp. 98-102.

30. TOPPLER, J.F., CHAUDHURI, B.K., and VAN DEN BERG, J. "Horizontally-curved Members: An Approximate Method of Design". Concrete, 2, 10, 1968, pp. 418-425.

31. WITTFOHT, H. "Kreisförmig gekrümmte Träger mit starrer Torsionseinspannung an den Auflagerpunkten: Theorie und Berechnung". Berlin, Springer-Verlag, 1964.

32. WITTFOHT, H. "Kreisförmig gekrümmte Träger mit exzentrischer Belastung". Bauingenieur, 43, 1, 1968, pp. 15-20.

33. VREDEN, W. "Die Berechnung des gekrümmten Durchlaufträgers". Berlin-München, Verlag von Wilhelm Ernst und Sohn, 1964.

34. VREDEN, W. "Neues Allgemeines Berechnungsverfahren beliebig gelagerter gekrümmte Träger". Berlin-München, Verlag von Wilhelm Ernst und Sohn, 1966.

35. SCHULZ, M. "Die praktische Berechnung von Kreisringträgern mittels Momentenausgleich". Bauingenieur-Praxis, Heft 18, Berlin-München, Verlag von Wilhelm Ernst und Sohn, 1970.

36. MICHALOS, J.P. "Numerical Analysis of Frames with Curved Girders". Trans. A.S.C.E., 121, 1956, pp. 521-543.

37. YAMASAKI, T. and OHTA, T. "A General Solution of Influence Lines Applied to Space Frames with Curved Members". (in English), Proc. 16th Japan National Congress for Applied Mech., Tokyo, 1966, Tokyo, Chuo Kagaku-Sha, 1967, pp. 44-58.

38. TEZCAN, S.S. and OVUNC, B. "Analysis of Plane and Space Frameworks with Curved Members". Publications I.A.B.S.E., 25, 1965, pp. 339-352.

39. MICHALOS, J. "Matrix Formulation of the Force Method for a Structure Curved in Space". Publications I.A.B.S.E., 26, 1966, pp. 327-336.

40. SAWKO, F. "Computer Analysis of Grillages Curved in Plan". Publications I.A.B.S.E., 27, 1967, pp. 151-170.

41. MORRIS, D.L. "Curved Beam Stiffness Coefficients". Proc. A.S.C.E. (Journ. Struct. Div.), 94 (ST5), 1968, pp. 1165-1174.

42. LEE, H.P. "Generalized Stiffness Matrix of a Curved Beam Element". Journ. A.I.A.A. (Technical Notes), 7, 10, 1969, pp. 2043-2045.

43. WANG, L.R. "Parametric Matrices of Some Structural Members". Proc. A.S.C.E. (Journ. Struct. Div.), 96 (ST8), 1970, pp. 1735-1759.

44. FASULLO, E.J. "Curving a Box Girder". Modern Steel Construction, A.I.S.C., II, 4, 1962, pp. 9-11.

45. SOTO, M.H. "Analysis of Suspended Curved Girders". Proc. A.S.C.E. (Journ. Struct. Div.), 92 (ST1), 1966, pp. 21-38.

46. BRAMALD, H.G. and GRALTON, J. "Design of Curved Bridges". Institution of Engineers, Australia, Queensland Division Technical Papers (pre-print), 10, 20, 1969.

47. VLASOV, V.Z. "Thin-Walled Elastic Beams". Washington, D.C., National Science Foundation, Second Edition, 1961.

48. WANSLEBEN, F. "Die Berechnung drehfester gekrümmter Stahlbrücken". Stahlbau, 21, 4, 1952, pp. 53-56.

49. DABROWSKI, R. "Equations of Bending and Torsion of Curved Thin-Walled Bars with Asymmetric Cross-Section". Archiwum Mechaniki Stosowanej, 12, 5-6, 1960, pp. 789-799.

50. DABROWSKI, R. "Zur Berechnung von gekrümmten dünnwandigen Trägern mit offenem Profil". Stahlbau, 33, 12, 1964, pp. 364-372.

51. DABROWSKI, R. "Einflusslinien der Biege-und Wölbkraft-momente in gekrümmten dünnwandigen Trägern". Stahlbau, 34, 7, 1965, pp. 214-222.

52. DABROWSKI, R. "Wölbkrafttorsion von gekrümmten Kasten-trägern mit nichtverformbarem Profil". Stahlbau, 34, 5, 1965, pp. 135-141.

53. DABROWSKI, R. "Gekrümmte dünnwandige Träger: Theorie und Berechnung". Berlin, Springer-Verlag, 1968.

54. KONISHI, I. and KOMATSU, S. "Three-Dimensional Analysis of Curved Girder with Thin-Walled Cross Section". Publications I.A.B.S.E., 25, 1965, pp. 143-204.

55. KONISHI, I. and KOMATSU, S. "On the Fundamental Theory of Thin-Walled Curved Girder". Trans. Japan Soc. of Civil Eng., 87, 1962, pp. 35-48.

56. KONISHI, I. and KOMATSU, S. "Three-Dimensional Analysis of Simply Supported Curved Girder Bridges". Trans. Japan Soc. of Civil Eng., 90, 1963, pp. 11-28.

57. KONISHI, I. and KOMATSU, S. "Three-Dimensional Analysis of Continuous Curved Girder Bridges". Trans. Japan Soc. of Civil Eng., 91, 1963, pp. 13-24.

58. KOMATSU, S. "Structural Analysis for Continuous S-Shaped Curved Girder Bridge". (in English), Proc. 13th Japan National Congress for Applied Mech., Tokyo, 1963, Tokyo, Chuo Kagaku-Sha, 1965, pp. 17-22.

59. KONISHI, I., SHIRAISHI, N., and KAMBE, S. "A Study on the Torsional Bending Theory of the Curved Girder Bridge with Thin-Walled Closed Cross Sections Taking the Secondary Shear Deformation into Account". Proc. Symposium on Thin-Walled Structures and Space Structures, Japan Science Council, National Committee for Bridge and Structure Engineering, Tokyo, March 1969, pp. 153-167.

60. BENSCOTER, S.U. "A Theory of Torsion Bending for Multi-cell Beams". Journ. Applied Mech., 21, 1, 1954, pp. 25-34.

61. HEILIG, R. "Beitrag zur Theorie der Kastenträger beliebiger Querschnittsform". Stahlbau, 30, 11, 1961, pp. 333-349.

62. KURANISHI, S. "Analysis of Thin-Walled Curved Beams". Trans. Japan Soc. of Civil Eng., 108, 1964, pp. 7-12.

63. FUKAZAWA, Y. "Fundamental Theory on Statical Analysis of Thin-Walled Curved Bars". Trans. Japan Soc. of Civil Eng., 110, 1964, pp. 30-51.

64. FUKAZAWA, Y. "Analysis of Thin-Walled Curved Beams with Variable Cross Section Taking into Account Discontinuity of Shear Centre Line". Proc. Symposium on Thin-Walled Structures and Space Structures, Japan Science Council, National Committee for Bridge and Structure Engineering, Tokyo, March 1969, pp. 135-152.

65. BAZANT, Z.P. "Non-Uniform Torsion of Thin-Walled Bars of Variable Section". Publications I.A.B.S.E., 25, 1965, pp. 17-39.

66. WASHIZU, K. "Some Considerations on a Naturally Curved and Twisted Slender Beam". Journ. Math. Phys., 43, 2, 1964, pp. 111-116.

67. GREBEN, E.S. "Contribution to Slender-Beam Theory". (in Russian). Inzhenernyi Zhurnal Mekhanika Tverdogo Tela, 5, 1967, pp. 67-72.

68. VESELOVSKII, G.V. "Calculation of Thin-Walled Circular Continuous Beams". (in Russian). Tr. Novocherk. Politekhn. In-ta, 163, 1966, pp. 70-77.

69. KARMAN, T. Zeitschrift des Vereins deutscher Ingenieure, 55, 1911, p. 1889.

70. TIMOSHENKO, S. "Bending Stresses in Curved Tubes of Rectangular Cross Section". Trans. A.S.M.E., 45, 1923, pp. 135-140.

71. ANDERSON, C.G. "Flexural Stresses in Curved Beams of I- and Box-Section". Proc. Inst. Mech. Engrs., 163 (War Emergency Proc., No. 62), 1950, pp. 295-306.

72. CORNELIS, A. and CARTILIER, G. "Theoretical Studies of Bending of Curved Beams with Thin Walls". (in French). Bull. Centre d'Etudes, Rech d'Essais Scient. Genie Civ. Liege, 11, 1960, pp. 27-69.

73. DZIEWOLSKI, R. "Flexion des tubes rectangulaires courbes à petit rayon de courbure". Construction Métallique, 4, 1964, pp. 20-24.

74. DABROWSKI, R. "Näherungsberechnung der gekrümmten Kastenträger mit verformbarem Querschnitt". I.A.B.S.E. 7th Congress, Rio de Janeiro, Preliminary Publication, 1, 1964, pp. 299-306.

75. BAZANT, Z.P. "Pièces longues à voiles épais et calcul des poutres à section déformable". Ann. des Ponts et Chaussées, 138, 3, 1968, pp. 155-169.

76. COULL, A. and DAS, P.C. "Analysis of Curved Bridge Decks". Proc. Institution of Civil Engrs., 37, 1967, pp. 75-85.

77. CERADINI, G. "Théorie des ponts courbes à poutres multiples". Publications I.A.B.S.E., 25, 1965, pp. 51-63.

78. YONEZAWA, H. "Moments and Free Vibrations in Curved Girder Bridges". Proc. A.S.C.E. (Journ. Eng. Mech. Div.), 88 (EM1), 1962, pp. 1-21.

79. HEINS, C.P. "The Presentation of the Slope-Deflection Fourier Series Method for the Analysis of Curved Orthotropic Highway Bridges". University of Maryland, Report, June 1967.

80. BELL, L.C. and HEINS, C.P. "The Solution of Curved Bridge Systems Using the Slope-Deflection Fourier Series Method. The Design of Curved Viaducts". University of Maryland, Civil Engineering Progress Report, June 1968.

81. BELL, L.C. and HEINS, C.P. "Analysis of Curved Girder Bridges". Proc. A.S.C.E. (Journ. Struct. Div.), 96 (ST8), 1970, pp. 1657-1673.

82. BELL, L.C. and HEINS, C.P. "Curved Girder Computer Manual". University of Maryland, Bureau of Public Roads (U.S.), Maryland State Roads Commission, Report HPR-PR-1(5), AW-70-85-46, Sept. 1969.

83. HEINS, C.P. and LOONEY, C.T.G. "The Analysis of Curved Orthotropic Highway Bridges by Finite Difference Technique". University of Maryland, Report, Jan. 1967.

84. HAILS, R.L. and HEINS, C.P. "The Study of a Stiffened Curved Plate Model using the Finite Difference Technique. The Design of Curved Viaducts". University of Maryland, Civil Engineering Progress Report, June 1968.

85. HEINS, C.P. and HAILS, R.L. "Behaviour of Stiffened Curved Plate Model". Proc. A.S.C.E. (Journ. Struct. Div.), 95 (ST-11), 1969, pp. 2353-2370.

86. YÜKSEL, F. "Berechnung gekrümmter Durchlaufplatten". Beton-und Stahlbetonbau, 61, 2, 1966, pp. 39-46.

87. PRZEMIENIECKI, J.S. "Theory of Matrix Structural Analysis". New York, McGraw-Hill Book Company, Inc., 1968, pp. 445-463.

88. ANEJA, I. and ROLL, F. "An experimental and Analytical Investigation of a Horizontally Curved Box Beam Bridge Model". Paper presented at Second International Symposium on Concrete Bridge Design, Chicago, April 1969.

89. ANEJA, I. "Experimental and Analytical Study of Horizontally Curved Box Beam Highway Bridges". Thesis presented to University of Pennsylvania at Philadelphia, Pa., in 1968 for the degree of Doctor of Philosophy.

90. CHAPMAN, J.C., DOWLING, P.J., LIM, P.T.K., and BILLINGTON, C.J. "The Structural Behaviour of Steel and Concrete Box Girder Bridges". Structural Engineer, 49, 3, 1971, pp. 111-120.

91. LIM, P.T.K. and MOFFATT, K.R. "Finite Element Analysis of Curved Slab Bridges with Special Reference to Local Stresses". Paper presented at Conference on Developments in Bridge Design and Construction, Cardiff, March-April 1971.

92. LIM, P.T.K., KILFORD, J.T., and MOFFATT, K.R. "Finite Element Analysis of Curved Box Girder Bridges". Paper presented at Conference on Developments in Bridge Design and Construction, Cardiff, March-April 1971.

93. SISODIYA, R.G., CHEUNG, Y.K., and GHALI, A. "Finite Element Analysis of Skew Curved Box Girder Bridges". Publications I.A.B.S.E., 30-II, 1970, pp. 191-199.

94. CHEUNG, Y.K., KING, I.P., and ZIENKIEWICZ, O.C. "Slab Bridges with Arbitrary Shape and Support Conditions; a General Method of Analysis Based on Finite Elements". Proc. Institution of Civil Engrs., 40, 1968, pp. 9-36.

95. CHEUNG, Y.K. "The Analysis of Cylindrical Orthotropic Curved Bridge Decks". Publications I.A.B.S.E., 29-II, 1969, pp. 41-52.

96. MEYER, C. and SCORDELIS, A.C. "Analysis of Curved Folded Plate Structures". University of California, Report UC SEMS 70-8, June 1970.

97. SAWKO, F. and MERRIMAN, P.A. "Finite Element Analysis of Bridges Curved in Plan". Paper presented at Conference on Developments in Bridge Design and Construction, Cardiff, March-April 1971.

98. DAVIES, J.D., SOMERAILLE, I.J., and ZIENKIEWICZ, O.C. "Analysis of Various Types of Bridges by the Finite Element Method". Paper presented at Conference on Developments in Bridge Design and Construction, Cardiff, March-April 1971.

99. SISODIYA, R.G. and CHEUNG, Y.K. "A Higher Order In-Plane Parallelogram Element and its Application to Skewed Curved Box Gorder Bridges". Paper presented at Conference on Developments in Bridge Design and Construction, Cardiff, March-April 1971.

100. CHEUNG, M.S. and CHEUNG, Y.K. "Analysis of Curved Box Girder Bridges by Finite Strip Method". Publications I.A.B.S.E., 31-I, 1971.

101. PULTAR, M. "Analysis of Continuous Folded Plate Structures". Thesis presented to Princeton University, Princeton, N.J., in 1964 for the Degree of Doctor of Philosophy.

102. PULTAR, M., BILLINGTON, D.P., and RIERA, J.D. "Folded Plates Continuous Over Flexible Supports". Proc. A.S.C.E. (Journ. Struct. Div.), 93 (ST5), 1967, pp. 253-277.

103. LEE, S.L., and MOUSA, A.M. "Prismatic Shells Continuous Over Transverse Diaphragms". Publications I.A.B.S.E., 27, 1967, pp. 43-60.

104. LO, K.S. "Analysis of Cellular Folded Plate Systems". Thesis presented to University of California, Berkeley, California, in 1967 for the Degree of Doctor of Philosophy.

105. SCORDELIS, A.C. "Analysis of Continuous Box Girder Bridges". A report of an investigation to the Division of Highways, Department of Public Works, State of California; and to U.S. Department of Transportation, Federal Highway Administration, Bureau of Public Roads. College of Engineering, Office of Research Services, University of California, Berkeley, California, Nov. 1967.

106. GOLDBERG, J.E. and LEVE, H.L. "Theory of Prismatic Folded Plate Structures". Publications I.A.B.S.E., 16, 1957, pp. 59-86.

107. FLÜGGE, W. "Stresses in Shells". Berlin, Springer-Verlag, 1960.

108. WILSON, B. "Asymmetrical Bending of Conical Shells". Proc. A.S.C.E. (Journ. Eng. Mech. Div.), 86 (EM3), 1960, pp. 119-139.

109. TIMOSHENKO, S.P. and WOINOWSKY-KRIEGER, S. "Theory of Plates and Shells". New York, McGraw-Hill Book Company, Inc., Second Edition, 1959.

110. TIMOSHENKO, S.P. and GOODIER, J.N. "Theory of Elasticity". New York, McGraw-Hill Book Company, Inc., Second Edition, 1951.

111. REHN, M. and SVED, G. "Stiffness Matrices of Sector Shaped Thin Shell Elements". Bulletin International Association for Shell Structures, no. 45, March 1971, pp. 3-22.

112. HOUGHTON, D.S. and JOHNS, D.J. "A Comparison of the Characteristic Equations in the Theory of Circular Cylindrical Shells". Aeronautical Quarterly, Vol. XII, Aug. 1961, pp. 228-236.

113. NOVOZHILOV, V.V. "The Theory of Thin Shells". Groningen, P. Noordhoff Ltd., 1959.

114. JENKINS, R.S. "Theory and Design of Cylindrical Shell Structures". Modern Building Techniques, Bulletin No. 1, London, Ove Arup and Partners, 1947.

[15. SCORDELIS, A.C. and LO, K.S. "Computer Analysis of Cylindrical Shells". Proc. A.C.I., 61, 5, 1964, pp. 539-560.

[16. WALLACE, G. "Structural Model Analysis with Thermoplastics". Strain, 3, 3, 1967, pp. 4-17.

[17. FIALHO, J.F.L. "The Use of Plastics for Making Structural Models". Bulletin R.I.L.E.M., 8, 1960, pp. 65-74.

[18. BREEN, J.E. "Fabrication and Tests of Structural Models". Proc. A.S.C.E. (Journ. Struct. Div.), 94 (ST6), 1968, pp. 1339-1352.

[19. ROLL, F. "Materials for Structural Models". Proc. A.S.C.E. (Journ. Struct. Div.), 94 (ST6), 1968, pp. 1353-1381.

[20. MASSACHUSETTS INSTITUTE OF TECHNOLOGY. "Stress: A User's Manual". Cambridge, Massachusetts, M.I.T. Press, 1967.

[21. MASSACHUSETTS INSTITUTE OF TECHNOLOGY. "Stress: A Reference Manual". Cambridge, Massachusetts, M.I.T. Press, 1966.